Model Tests of a Series of Six Patrol Boats

SIT

Model	Lpx		Lwl		Bpx		Dep		βχ	βτχ	Centroid	Lcg aft of Centroid	Lcg from Transom		Lcg/Lpx	Centerline	Ap		Twisted	Lpx/Bpx	Ap/Vol	Lpx/Ap	Lpx/Vol	Cv	Vcg/Lpx	Shaft	Lce	
4928	31,89	in	31,60	in	9,88	in	13,06	Lb	18,00	8,50	48,70	-6,70	13,427	in	0,421	-2,30	1,92	ft^2	9,50	3,23	5,444	3,677	4,474	0,365	----------	10,80	0,000	ft
	0,81	m	0,80	m	0,25	m	5,92	kg					0,341	m			0,1785	m^2									0,0000	m
4929	41,33	in	40,46	in	8,03	in	13,06	Lb	18,50	5,70	49,10	-5,90	17,855	in	0,432	-1,60	1,92	ft^2	12,80	5,15	5,444	6,175	5,798	0,680	----------	10,80	0,000	ft
	1,05	m	1,03	m	0,20	m	5,92	kg					0,454	m			0,1785	m^2									0,0000	m

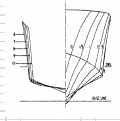

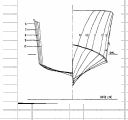

LITERATURE =

Pv

Salt Water
ATTC
1.90-4.25

REPORTS

R-985

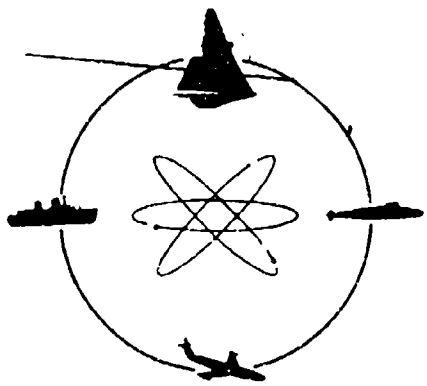

DAVIDSON LABORATORY

REPORT 985

MODEL TESTS OF A SERIES OF SIX PATROL BOATS IN SMOOTH AND ROUGH WATER

by

Young Chey

October 1963
Revised August 1964

STEVENS INSTITUTE OF TECHNOLOGY
CASTLE POINT STATION
HOBOKEN, NEW JERSEY

DAVIDSON LABORATORY

REPORT 985

October 1963

Revised August 1964

MODEL TESTS OF A SERIES OF SIX PATROL BOATS IN SMOOTH AND ROUGH WATER

by

Young Chey

Sponsored by
Bureau of Ships, Department of the Navy
Administered by David Taylor Model Basin
Contract NObs 78349, T/O 14
DL Project 2648(223)

Approved

Edward Numata

Edward Numata, Chief
Ship Research Division

xii + 31 pages
43 figures, 9 plates
frontispiece

ABSTRACT

Three round-bottom models and three hard-chine models, with length-beam ratios of 3, 4 and 5 in each group and with constant displacement, were tested in smooth water and in irregular waves of Sea States 3 and 5. The hard-chine model and the round-bottom model of length-beam ratio 4 were used to evaluate relative broaching tendencies in regular following waves.

The resistance data in smooth and rough water were expanded to boat weights of 55,000 pounds. The measured values of accelerations, at the forward quarter point and LCG position, and of heave, are presented. In the evaluation of relative broaching tendencies in regular following waves, experimental results were combined with theoretical results to derive indices of broaching.

Keywords: Planing Hulls, Seakeeping,
Resistance, Porpoising
Broaching

TABLE OF CONTENTS

NOMENCLATURE

A_p	projected planing bottom area, excluding area of external spray strips
B	maximum beam at water line
b	local beam at water line; bow
c	wave celerity
C_L	lift coefficient
C_{SF}	side force coefficient $= \frac{SF}{1/2\ \rho\ \nabla^{2/3}\ V^2}$
C_{YM}	yaw moment coefficient $= \frac{YM}{1/2\ \rho\ \nabla^{2/3}\ V^2 L}$
$\frac{dC_L}{d\delta}$	lift curve slope of rudder
EHP	effective horsepower
F	force
F_A	side force due to mean wave slope
F_B	side force due to local wave slope
F_{bw}	side force due to wave-body interaction
F_∇	volume Froude number $= \frac{V}{\sqrt{g\ \nabla^{1/3}}}$
g	gravitational acceleration
H'	local draft
H	wave double amplitude
h	wave amplitude
k'	coefficient of accession to inertia in sway motion
LBP, L	length between perpendiculars
LCG	longitudinal center of gravity position

M_B	yaw moment due to local wave slope
M_{bw}	yaw moment due to wave-body interaction
P	pressure
R	radial distance to a point in the fluid
r	radius
SF	side force
$\frac{S_w}{\nabla^{2/3}}$	wetted surface area coefficient
S	sectional area of hull
s	stern
V	model speed
v	horizontal component of wave orbital velocity perpendicular to the ship longitudinal center line
x,y,z	coordinates
YM	yaw moment
α	angle with horizontal of tangent to mean buttock at stern, in degs when model is advancing in water
Δ	displacement at rest
δ	rudder angle in degs
θ	relative heading between ship and waves
λ	wave length
ξ	longitudinal distance from CG of any section in ship
ρ	water density
τ	trim angle
Φ	velocity potential
Φ_{bw}	velocity potential due to body-wave interaction
Ψ	yaw angle
∇	volume of displacement at rest

INTRODUCTION

Many reports on systematic studies of planing boats have appeared recently. The hydrodynamics of planing hulls in smooth water, for example, is extensively covered in a paper by A. B. Murray.[1] This paper demonstrates the precise importance of trim effect on the total resistance of planing hulls, and of other parameters affecting the resistance. E. P. Clements[2,3] discusses a logical method of presenting experimental data, and the effects on performance of variations in some of the primary parameters of planing hulls. E. P. Clement and C. W. Tate[4] present resistance data for a number of planing-boat designs in smooth water, and list desirable features of stepless planing-hull design. S. C. McGown[5] emphasizes seaworthiness as an important design consideration for high-speed small craft. Peter DuCane[6] and DuCane and G. J. Goodrich[7] describe experimental and theoretical methods of evaluating broaching tendencies of high-speed hull forms. K. S. M. Davidson[8] presents a practical method of determining the broaching tendency of a ship in following regular waves. Theoretical study of surging motion and broaching tendencies in irregular seas is described by O. Grim.[9]

Only a few experimental studies on the seakeeping qualities of planing-hull models in rough water (particularly in irregular waves) have been made. D. Lueders[10] presents the results of model tests of two planing-hull forms and a round-bottom hull form, in irregular head seas.

Small-craft designers are of late becoming more and more interested in the over-all performance of craft under actual sea conditions. This report presents the results of an experimental study on the effects of hull characteristics of high-speed small craft on smooth-water resistance and on performance in irregular waves. The results will help to promote a better understanding of how the two most fundamental parameters — hull form and length-beam ratio — affect smooth-water resistance and behavior of craft in irregular seas.

The study was conducted at Davidson Laboratory, Stevens Institute of Technology, for the David Taylor Model Basin, under Contract NObs 78349, Task Order 14.

DESCRIPTION OF MODELS

Six 1/16-scale models were used in this experiment. Three of them, Models 4925, 4926, and 4927 were round-bottom hull forms, with nominal length-beam ratios of 3, 4, and 5, respectively. The other three, Models 4928, 2387, and 4929, were hard-chine vee-bottom hull forms, with nominal L/B ratios of 3, 4, and 5, respectively. The body plans and profiles of these models are shown in Figs. 1 through 6.

The models, with the exception of Model 2387, were constructed by the David Taylor Model Basin. Model 2387 was built by Davidson Laboratory. All models had a displacement of 13.06 lb (ship displacement of 55,000 lb) and they were tested at this displacement only. Tables I-A and I-B, following, show the characteristics of the models.

TABLE I-A

CHARACTERISTICS OF ROUND-BOTTOM MODELS

	Models		
	4925	4926	4927
Nominal L/B ratio	3	4	5
Length overall	33.9"	38.7"	42.9"
Length between perpendiculars	31.2"	35.6"	40.2"
Length at water line	31.2"	36.05"	40.45"
Maximum beam	11.25"	9.69"	8.56"
Beam at water line	10.5"	9.035"	8.0"
Draft	2.20"	2.30"	2.39"
Longitudinal center of gravity abaft amidships in % of LBP	9.9%	7.9%	9.4%
Longitudinal radius of gyration, in % of LBP	26%	26%	26%
$A_p/\nabla^{2/3}$	5.2	5.3	5.3

TABLE I-B

CHARACTERISTICS OF HARD-CHINE MODELS

	Models		
	4928	2387	4929
Nominal L/B ratio	3	4	5
Length overall	34.0"	39.0"	43.0"
Length between perpendiculars	31.2"	35.6"	40.2"
Length at water line	31.6"	36.0"	40.46"
Maximum beam	11.88"	10.75"	9.85"
Beam at water line	10.5"	9.15"	8.25"
Draft	2.63"	2.63"	2.55"
Longitudinal center of gravity abaft amidships, in % of LBP	6.7%	6.2%	5.9%
Longitudinal radius of gyration in % of LBP	26%	26%	26%
$A_p/\nabla^{2/3}$	5.5	5.5	5.5

The models were made of pine and coated with grey paint. Basically, there were two configurations for each model: one without skeg and the other with skeg.

The profiles of hard-chine-hull model forms exhibit curves where buttock lines abaft midships are close to keels, with the radii of curvature pointed downward; but the corresponding buttock lines of the round-bottom hulls are straight. If one relates these shapes with airfoil sections, for purposes of comparison, they are found to resemble, respectively, cambered and straight airfoil sections. Also, the ratio of the vertical distance between keel and water line, at the forefoot, to the corresponding vertical distance at the transom is, for hard-chine models, about 30% greater than that for round-bottom models.

For the broaching-tendency evaluation experiment, Models 4926 and 2387 were fitted with twin rudders. The locations of the rudders for both models were identical. The arrangement sketch of the rudders is shown in Fig. 37.

TEST CONDITIONS AND PROCEDURES

Smooth-Water Resistance Test

The smooth-water resistance experiment was conducted at Tank No. 1 of the Davidson Laboratory; the standard test apparatus and method described in an earlier paper[1] were used. Additional tests were conducted in the Laboratory's Tank No. 3, to investigate porpoising tendency.

On each of the six models, a turbulence stimulation strut 0.04 in. in diameter was located 5 in. forward of the stem and was immersed to keel level.

Model 4927 (round bottom, L/B of 4) was initially tested with a spray strip covering only the forward 40% of the length. Photographs of this configuration at full-size-ship speeds of 25, 30, 35, 40, 45, and 50 knots are shown in Plate 1. At speeds above 35 knots, water spray wetted the sides of the model all the way up to deck level. Since this was unrealistic for the prototype, the spray strip was extended all the way aft, to the transom. The spray strips of Models 4926 and 4927 (round bottom) were also extended to the transoms.

The smooth-water resistance test was conducted for a total of 12 configurations — that is, with and without skeg for each of the six models. The static trim angles of all models were even keel; the water lines of the models coincided with the designer's water lines as they appear in Figs. 1 through 6. Shaft angles with the horizontal were 10 deg for the round-bottom models and 10.8 deg for the hard-chine models.

Performance Test in Irregular Waves

The performance test in irregular waves was conducted at Tank No. 3 of the Davidson Laboratory. All six models were tested without skegs.

Each model was towed by a falling weight; transducer wires followed the model through the follow-up servo-carriage. Each model was balanced so that the longitudinal radius of gyration was 26% of its LBP. The models were free to heave and free to pitch about the CG axis. Accelerometers were located at the LCG and 1/4-LBP aft of station zero. Turbulence stimulation was not applied, either on bow or ahead of model, for this test in waves. The following items were measured and their time histories recorded on tape:

1. Acceleration at forward quarter point
2. Acceleration at LCG
3. Heave amplitude (head seas only)
4. Waves

Characteristics of irregular waves are summarized below.

TABLE II

CHARACTERISTICS OF IRREGULAR WAVES*

	Irregular waves(1) (Ship Size)	Irregular waves(2) (Ship Size)
Average wave height	2.47 ft	5.50 ft
Average of 1/10 highest wave heights	4.42 ft	9.40 ft
Average period	4.5 sec	6.0 sec

* Irregular waves (1) and (2) correspond approximately to Sea States 3 and 5, respectively.

In order to have at least 25 to 30 cycles of acceleration records, two runs were made for each speed, in the speed range of 40 to 50 knots. On every run, the models started from a fixed location in the tank. For the second run in the speed range of 40 to 50 knots, a longer period of time was allowed to elapse between wave-machine start and model start, so that the wave program of the second run would be different from that of the first run. Waves encountered by a model at a given speed were practically identical to those encountered by any other model at that speed. This procedure was employed for the sake of consistence and of ease in making a comparison of data for the models.

Movies of selected portions of the runs were taken, to record observation of the models' behavior in these irregular seas.

Broaching-Tendency Evaluation Test

In order to find static derivatives of side force and yaw moment with respect to yaw angle, two models, 4926 and 2387, were towed with constant speeds in smooth water. The models were free to heave and pitch, so that they could be in the equilibrium positions during a run. The axes of the dynamometer measuring yaw moment and side force were aligned with the axes of the models at the CG in still water, and they yawed with the models. Therefore the side force was measured about the ship axes, but the yaw moment was measured about a vertical axis through the CG.

The models were also towed with constant speed in regular following waves. The models' longitudinal moments of inertia were identical to those noted during the performance test in the irregular seas.

The dimensions of the regular waves are summarized in the table below.

TABLE III

REGULAR FOLLOWING WAVES

	Wave Length	$\frac{\text{Wave Double Amplitude}}{\text{Wave Length}}$
Regular wave (1)	50 ft	1/25
Regular wave (2)	50 ft	1/50
Regular wave (3)	100 ft	1/25
Regular wave (4)	100 ft	1/50

Originally, wave-height-to-wave-length ratios of 1/20 and 1/40 were planned. However, because of the limited capacity of the existing dynamometer, wave-height-to-wave-length ratios of 1/25 and 1/50 were selected instead. Both models were tested in regular waves (1) and (3), but for a linearity check only Model 2387 was tested in regular waves (2) and (4). In regular wave (1), speeds of the models were 1.15 and 1.5 times the wave speed. These speeds correspond, respectively, to 10.9 knots and 14.2 knots.

In regular wave (3), speeds of the models were 0.75, 1.10, and 1.5 times the wave speed. These speeds correspond to 10 knots, 14.8 knots, and 20 knots, respectively. Originally, a maximum model speed of 3 times the wave speed for each regular wave was planned. However, because the natural frequency of yaw-moment balance is too close to the exciting frequencies at these high speeds, the data analysis for the runs in this speed range would have been complicated. Therefore, these high-speed runs were not made. The highest encounter frequency of the test was approximately 1/5 of the natural frequency of the yaw-moment balance. Hence no correction for the dynamic response of the dynamometer was applied to the amplitude data.

A few runs were made without rudders for Model 2387, in both smooth water and in the waves, to see the effect on the forces and moments.

RESULTS OF TESTS

Smooth-Water Resistance Test

The results of the smooth-water resistance test are presented in Figs. 7 through 12. Predictions are for salt water at 59°F, based on Schoenherr's friction formulation for both model and boat. The roughness allowance coefficient of 0.4×10^{-3} was added to the friction resistance coefficient of the prototype. Figure 7 shows the specific resistance and α, the angle with the horizontal of the mean buttock at the stern, in degrees, for each boat without skeg. Figure 8 shows the specific resistances of the boats with skegs. The α values are the same for a boat with skeg and without skeg. The wetted area coefficients and the CG rise coefficients of the models without and with skegs are plotted in Figs. 9 and 10, respectively. The EHP's of the boats without and with skegs are shown in Figs. 11 and 12, respectively. The photographs of the models running in smooth water are presented in Plates 1 through 9.

Performance Test in Irregular Waves

The results of the performance test in irregular seas are presented in Figs. 13 through 36. The specific resistances of the boats in State 3 head seas, State 3 following seas, State 5 head seas, and State 5 following seas are shown, respectively, in Figs. 13, 14, 15, and 16. The resistance of a boat in waves was obtained by summing up the smooth-water resistance of the boat and the product of the cube of the scale ratio and the added model resistance in waves. Performance tests in following irregular seas were conducted for only three models: 4926, 4927, and 2387. In these tests it was found that the acceleration levels in following seas were relatively low, and it was decided to eliminate tests of the remaining three models in following seas.

EHP's of the boats in State 3 head seas, State 3 following seas, State 5 head seas, and State 5 following seas are shown in Figs. 17, 18, 19, and 20 respectively.

The average values and the average values of 1/10 highest accelerations, at the forward quarter points of the models in State 3 head seas, are plotted in Figs. 21 and 22, respectively. The accelerometer was located at the forward quarter point along the longitudinal center line on the inner bottom of each model.

Figures 23 and 24 show the average values and the average values of 1/10 highest accelerations, at the LCG in State 3 head seas, respectively. The accelerometer was located at the intersection of the transverse plane, through the LCG, with the starboard inner side of the hull. The models were restrained from roll during the performance test in the irregular seas.

The average heave double amplitudes and the averages of 1/10 highest heave double amplitudes in State 5 head seas are shown in Figs. 25 and 26, respectively. The average acceleration amplitudes at the forward quarter point and LCG in State 3 following seas are shown in Figs. 27 and 28, respectively. The average vertical accelerations and the averages of 1/10 highest vertical accelerations, at the forward quarter points of the models in the head sea of State 5, are plotted in Figs. 29 and 30, while the corresponding accelerations at the LCG's of the models are shown in Figs. 31 and 32, respectively. Figures 33 and 34 show, respectively, the average heave double amplitudes and the average values of 1/10 highest heave double amplitudes of the models in State 5 head seas. The average amplitudes of vertical accelerations at the forward quarter points and the LCG's of the models, in State 5 following seas, are presented in Figs. 35 and 36, respectively.

Broaching-Tendency Evaluation Test

The side force coefficients of Models 4926 and 2387 in smooth water are plotted in Fig. 38. The yaw moment coefficients of the models in smooth water are plotted in Fig. 39 for the volume Froude numbers of 0.92, 1.37, and 1.83. The yaw moment coefficients in smooth water for the Froude numbers of 0.97, 1.29, 1.94, and 2.59 are plotted in Fig. 40. The side force coefficient and the yaw moment coefficient are defined as follows:

$$C_{YM} = \frac{YM}{\frac{1}{2}\rho V^2 \nabla^{2/3} L} \qquad C_{SF} = \frac{SF}{\frac{1}{2}\rho V^2 \nabla^{2/3}}$$

Figures 41 and 42 show the side force coefficients and the yaw moment coefficients of Model 2387 in regular waves (1), (2), (3), and (4). They are plotted against H/λ, so that the linearity of the force and moment, with respect to wave height, can be easily checked.

During the broaching-tendency evaluation test, the models moved parallel to the longitudinal center line of the tank. The model's yaw angle was fixed during a run in both smooth water and in waves. Therefore, measured side force and yaw moment in waves are the sum of two components: one due to relative model-wave heading in waves and the other due to drift angle in waves. These two components could be experimentally determined in Tank No. 2 of the Davidson Laboratory. Unfortunately, however, the speed capacity of the existing carriage could not meet the speed requirement of the experiment. Therefore the side force component and the yaw moment component due to relative ship-wave heading was estimated by the theoretical analysis which is presented in the next section.

A photograph of Model 2387, underway in regular following waves, is presented as the Frontispiece.

THEORETICAL ANALYSIS OF THE FORCES AND MOMENTS ACTING ON A SHIP IN REGULAR FOLLOWING WAVES

Forces and moments can be conveniently separated into the following three components.

1. The force generated by the mean inclination of the water surface
2. The force and moment produced by the local slope of the wave profile at various stations along the ship
3. The force and moment produced by the inertial interaction between the ship and wave

For the following analysis, the angle of heading θ, with respect to the normal to the wave crests, is reasonably small, so that $\sin\theta \approx \theta$ and $\cos\theta \approx 1.0$.

When the ship is advancing in following waves, so that encounter frequency is much smaller than the natural frequency in pitch, the trim of the ship at any instant of time will be essentially identical with the

mean slope of the wave on which the ship is floating. If we designate the trim angle in radians by τ and the displacement by Δ, there is a forward-acting component of the displacement, in a direction normal to the wave crests, equal to $\Delta\tau$; and there is a lateral component of this force equal to $\Delta\tau\theta$.

Additional force and moment are produced at various stations because of difference in the water level at the starboard side and at the portside of the hull. If the wave slope is $(dy/dx)_w$, then its component normal to the ship's longitudinal center line is $\theta(dy/dx)_w$. Pressure force difference between the starboard and port sides of the hull, for a unit-length strip section, will be

$$\rho g H' b \beta_1$$

where

H' = local draft
b = local beam
$\beta_1 = \theta\,(dy/dx)_w$

Total force and moment due to the local wave slope are:

$$F_B = \rho g \int_s^b H' b \beta_1 dx \qquad (1)$$

$$M_B = \rho g \int_s^b H' b \beta_1 x dx \qquad (2)$$

Using the notation of Fig. 43, the velocity potential of the wave is

$$\phi_w = hc\, e^{2\pi z/\lambda} \cos\left[\frac{2\pi}{\lambda}(x\cos\theta + y\sin\theta - ct)\right] \qquad (3)$$

and the component of horizontal wave orbital velocity perpendicular to the

ship longitudinal center line is

$$v = -\frac{\partial \Phi_w}{\partial y} = \frac{2\pi}{\lambda} hc\, e^{2\pi z/\lambda} \sin\left[\frac{2\pi}{\lambda}(x\cos\theta + y\sin\theta - ct)\right]\sin\theta \qquad (4)$$

Then the potential due to wave-body interaction becomes, with the assumption of $\cos\theta \approx 1.0$ $\sin\theta \approx \theta$,

$$\Phi_{bw} = +v\frac{r^2}{R}\cos\alpha = \frac{2\pi hc\, r^2}{\lambda R} e^{2\pi z/\lambda} \sin\left[\frac{2\pi}{\lambda}(x + y\theta - ct)\right] \theta\cos\alpha \qquad (5)$$

Neglecting small perturbation velocities,

$$P_{bw} = \rho\frac{\partial \Phi_{bw}}{\partial t} = -\rho\frac{4\pi^2 c^2 h\theta\, r^2}{\lambda^2 R} e^{-2\pi R\sin\alpha/\lambda} \cos\left[\frac{2\pi}{\lambda}(x + y\ \theta - ct)\right]\cos\alpha$$

$$+ \rho\frac{2r\dot{r}}{R}\ \frac{2\pi h c\ \theta}{\lambda} e^{-2\pi R\sin\alpha/\lambda} \sin\left[\frac{2\pi}{\lambda}(x + y\ \theta - ct)\right]\cos\alpha \qquad (6)$$

On the surface of the body $R = r$, and

$$c^2 = \frac{g\lambda}{2\pi} \qquad (7)$$

$$P_{bw} = -\left[\frac{2\pi\ \rho\ g\ h\theta}{\lambda}\cos\frac{2\pi}{\lambda}(x + y\ \theta - ct)\right] r\cos\alpha\, e^{-2\pi r\sin\alpha/\lambda}$$

$$+\left[\frac{2\ \rho\ g\ h\theta}{c}\sin\frac{2\pi}{\lambda}(x + y\ \theta - ct)\right]\dot{r}\cos\alpha\, e^{-2\pi r\sin\alpha/\lambda} \qquad (8)$$

$$\left(\frac{dF}{dx}\right)_{bw} = -\int_0^{\pi} P_{bw}\, r\cos\alpha\, d\alpha \qquad (9)$$

$$e^{-2\pi\, r\sin\alpha/\lambda} = 1 - \frac{2\pi\, r\sin\alpha}{\lambda} + \frac{4\pi^2 r^2\sin^2\alpha}{2\lambda^2} + \ldots \qquad (10)$$

$$\left(\frac{dF}{dx}\right)_{bw} = \left[\left\{ \frac{2\pi\ \rho\ g\ h\theta\ r^2}{\lambda} \cos \frac{2\pi}{\lambda} (x + y\ \theta - ct) \right\} \right.$$

$$\left. - \left\{ \frac{2\ \rho\ g\ h\theta\ r\dot{r}}{c} \sin \frac{2\pi}{\lambda} (x + y\ \theta - ct) \right\} \right]$$

$$X \int_0^{\pi} \cos^2\alpha\ \ e^{-2\pi r\ \sin\alpha/\lambda}\ d\alpha \qquad (11)$$

Substituting Eq.(10) into the integrand of the last term of Eq.(11),

$$\int_0^{\pi} \cos^2\alpha\ \ e^{-2\pi\ r\ \sin\alpha/\lambda}\ d\alpha = 2\left[\frac{\pi}{4} - \frac{2\pi r}{3\lambda} + \frac{\pi^3 r^2}{8\lambda^2} + \ \ldots\right] \qquad (12)$$

Therefore,

$$\left(\frac{dF}{dx}\right)_{bw} = \left[\left\{ \frac{4\pi\ \rho\ g\ h\theta}{\lambda}\ \ r^2 \cos \frac{2\pi}{\lambda} (x + y\ \theta - ct) \right\} \right.$$

$$\left. - \left\{ \frac{4\ \rho\ g\ h\theta\ r\dot{r}}{c} \sin \frac{2\pi}{\lambda} (x + y\ \theta - ct) \right\} \right] X \left[\frac{\pi}{4} - \frac{2\pi r}{3\lambda} + \frac{\pi^3 r^2}{8\lambda^2}\right.$$

$$\left. + \ \ldots \right] \qquad (13)$$

Retaining (see Ref. 11) up to the square of $\frac{r}{\lambda}$ for the first term and the first power of $\frac{r}{\lambda}$ for the coefficients of $\dot{r}$ in the second term, and neglecting the terms with the coefficient of θ^2 ,

$$\left(\frac{dF}{dx}\right)_{bw} = 2\ \rho\ g\ h\ r\ \theta \left[\left\{ \frac{\pi^2 r}{2\lambda} - \frac{4\pi^2 r^2}{3\lambda^2} \right\} \cos \frac{2\pi}{\lambda} (x - ct) \right.$$

$$\left. - \frac{\dot{r}}{c} \left(\frac{\pi}{2} - \frac{4\pi r}{3\lambda}\right) \sin \frac{2\pi}{\lambda} (x - ct) \right] \qquad (14)$$

Now, designating the angle between the longitudinal tangent to the body surface and the x axis by β ,

$$\dot{r} = \frac{dr}{d\xi}\ \frac{d\xi}{dt} = - V \tan \beta \qquad (15)$$

For generalized ship form, r is to be interpreted as a measure of section area:

$$r = \left(\frac{2S}{\pi}\right)^{\frac{1}{2}} \quad ; \quad \tan\beta = \frac{1}{(2\pi S)^{\frac{1}{2}}} \frac{dS}{d\xi} \tag{16}$$

The term $\frac{\rho\pi r^2}{2}$ is the virtual mass of the semi-cylinder having a coefficient of accession to inertia k' equal to unity.[12] For a ship section, this term is expressed as $\rho S k'$. The term $\rho \pi r \tan\beta$ is the derivative of $\rho S k'$ with respect to ξ.

Then, for $t = 0$,

$$\left(\frac{dF}{dx}\right)_{bw} = g \rho S k' \theta \frac{2\pi h}{\lambda} \cos\frac{2\pi x}{\lambda} \left[1 - \frac{8}{3\lambda}\left(\frac{2S}{\pi}\right)^{\frac{1}{2}}\right]$$

$$+ \frac{V}{c} \frac{d}{d\xi}(g \rho S k') \theta h \sin\frac{2\pi x}{\lambda} \left[1 - \frac{8}{3\lambda}\left(\frac{2S}{\pi}\right)^{\frac{1}{2}}\right] \tag{17}$$

The total force acting on the ship can be expressed as

$$F_{bw} = \int_s^b g\theta \left[1 - \frac{8}{3\lambda}\left(\frac{2S}{\pi}\right)^{\frac{1}{2}}\right] \left[\rho S k' \frac{2\pi h}{\lambda} \cos\frac{2\pi x}{\lambda}\right.$$

$$\left. + \frac{V}{c} \frac{d}{d\xi}(\rho S k') h \sin\frac{2\pi x}{\lambda}\right] dx \tag{18}$$

where b = bow
and s = stern

Computing the integrand of Eq.(18) at each station of the model and integrating by the Simpson's rule, one can estimate the side force due to the inertial interaction of wave and ship. The coefficient k' can be estimated from several of the listed references, such as Refs. 13, 14, and 16.

$$M_{bw} = \int_{s}^{b} \frac{dF}{dx} \left(\xi + \frac{1}{\pi} \frac{dS}{d\xi} \right) dx \qquad (19)$$

where M_{bw} = yaw moment due to ship-wave interaction.

Integrating Eq.(19) in a similar fashion, one can estimate the moment. Tables IV and V on the following page summarize the force and moment components of the models in regular waves (1) and (3).

TABLE IV

SIDE FORCE AND YAW MOMENT IN REGULAR WAVES (1)

Model	Model Speed / Wave Speed	F_A/θ (lb)	F_B/θ (lb)	F_{bw}/θ (lb)	M_B/θ (in-lb)	M_{bw}/θ (in-lb)
4926	1.0	-0.003	-0.0067	-0.0013	0.195	0.105
4926	1.50	-0.008	-0.0067	-0.0012	0.195	0.096
2387	1.0	-0.003	-0.0047	-0.0014	0.221	0.070
2387	1.50	-0.0084	-0.0047	-0.0016	0.221	0.057

TABLE V

SIDE FORCE AND YAW MOMENT IN REGULAR WAVES (3)

Model	Model Speed / Wave Speed	F_A/θ (lb)	F_B/θ (lb)	F_{bw}/θ (lb)	M_B/θ (in-lb)	M_{bw}/θ (in-lb)
4926	0.75	-0.0047	-0.11	-0.0082	0.269	0.236
4926	1.0	-0.01	-0.11	-0.0075	0.269	0.251
4926	1.50	-0.01	-0.11	-0.0061	0.269	0.281
2387	0.75	-0.004	-0.074	-0.0045	0.282	0.239
2387	1.0	-0.01	-0.074	-0.0037	0.282	0.252
2387	1.50	-0.0075	-0.074	-0.0020	0.282	0.277

In these tables, forces to starboard are positive; and moments clockwise are positive.

DERIVED RESULTS

There are two ways of approaching the ship-broaching problem. The first method depends on the equations of static equilibrium, the second on the equations of motion in dynamics. Solving of the latter equations would require values of coefficients of accession to inertia and coefficients of damping of hull and rudder with respect to yaw and yaw rate. Since all values of these coefficients for the models are not available at present, only the first method will be presented here.

The equations of static equilibrium are

$$\Sigma F = \frac{\partial F}{\partial \psi} \psi + \frac{\partial F}{\partial \delta} \delta + \frac{\partial F}{\partial \theta} \theta = 0 \qquad (20a)$$

and

$$\Sigma M = \frac{\partial M}{\partial \psi} \psi + \frac{\partial M}{\partial \delta} \delta + \frac{\partial M}{\partial \theta} \theta = 0 \qquad (20b)$$

where ψ = yaw angle

and δ = rudder angle

These equations represent the physical situation only when ψ, δ, and θ are small enough for the force and moment derivatives to be constants within this range. Under this assumption, ψ/θ and δ/θ solved from the above equations could provide the indices of static stability. For a given θ, the larger the values of the above two ratios, the poorer the stability. Values of δ/θ will provide immediate comparison as to the rudder angle required to maintain equilibrium in the horizontal plane for the two models.

As mentioned previously, the direct data obtained from the Tank No. 3 force and moment test in regular following waves consist of the two components. Theoretical values of the wave-exciting force and moment were subtracted from the direct data to obtain the force and moment components due to yaw angle ψ in waves. Obviously, the theoretical values to be

subtracted from the experimental maximum values had to be evaluated at the same phase as that of the experiment. The maximum forces and moments always took place when the LCG's of the models coincided with troughs of regular waves.

In order to evaluate the rudder force, the following assumptions were made.

1. Stream velocities at the rudder, for the two models for a given model speed, are identical. The stream velocity here is equal to the algebraic sum of the model speed and the horizontal component of the mean orbital velocity of the wave at the location of the rudder.
2. For both, $(\frac{dC_L}{d\delta})_r = 0.03$ per degree.
3. The angle of incidence of flow to the rudder is equal to the angle of rudder deflection.

The above assumptions do not necessarily represent actual phenomena. But without detailed data for the rudder, and, particularly, for the comparison of performances of the two models with the same rudders, these assumptions may be justified.

Listed in Table VI, on the following page, are $\partial F/\partial\delta$ and $\partial M/\partial\delta$ values for the two models, calculated on the basis of the above assumptions.

TABLE VI

$\partial F/\partial\delta$ AND $\delta M/\partial\delta$

Regular Waves (1):

Model	Model Velocity / Wave Velocity	$\partial F/\partial\delta$ (lb/δ deg)	$\partial M/\partial\delta$ (in-lb/δ deg)
4926	1.15	0.018	-0.25
4926	1.50	0.034	-0.473
2387	1.15	0.018	-0.258
2387	1.50	0.034	-0.488

Regular Waves(3):

4926	0.75	0.0205	-0.285
4926	1.0	0.0355	-0.495
4926	1.5	0.080	-1.115
2387	0.75	0.0205	-0.295
2387	1.0	0.0355	-0.510
2387	1.50	0.080	-1.148

Using the theoretically determined $\partial F/\partial\theta$ and $\partial M/\partial\theta$ and the derived values of $\partial F/\partial\dot{\psi}$ and $\partial M/\partial\dot{\psi}$, together with $\partial F/\partial\delta$ and $\partial M/\partial\delta$ as listed in previous tables, Eq.(20a) and (20b) were solved for δ/θ and ψ/θ. These results are summarized on Table VII, on the following page.

TABLE VII

δ/θ AND ψ/θ OF TWO MODELS

Model	Model Speed / Wave Speed	δ/θ	ψ/θ	Regular Waves
4926	1.15	1.12	-0.053	(1)
2387	1.15	1.06	-0.055	(1)
4926	1.50	0.62	-0.014	(1)
2387	1.50	0.57	-0.014	(1)
4926	0.75	2.28	0.270	(3)
2387	0.75	2.06	0.145	(3)
4926	1.0	1.01	0.186	(3)
2387	1.0	0.985	0.111	(3)
4926	1.50	0.48	0.156	(3)
2387	1.50	0.55	0.051	(3)

DISCUSSION OF RESULTS

Smooth-Water Test

In Fig. 7, both the specific resistances and the trim angle in smooth water are plotted against the Froude number. It was found that all three round-bottom models and one hard-chine model (4928 [L/B = 3]) were porpoising in smooth water. The speed ranges in which the models porpoised, and the degree of porpoising, are summarized below:

Model	L/B	Froude No.	Oscillatory Pitch Double Amplitude (Degrees)	Oscillatory Heave Double Amplitude (Ship Size, Ft)
4925	3	3.1	1.2	1.65
4925	3	3.3	1.7	2.40
4926	4	4.0	.7	.80
4926	4	4.3	2.0	3.00
4927	5	4.85	2.7	4.00
4928	3	4.3	.8	.40
4928	3	4.45	1.2	.70
4928	3	4.85	1.6	.80

As shown in the above table, the oscillatory pitch and heave amplitudes increased with speed. In order to prevent possible diving at higher speeds, the test speeds were limited to Froude numbers of 3.3 and 4.3, respectively, for Models 4925 and 4926. Each model listed in the above table was stable at the speeds slower than that corresponding to the smallest Froude number in the table.

In the stable range of operation, the hard-chine hull forms showed, in general, better smooth-water resistance and stability characteristics than the round-bottom hull forms of corresponding L/B. Among models of the same hull form, the larger the L/B ratio the lower the running trim angle

and the less the resistance at Froude numbers below 2.5 . Model 4929, with L/B 5, had the best resistance characteristics in smooth water throughout the Froude-number range tested, except at Froude numbers between 2.5 and 3.5, where Model 4928, with L/B 3, had the least resistance. The specific resistances of the boats with skegs, shown in Fig. 8, indicated in general that there were approximately 4% to 8% resistance-increases over those of respective hulls without skegs.

EHP's in smooth water are plotted against trim angle in Fig. 11-A. For the low Froude numbers of 1.5 and 1.9, EHP diminishes as trim angle decreases. However, the EHP curves definitely show the presence of minima for the Froude numbers of 2.4 and 3.0 . The minima are found at trim angles of 5 and 4.5 deg, respectively, for the Froude numbers of 2.4 and 3.0 .

As mentioned earlier, the curvatures at the bilges of the round-bottom models are believed to have developed suction at the bilges causing the sides of the models to become wet. With aft-extended spray strips, the sides of these models above the strips remained dry, but the suction effect at the bilges remained.[15] This effect causes a greater bow-up moment to act on the hull form than in the case of the hard-chine hull form. In addition, the distance between the transom and the LCG of the round-bottom hull was shorter, by approximately 3% of the length, than the corresponding distance for the hard-chine hull. These two factors combined to make the bow-up trim moment and the trim angle of the round-bottom hull larger than those of the corresponding hard-chine hull, and hence increased the porpoising tendency of the round-bottom hull.

Performance Test in Irregular Waves

A comparison of Fig. 7 and Fig. 13 shows that, for both types of models, the smaller the L/B ratio the greater the added resistance in waves of State 3 head seas. Since the resistance of a ship in a seaway is greatly influenced by the motion and acceleration of the ship, these data must be analyzed simultaneously. Fig. 25 shows that the average heave amplitudes of the round-bottom hulls were about 10% to 25% higher than those of the corresponding hard-chine hulls, in the speed range of 25 to 30 knots. The averages of 1/10 highest heave double amplitudes of the round-bottom hulls

are again larger than those of the hard-chine hulls by approximately 15% to 35%, in the same speed range – as shown in Fig. 26. The average and the average of 1/10 highest bow accelerations show a trend similar to that of the heave amplitudes in State 3 head seas.

Since the bow-up trim angles of the round-bottom hulls in smooth water were larger than those of the corresponding hard-chine hulls in the above speed range, the mean running trim of the round-bottom boat in waves would be larger than that of the hard-chine boat by nearly the same order of magnitude. Because of this effect, the lift developed on the bottom at the forward quarter of the round-bottom hull (when running in head seas) was larger than that developed by the hard-chine boat, with the result that the forward quarter-point acceleration and the heave amplitude of the round-bottom hulls were higher than those of the hard-chine boat in waves. For example, as shown in Fig. 21, the average bow accelerations were 2.0, 1.35, and 1.1g for the round-bottom hulls 4925, 4926, and 4927 respectively, at 30-knots speed in State 3 head seas. The corresponding average bow accelerations for the hard-chine hulls were 1.4, 1.1 and 1.0g respectively. The CG accelerations in the same head seas followed the same trend, but the amplitudes were approximately 50% of those for the bow accelerations.

In State 3 following seas, the acceleration amplitudes (Fig. 27) were insignificant compared with those of State 3 head seas. When the course changed from head to following seas, the bow acceleration and the CG acceleration were reduced about one-half at 30 knots speed. An evaluation of the models from an over-all point of view indicated that for the given loadings and test conditions, the hard-chine hulls with L/B 5 and L/B 4 were to be preferred over all other hulls in State 3 seas.

The general tendencies outlined in the previous paragraphs for Sea State 3 also apply for the specific resistances of the models in State 5 sea. The average heave double amplitudes of the round-bottom models were about 15% to 40% higher than those of the corresponding hard-chine models, throughout the speed range in State 5 head sea. However, among the models of each basic hull type, those with L/B 4 had the least heave double amplitudes. The average forward quarter-point accelerations of the round-bottom hulls in State 5 head sea are consistently higher than those of the

hard-chine hulls, throughout the speed range. With respect to CG accelerations of the models in this sea state, it was found that the round-bottom and hard-chine hulls of the same L/B ratios showed almost identical accelerations throughout most of the speed range, excepting the round-bottom models 4926 and 4927, which had the least amplitudes in the range of 20 to 35 knots. It should be noted here that the accelerations were very extreme (in excess of 4g) at the higher speeds in a State 5 sea, thus making such speeds impractical to attain.

In State 5 following sea, there was difficulty in operating the apparatus for accelerating models in the high-speed range. In addition, great irregularities were found in the speed of models during a run, due to the steep positive slopes and negative slopes of waves encountered. Therefore, the maximum Froude number was limited to about 3.5 . The acceleration amplitudes of the models in State 5 following sea were quite insignificant (in most runs, less than 1g) compared with those in State 5 head sea.

Broaching-Tendency Evaluation Test

According to the derived results of the evaluation of broaching tendencies of Models 4926 and 2387, the latter (hard-chine) showed slight superiority over the former (round-bottom) throughout the ranges of waves and speeds covered in the experiment, except at the ship-speed-to-wave-speed ratio of 1.5 in 100 ft waves, where the round-bottom model was better. This comparison was based on the assumption that rudder effectiveness for the two hulls was the same. It can be said that the hard-chine hull is easier to steer in following waves, at speeds below 20 knots.

It was observed, during the run of Model 2387 in 100 ft x 4 ft waves at 20-knots speed, that this model produced a considerable amount of water spray around the pressure side of the bow. The time at which the water spray was observed coincided with the time at which the maximum yaw moment was recorded. The yaw-moment derivative for the hard-chine hull, with respect to yaw angle in the waves, was larger than that for the round-bottom hull at this speed.

According to Table VII, the values of δ/θ decrease as speed increases. This result is based strictly on static equilibrium. Peter DuCane[6]

showed that broaching tendency still exists even when ship speed becomes faster than wave speed. When a ship is in waves, rudder angle must be continuously varied in order to maintain a desired course. The faster the ship speed, the more rapid the rudder movement must be. In predicting the behavior of a ship in a following sea, with varying rudder angle with respect to time, one must solve the dynamic equations of motion. However, the dynamic equations of motion in the horizontal plane alone may not give accurate answers, because the forces and moments are also influenced by pitch and heave. It is recommended that, in parallel with an experimental evaluation of broaching tendency with controlled rudder in waves, the motions of a ship in an oblique following sea be solved by setting up the dynamic equations involving four modes of motion — sway and heave, and the two angular motions of pitch and yaw.

Figure 38 indicates that the side force coefficients of the two models 4926 and 2387 in smooth water are very similar through the speed range and yaw-angle range tested. It also shows that the side force coefficients of the model without rudder are somewhat smaller than those of the model with rudder, as expected. Figures 39 and 40 show that the hard-chine hull always has greater negative yaw moment coefficients for a given yaw angle and speed. Negative yaw moment coefficient implies stabilizing moment in yaw. It is interesting to observe that the sign of the yaw moment changes from positive to negative at a Froude number near 1.0 . These figures show that elimination of the rudders has a destabilizing effect on yaw moment.

Linearity of the forces and moments in regular waves can be examined in Figs. 41 and 42. The forces and moments for deriving the coefficients in these figures are the sum of the forces and moments due, respectively, to relative heading between model and waves and to the drift angle of the model in waves. According to the figures, the linearity of the force and moment, with respect to wave height, holds except at waves with λ/L 2.0 and model-speed-to-wave-speed ratios of 1.5 .

In deriving the equations for theoretical determination of the wave-exciting forces and moments on a ship (in the preceding section), the effect of heave motion was not considered. Hence there is doubt concerning the accuracy of $\delta/6$ values of the two models at this combination of speed and

wave, where a nonlinearity is present. Since the tendency of the bow to plunge into wave crests made the broaching condition worse, and since the mean trim angles of the models in following waves were approximately the same as those i smooth water at the same speed, within a hull group of the same types, a hull having large bow-up trim in smooth water would be better with respect to broaching tendency in following waves. Furthermore, if a boat's trim angle can be controlled so as to prevent the bow from plunging into a wave crest, or to prevent the emergence of the bow from water in following waves, broaching tendency will be lessened.

In summarizing the desirable values of trim angles, one may point out that there will be, altogether, two different optimum angles. At this stage of investigation, it may be fair to state that, depending on dead rise, they will be (in the range of Froude numbers between 2.4 and 3.0):

1. Four to 5 degrees in smooth water
2. A mean of 3 to 4 degrees in head seas

Somewhat more detailed study of the effect of trim angle on broaching tendencies in following seas is indicated.

CONCLUSIONS

1. The round-bottom models had a tendency to porpoise in smooth water, and the smaller the L/B ratio the lower the speed at which porpoising developed. The hard-chine hulls had less resistance than the corresponding round-bottom hulls in the stable speed range of the tests in smooth water. For the hard-chine hulls, the larger the L/B ratio the less the resistance, through most of the Froude-number range tested.

2. With respect to hull resistance in head seas of State 3 and State 5, for a given L/B ratio, the larger the trim angle, the greater the added resistance in waves. Of the round-bottom models, that with the largest L/B ratio had the smallest increase in resistance due to the presence of waves. The resistance increases in waves for the hard-chine hulls with L/B ratios

of 4 and 5 were practically identical. The hard-chine hull with L/B 5 had the preferable rough-water resistance characteristics throughout most of the Froude-number range tested.

3. In state 3 head seas, the average forward quarter-point acceleration was about 50% higher than the average acceleration at the CG. For the hard-chine hulls, the former was 1.5g and the latter was 0.95g, at 40 knots. The round-bottom hulls had the higher amplitudes of acceleration, at both forward quarter-point and CG. For both types of hull, the accelerations varied inversely as the L/B ratios, throughout most of the speed range tested. The above trend held also for heave amplitudes in State 3 head sea.

4. In following seas, the accelerations at the forward quarter-point and at the CG were small compared with those in head seas of the same sea states.

5. The general trend of accelerations in State 3 sea held also for the accelerations in State 5 sea. Exceptions were that the round-bottom hulls with L/B 4 and 5 had the smallest CG accelerations in the speed range between 20 and 35 knots and that, among the models of each hull type, the model with L/B 4 had the smallest heave amplitude. The average heave double amplitude of the round-bottom hull was higher than that of the corresponding hard-chine hull by 25%, in State 5 head sea. In this sea state, the higher speeds are impractical to attain, because of severe accelerations.

6. The hard-chine hull with L/B 4 required less angle of rudder deflection than the round-bottom hull with the same L/B ratio, for static equilibrium in the horizontal plane in following regular waves, through most of the speed range. However, in 100 ft x 4 ft waves, at a speed of 20 knots, the hard-chine hull required the larger rudder deflection. At this combination of wave and speed, a nonlinearity of the

lateral force and yaw moment, with respect to wave height, was found.

RECOMMENDATIONS

The following studies are recommended for obtaining basic design information on high-speed craft of planing or semi-planing hull forms to be operated in smooth and rough water:

1. Effects of LCG shift, stern flap, and afterbody buttock-line curvature on the porpoising tendencies of the round-bottom models
2. Scale effect on porpoising of round-bottom hulls
3. Effects of a trim-control device on resistance in smooth water and on resistance, seakeeping quality, and broaching tendency in waves
4. Experimental evaluation of the broaching tendencies of self-propelled models with controlled rudders, in following seas
5. Resistances and seakeeping qualities of hybrid-type hull forms such as, for example, the hard-chine hull with rounded bilge near the transom, or the round-bottom hull with the hard-chine near the transom
6. Solutions of the dynamic equations of motion in the horizontal and vertical planes, for a high-speed boat in oblique following seas

ACKNOWLEDGEMENTS

The author wishes to thank Mr. Paul R. Van Mater, Jr., for his valuable suggestions concerning experimental technique. The author also wishes to express grateful acknowledgement to Mr. Daniel Savitsky, Manager of the Applied Mechanics Group, Davidson Laboratory, for his guidance in the experiment, and to Mr. Edward Numata, Chief of the Ship Research Division, Transportation Research Group, Davidson Laboratory, for his guidance in the experiment and for his review of the report.

CITED REFERENCES

1. Murray, A. B.: "The Hydrodynamics of Planing Hulls," paper presented at the February 1950 Meeting of the New England Section of the Society of Naval Architects and Marine Engineers.

2. Clement, E. P.: "Hull Forms of Stepless Planing Boats," paper presented at the January 1955 Meeting of the Chesapeake Section of the Society of Naval Architects and Marine Engineers.

3. Clement, E. P.: "Analyzing the Stepless Planing Boats," DTMB Report 1093, November 1956.

4. Clement, E. P. and Tate, C. W.: "Smooth Water Resistance of a Number of Planing Boat Designs," DTMB Report 1378, October 1959.

5. McGown, S. C.: "The Seaworthiness Problem in High-Speed Small Craft," paper presented at the January 1961 Meeting of the New York Metropolitan Section of the Society of Naval Architects and Marine Engineers.

6. DuCane, P.: "Model Evaluation of Four High Speed Hull Forms in Following and Head Sea Conditions," paper presented at the September 1957 Symposium on the Behavior of Ships in a Seaway, Vol. II of the Proceedings.

7. DuCane, P. and Goodrich, G. J.: "The Following Sea, Broaching and Surging," Trans. INA 1961.

8. Davidson, K. S. M.: "A Note on the Steering of Ships in Following Seas," DL Note 80, June 1948.

9. Grim, O.: "Surging Motion and Broaching Tendencies in a Severe Irregular Sea," DL Report 929, November 1962.

10. Lueders, D.: "Model Tests of Two Planing Forms and a Round Bottom Form in an Irregular Head Sea," DL Report 746, April 1959.

11. Korvin-Kroukovsky, B. V. and Jacobs, W. R.: "Pitching and Heaving Motions of a Ship in Regular Waves," Trans. SNAME, May 1957.

12. Paoli, A. D.: "Yawing and Swaying Motions of a Ship in Regular Waves," M.S. thesis SIT, 1961.

13. Landweber, L. and Macagno, M.: "Added Mass of Three Parameter Family of Two Dimensional Forces Oscillating in a Free Surface," J. of Ship Res., March 1959.

14. Hu, P. N.: "Lateral Force and Moment on Ship in Oblique Waves," J. of Ship Res., June 1962.

15. Korvin-Kroukovsky, B. V.: "Hydrodynamic Principles of Planing-Boat Design," ETT Note 178, March 1952.

16. Tasai, F.: "Hydrodynamic Force and Moment Produced by Swaying Oscillation of Cylinders on the Surface of a Fluid," JSNA, Vol. 110, 1961.

UNCITED REFERENCE

Korvin-Kroukovsky, B. V., Savitsky, D. and Lehman, F. W.: "Wetted Area and Center of Pressure of Planing Surfaces," Sherman M. Fairchild Publication Fund Paper No. 244, Institute of the Aeronautical Sciences, New York, August 1949.

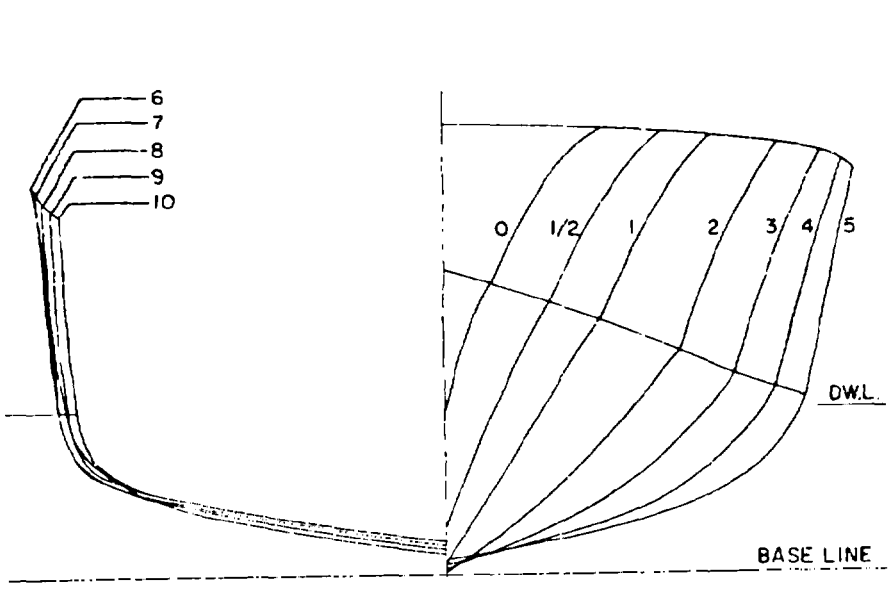

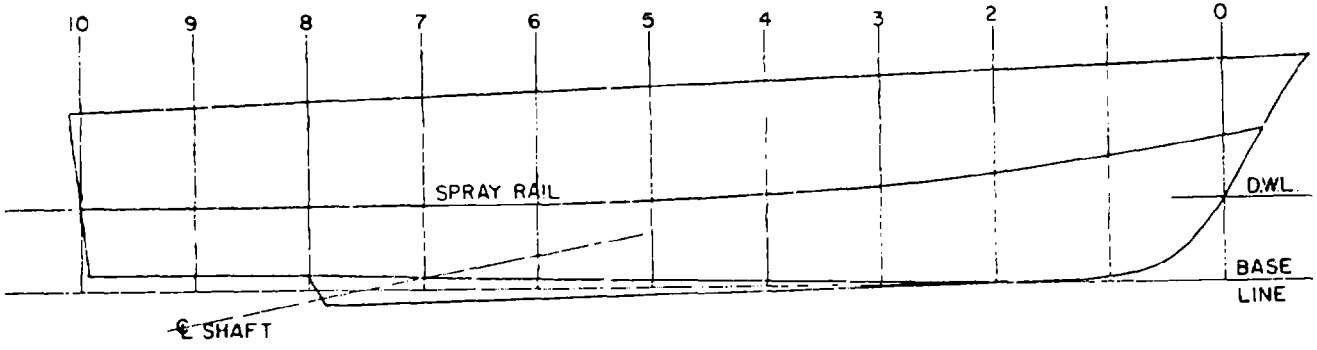

FIGURE 1. LINES OF MODEL 4925

R-985

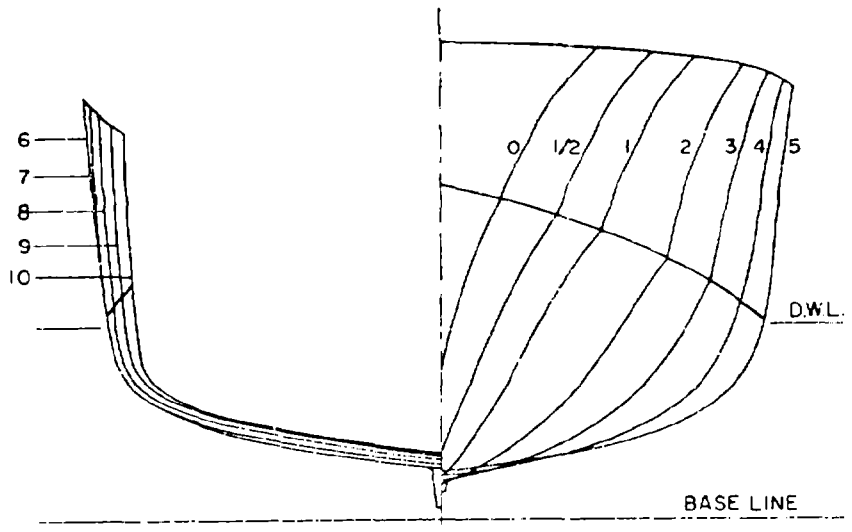

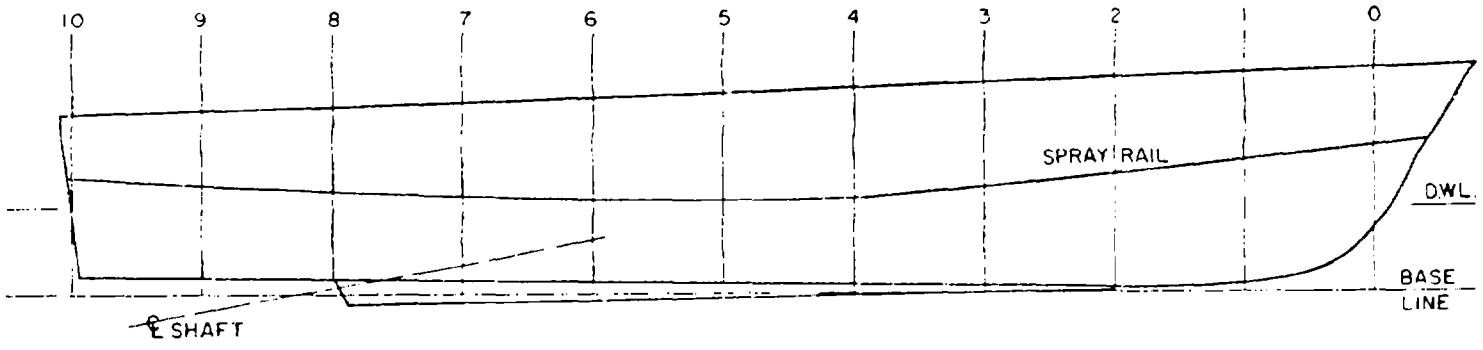

FIGURE 2. LINES OF MODEL 4926

R-985

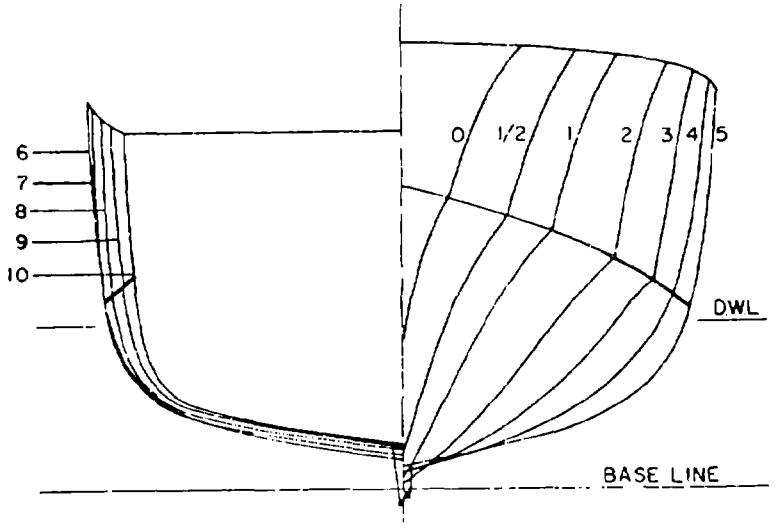

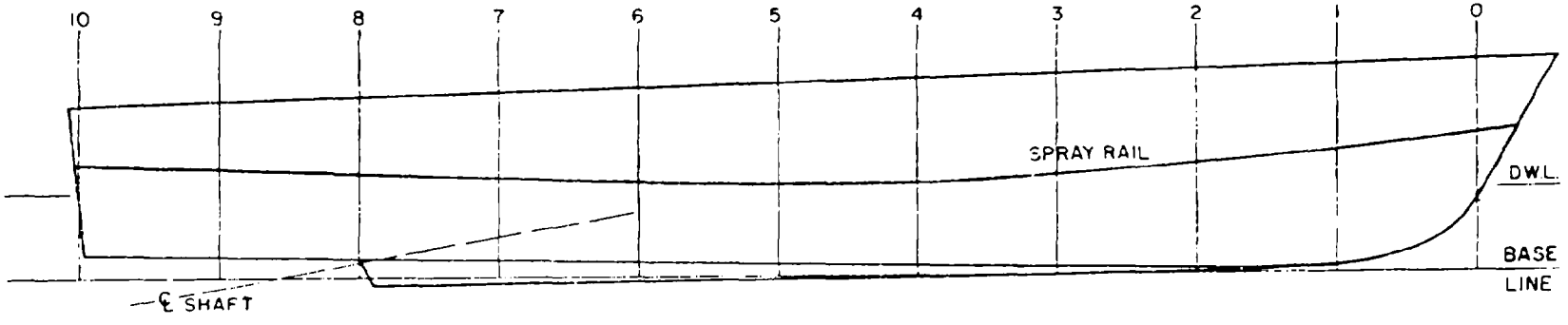

FIGURE 3. LINES OF MODEL 4927

R-985

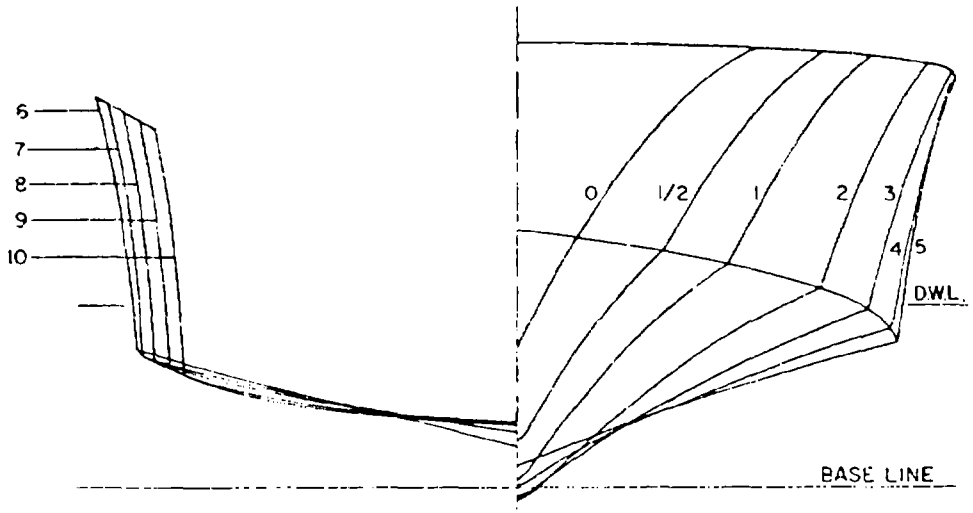

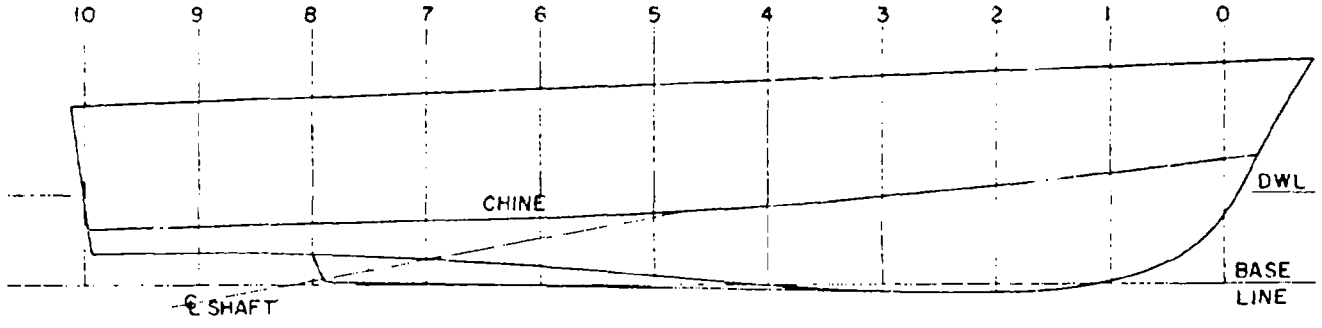

FIGURE 4. LINES OF MODEL 4928

R-985

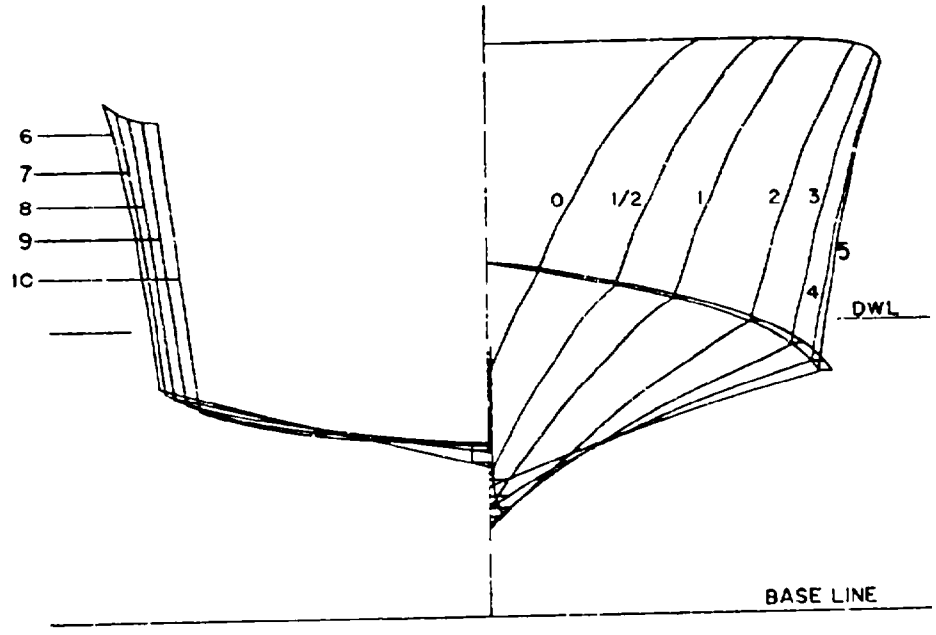

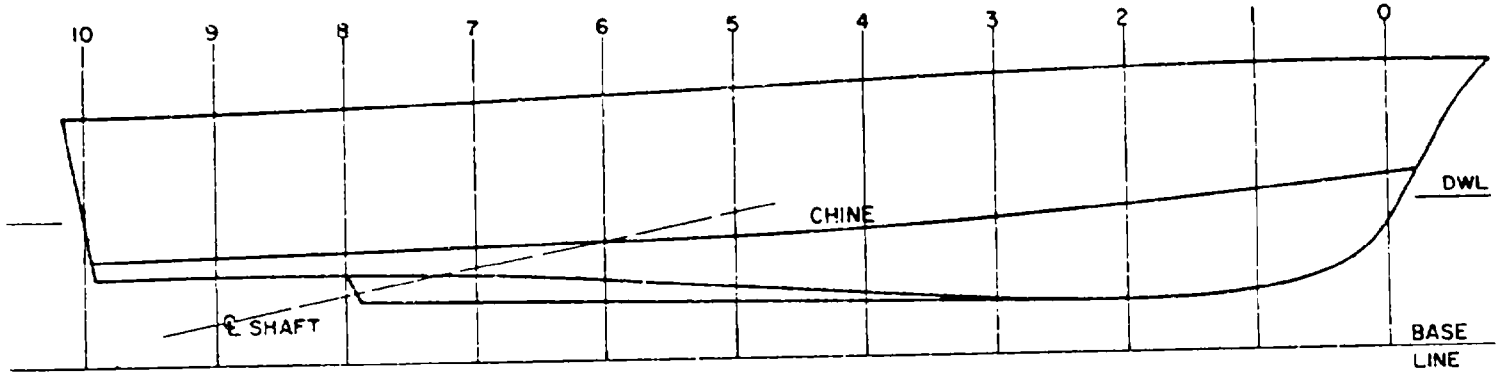

FIGURE 5. LINES OF MODEL 2387

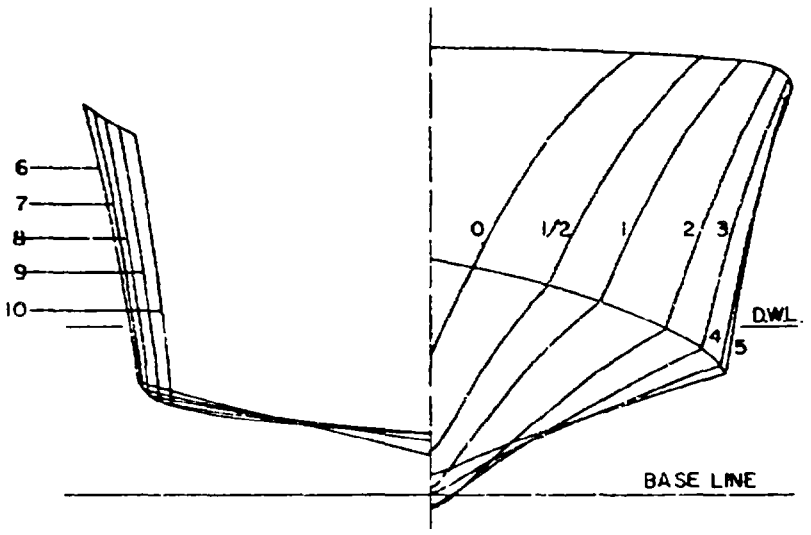

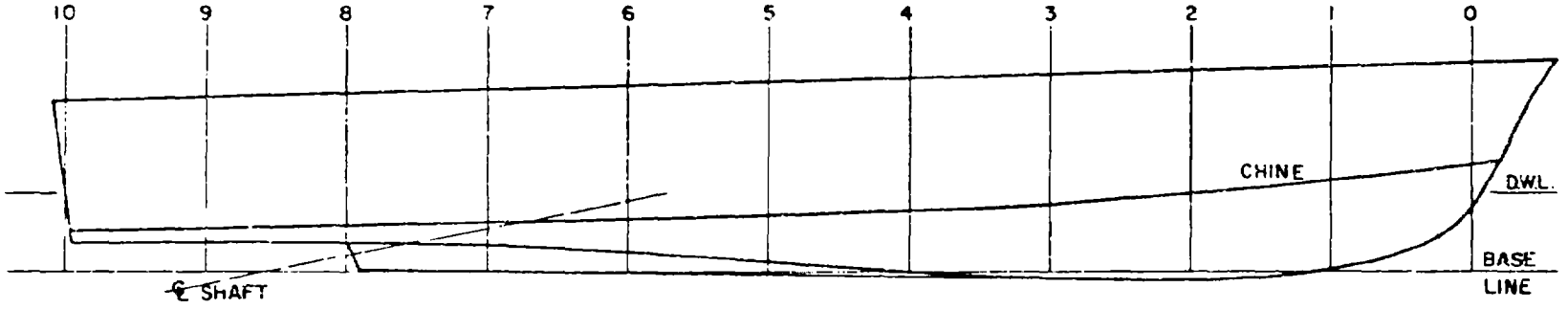

FIGURE 6. LINES OF MODEL 4929

R-985

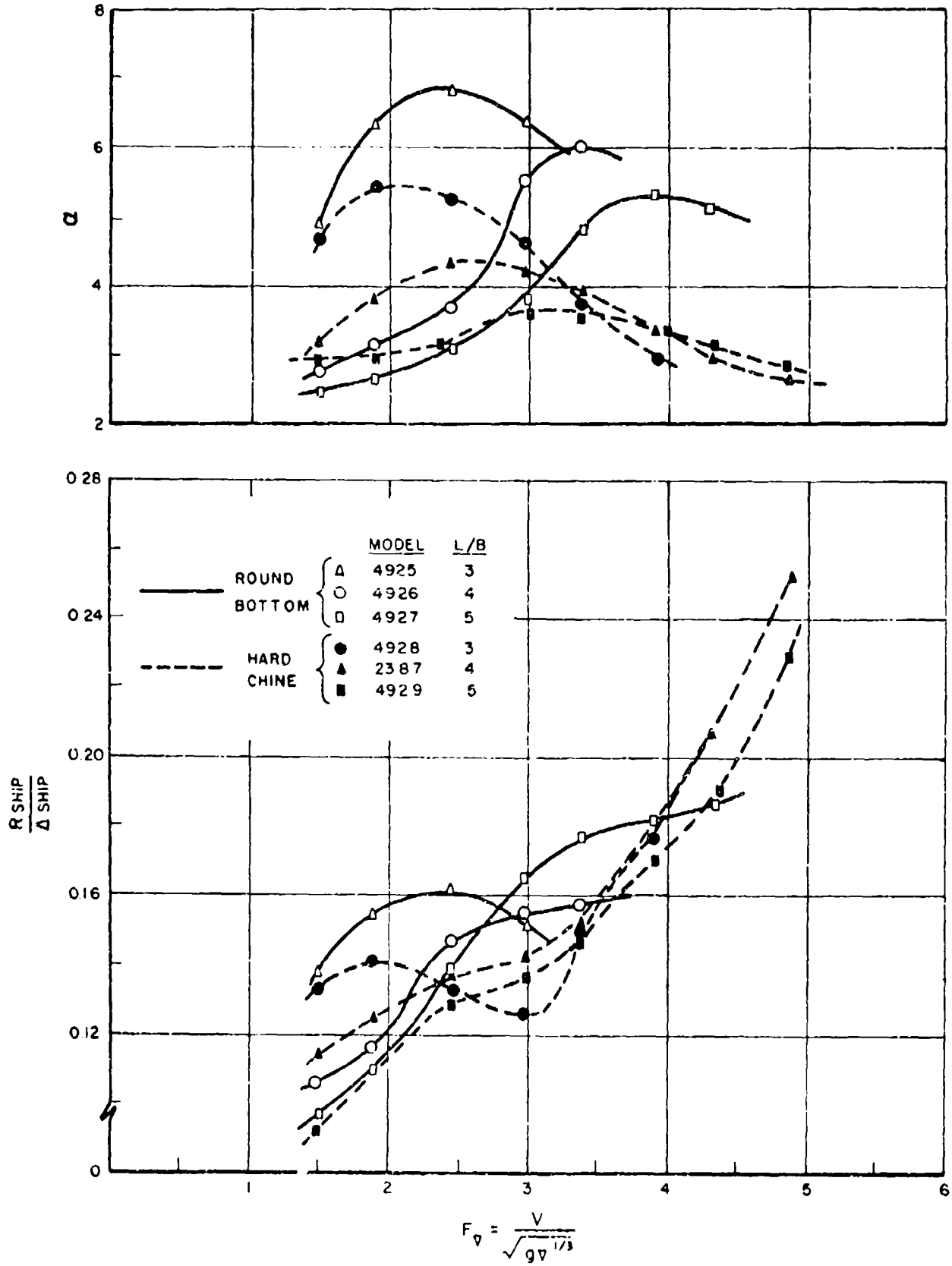

FIGURE 7. SPECIFIC RESISTANCE AND α OF MODELS WITHOUT SKEGS IN CALM WATER.

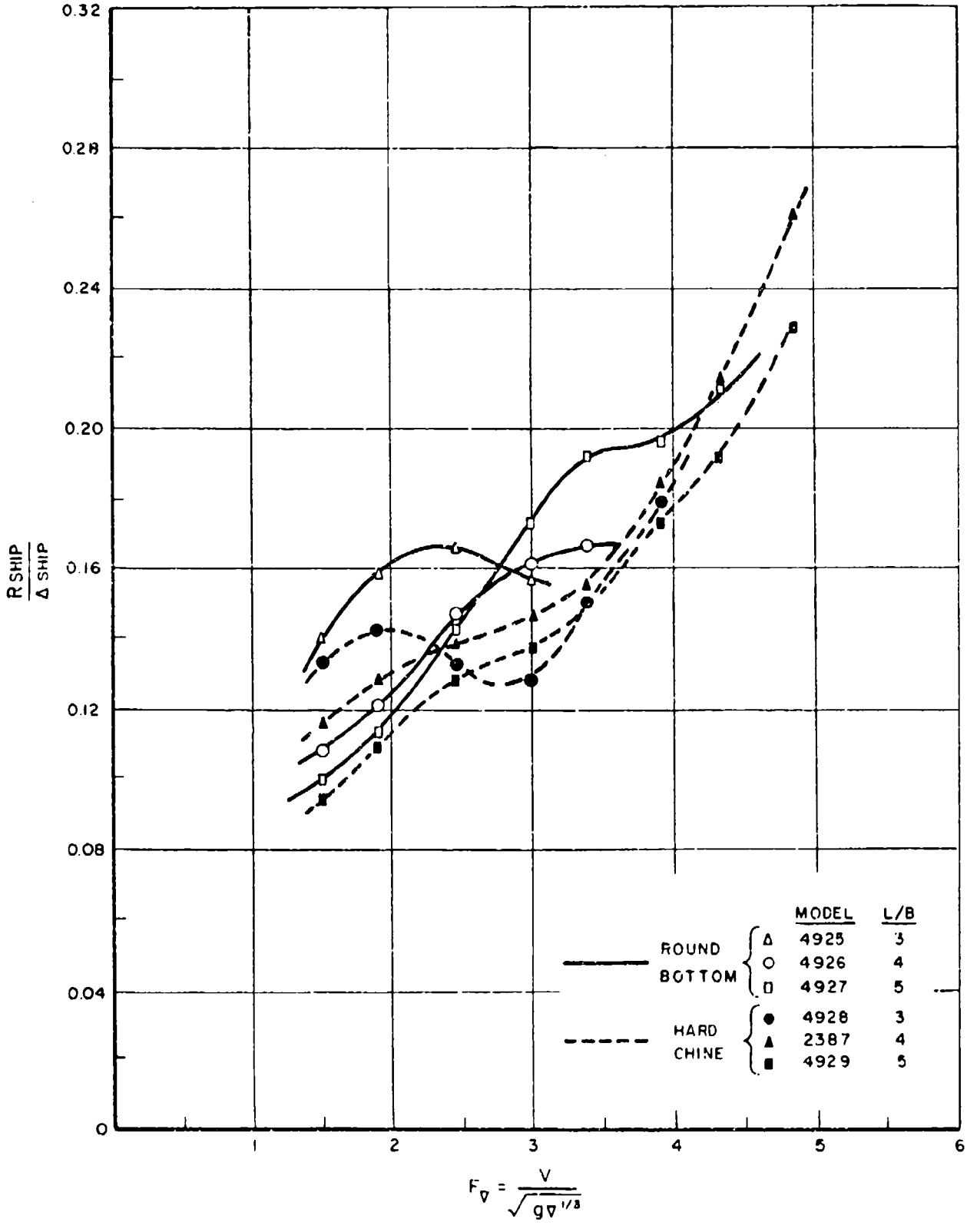

FIGURE 8. SPECIFIC RESISTANCE OF MODELS WITH SKEGS IN CALM WATER.

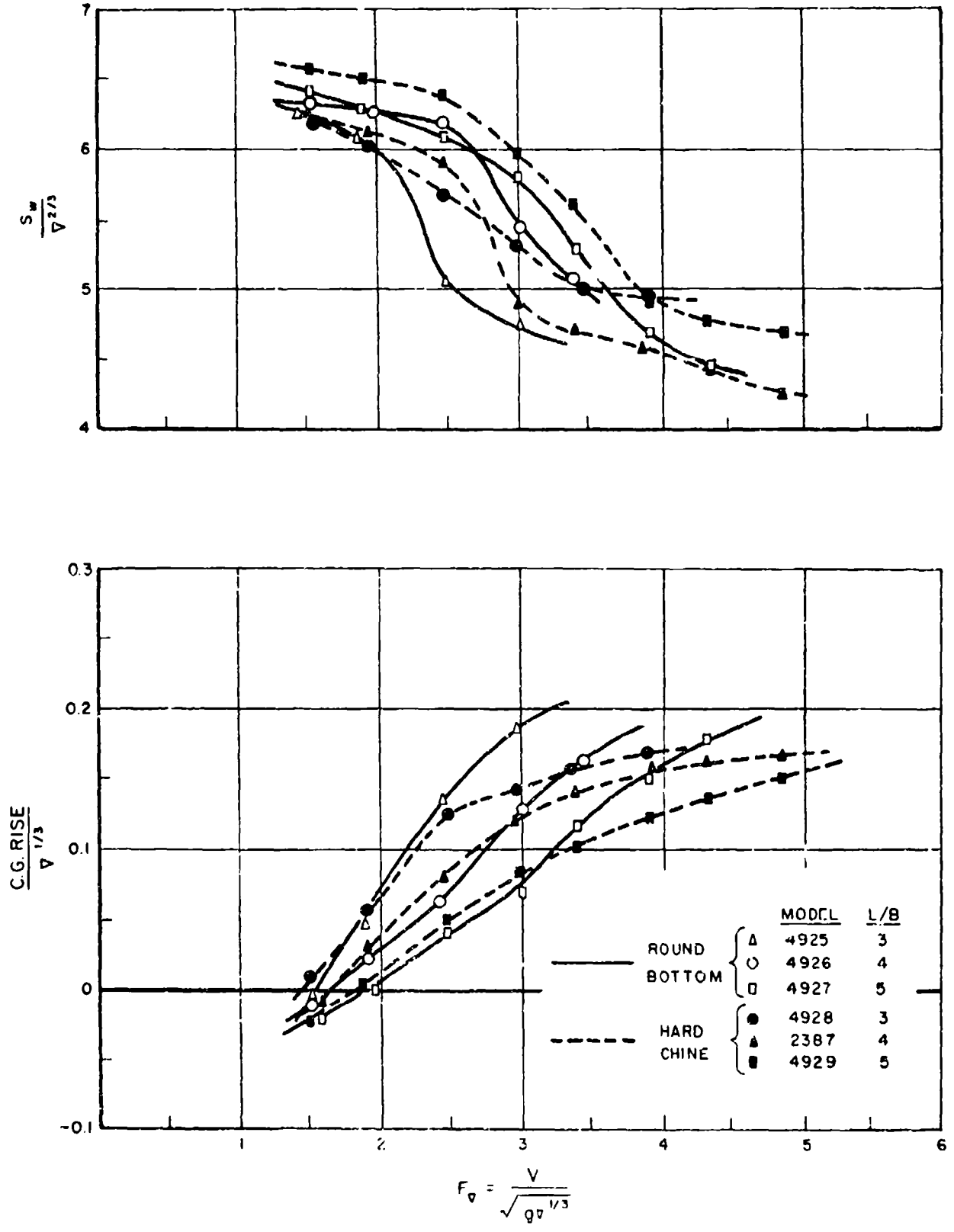

FIGURE 9. WETTED AREA AND C.G. RISE COEFFICIENTS OF MODELS WITHOUT SKEGS IN CALM WATER.

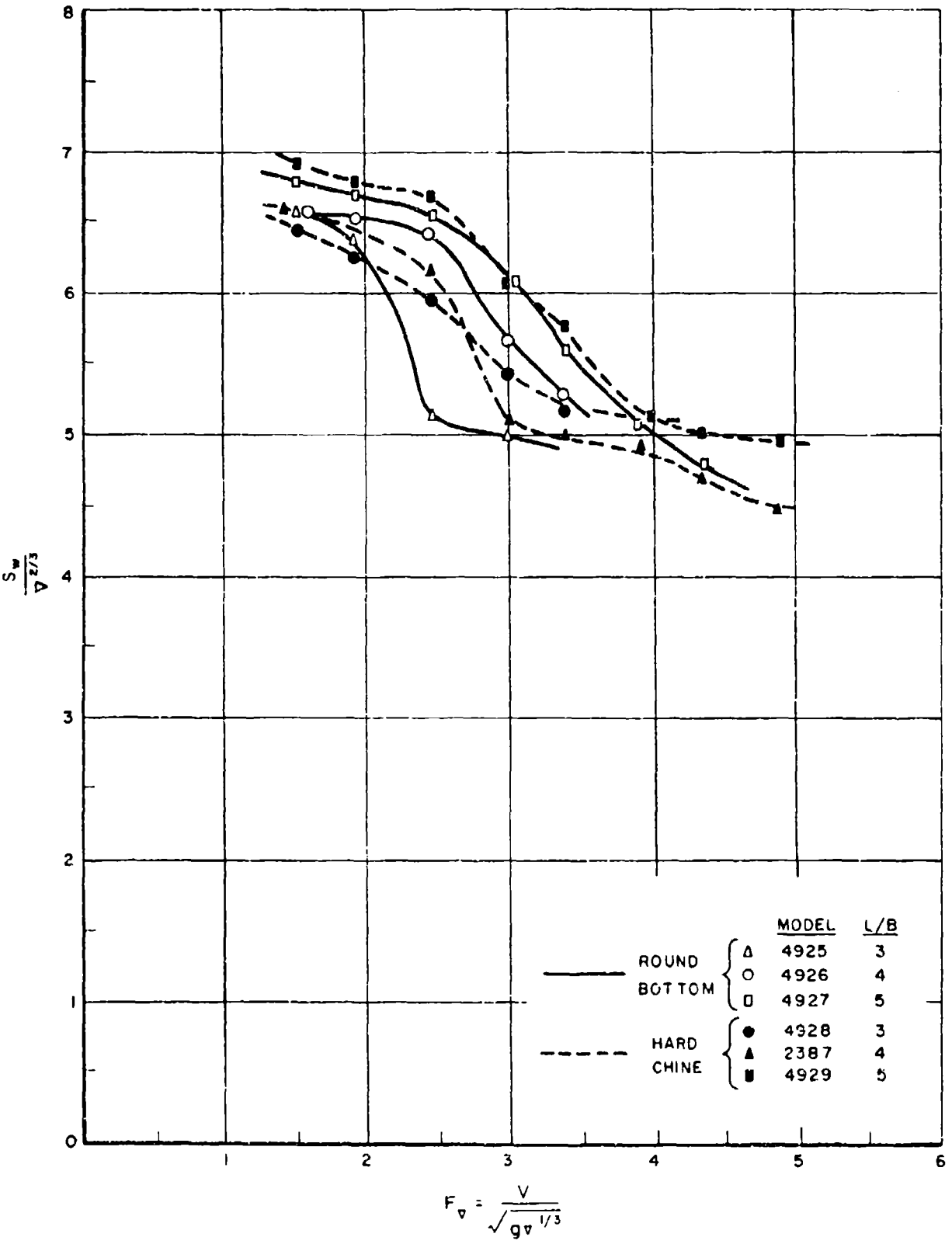

FIGURE 10. WETTED AREA COEFFICIENTS OF MODELS WITH SKEGS IN CALM WATER

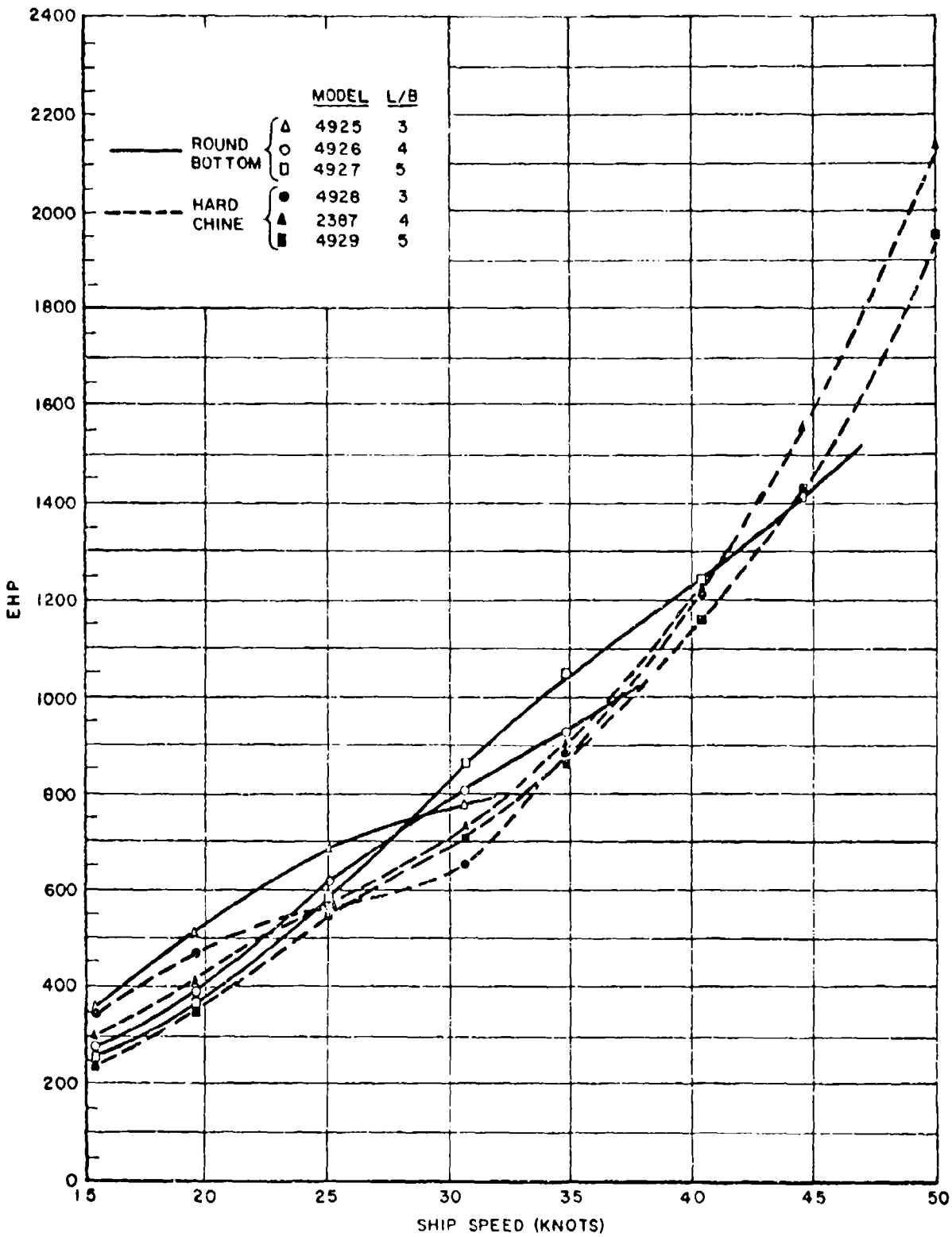

FIGURE 11. EHP's OF SHIPS WITHOUT SKEGS IN CALM WATER

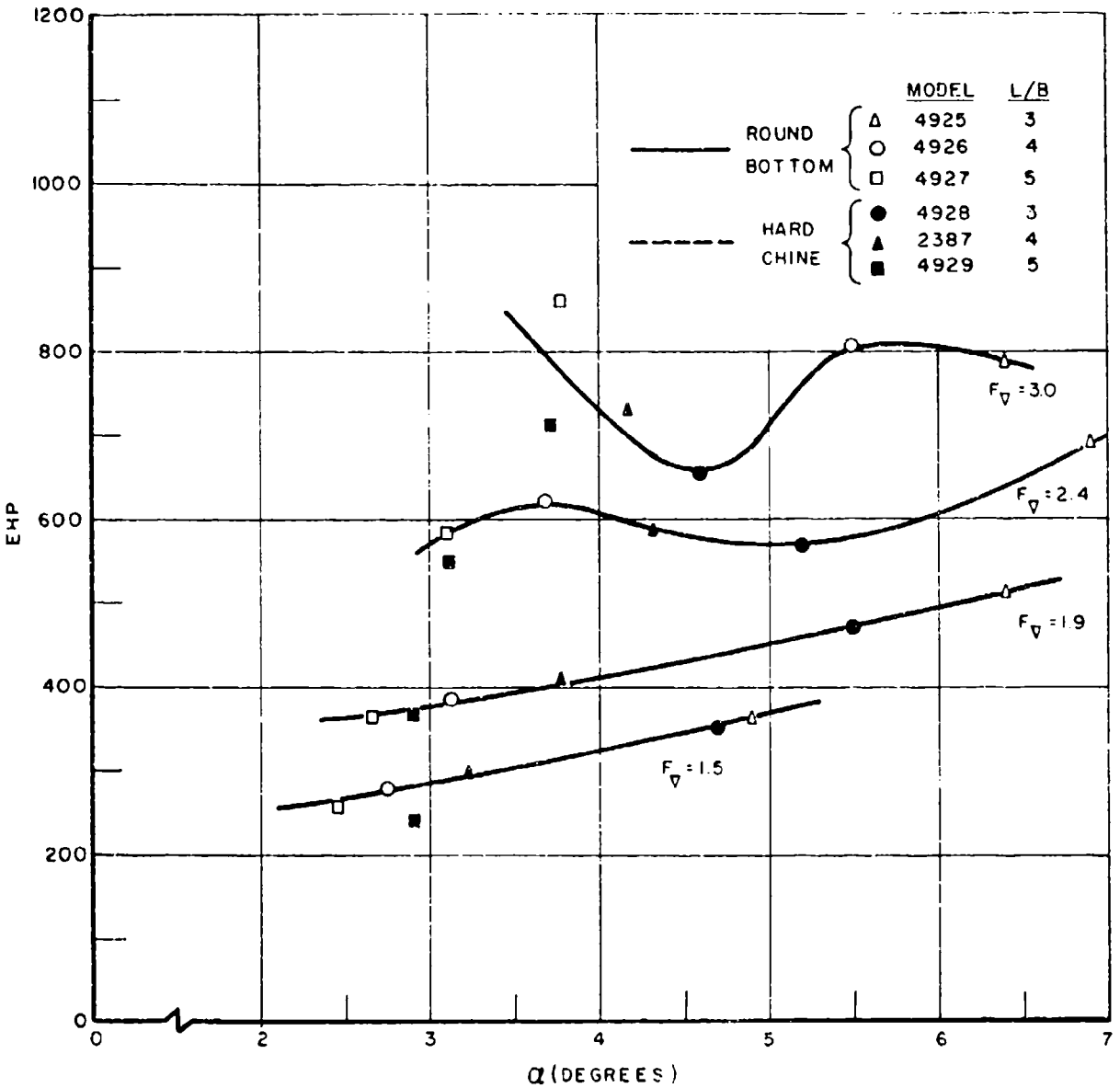

FIGURE 11A. EHP VERSUS α IN CALM WATER

R-985

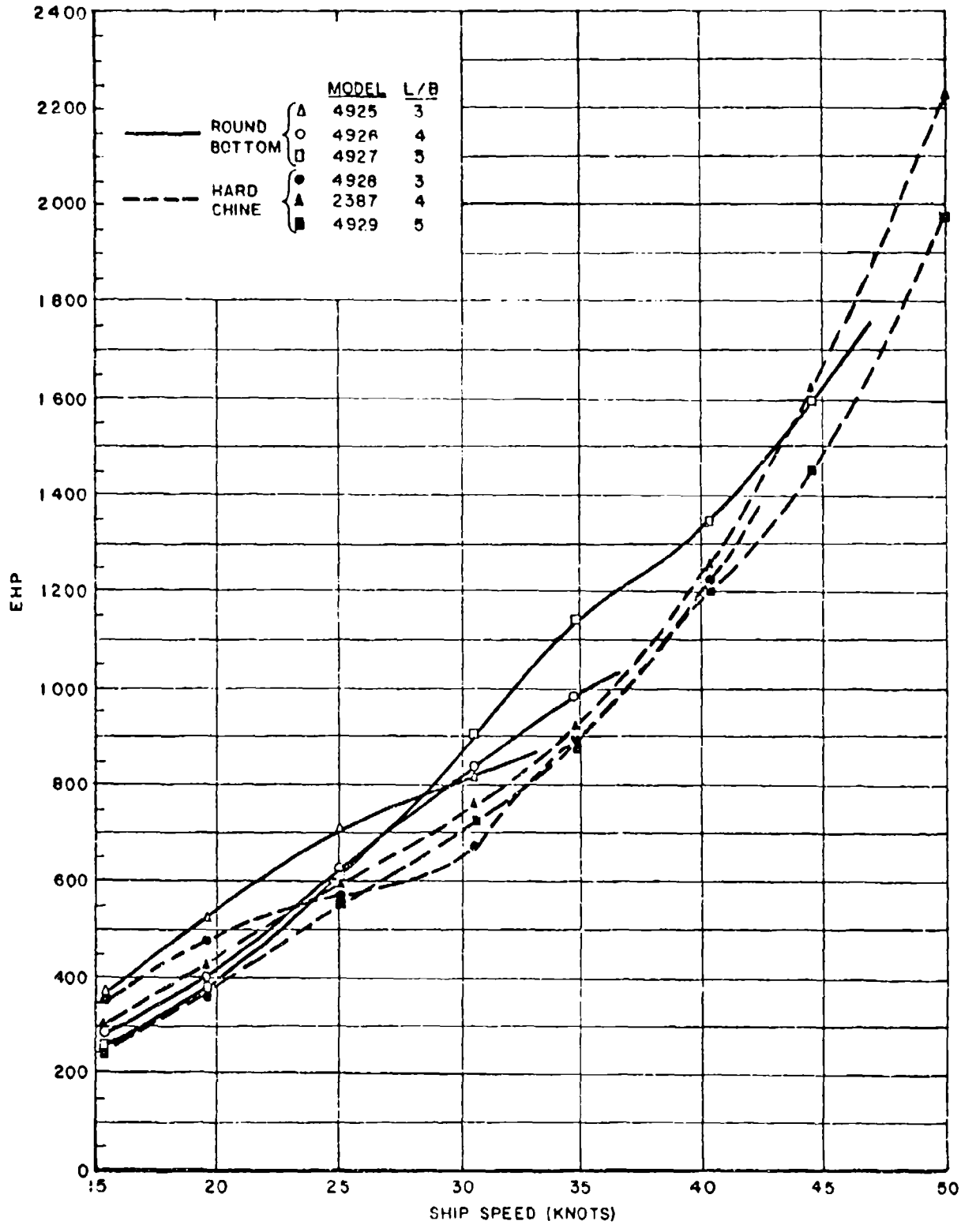

FIGURE 12. EHP's OF SHIPS WITH SKEGS IN CALM WATER

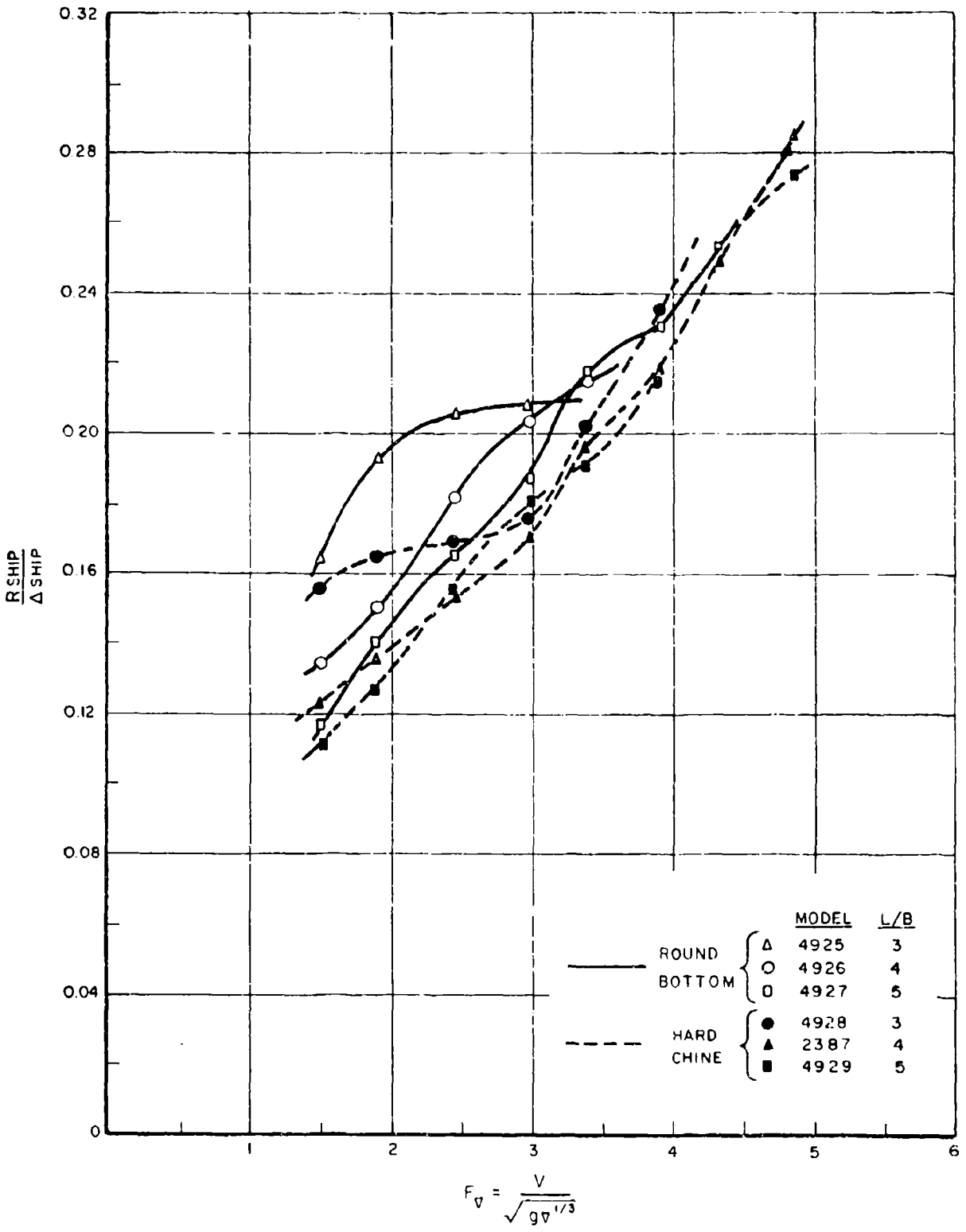

FIGURE 13. SPECIFIC RESISTANCE IN AHEAD SEA STATE 3.

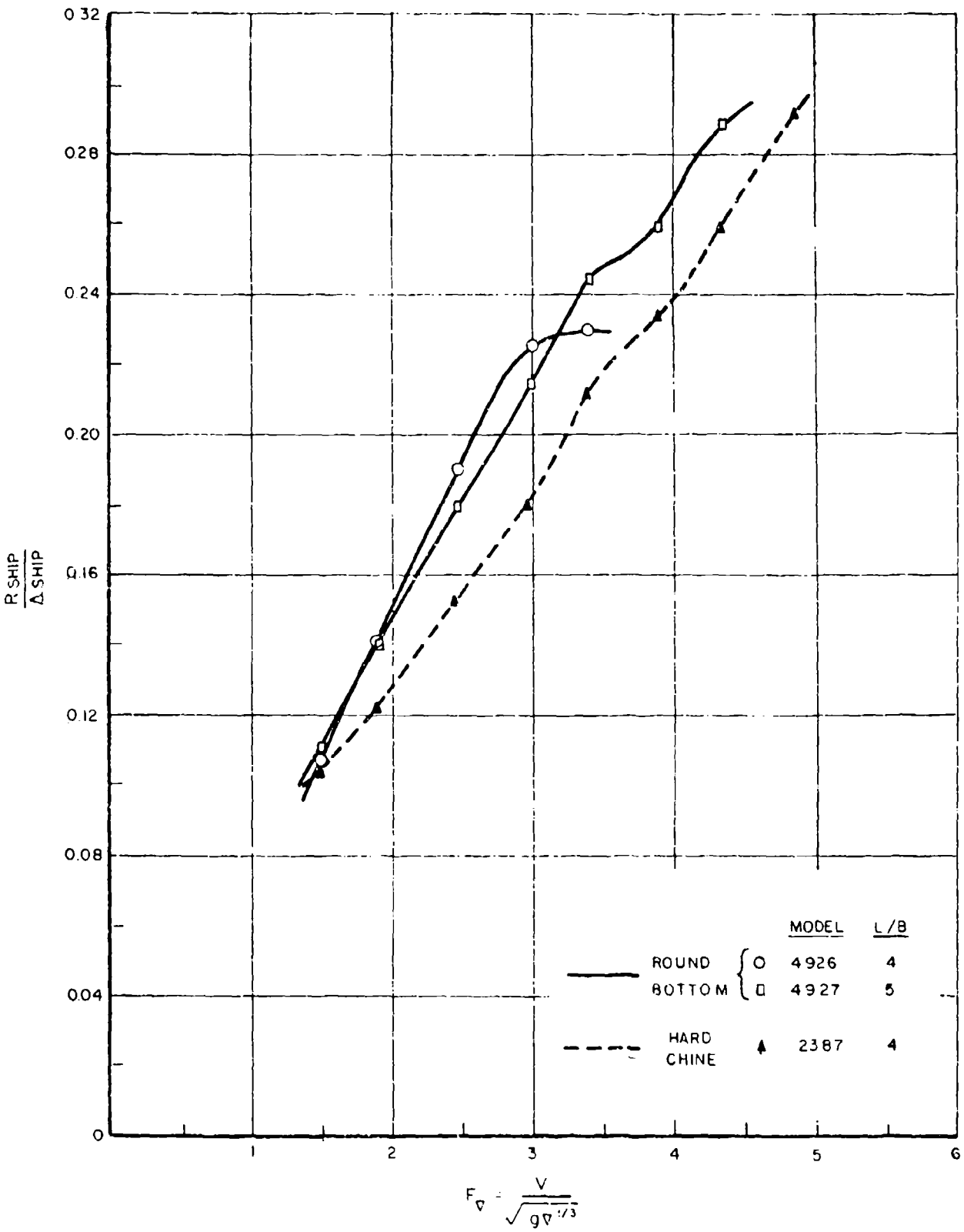

FIGURE 14. SPECIFIC RESISTANCE IN FOLLOWING SEA STATE 3.

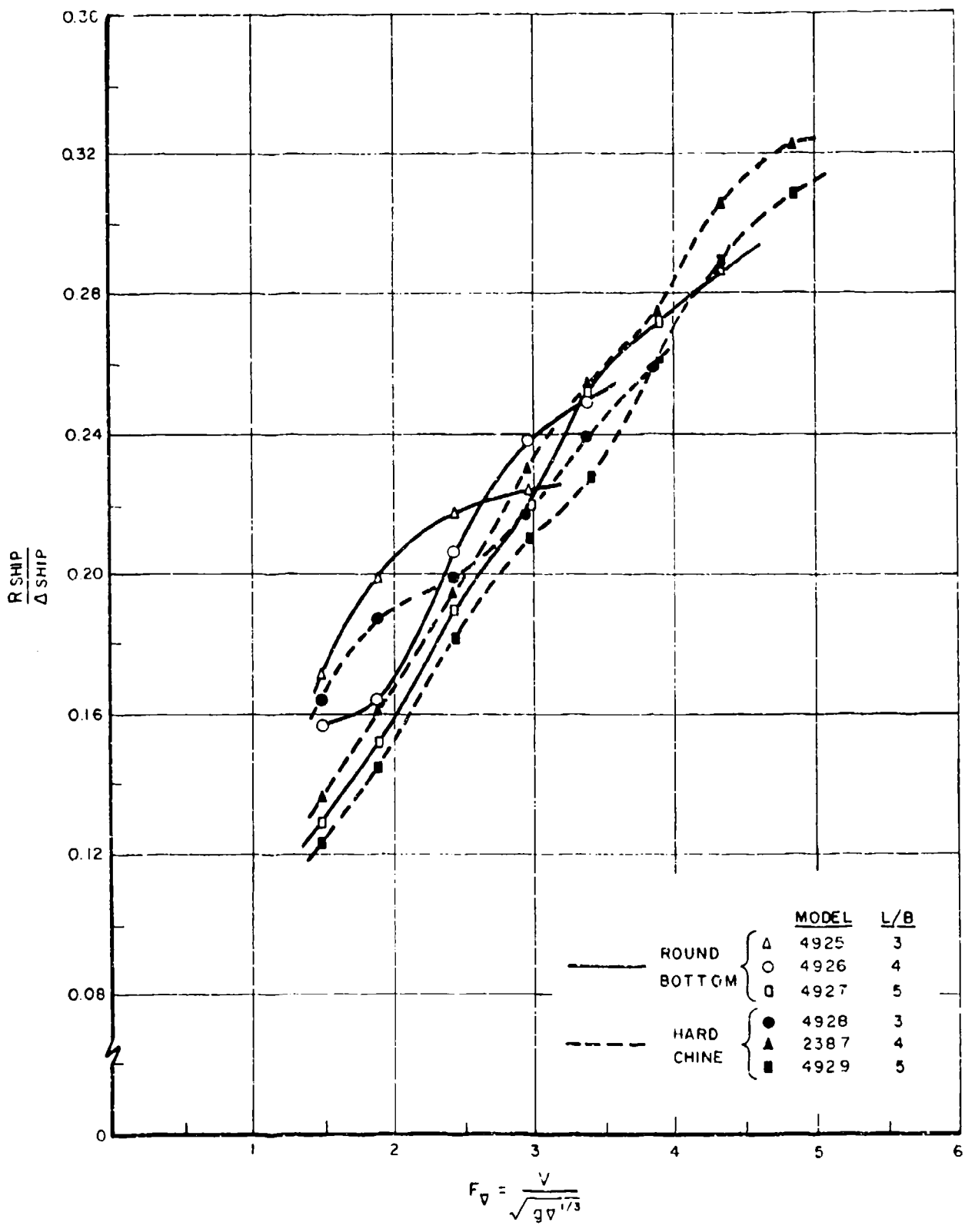

FIGURE 15. SPECIFIC RESISTANCE IN AHEAD SEA STATE 5.

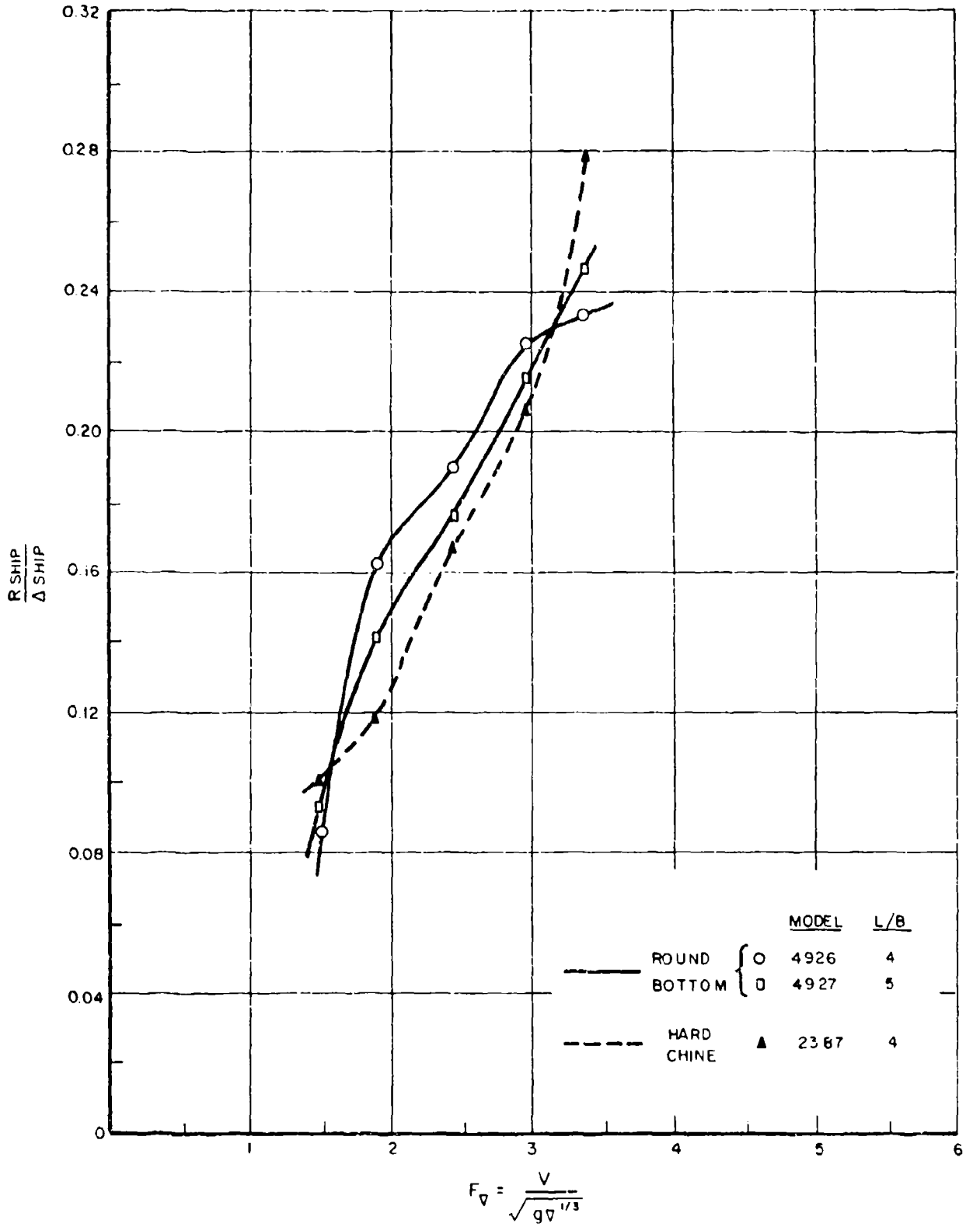

FIGURE 16. SPECIFIC RESISTANCE IN FOLLOWING SEA STATE 5.

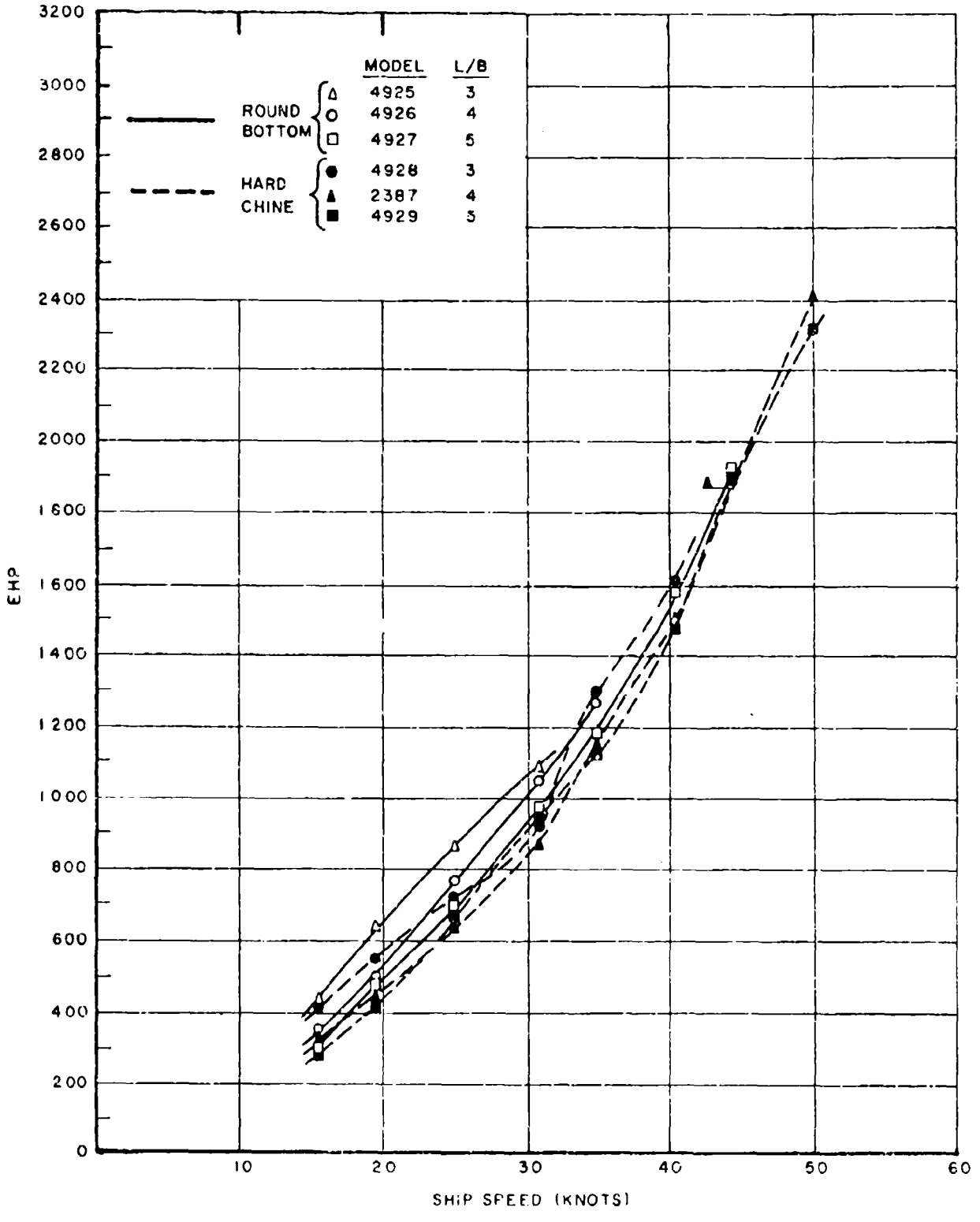

FIGURE 17. EHP IN AHEAD SEA STATE 3

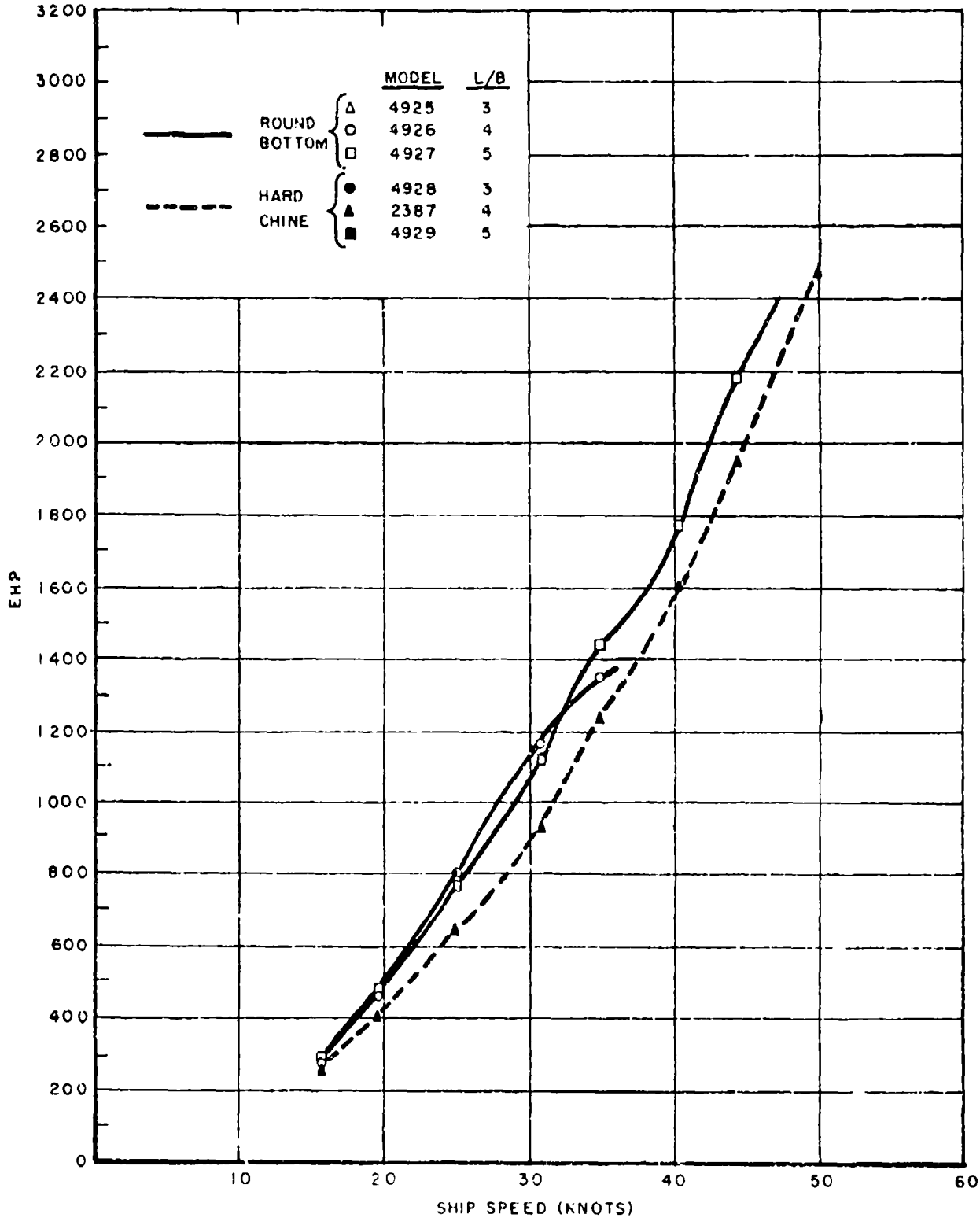

FIGURE 18. EHP IN FOLLOWING SEA STATE 3

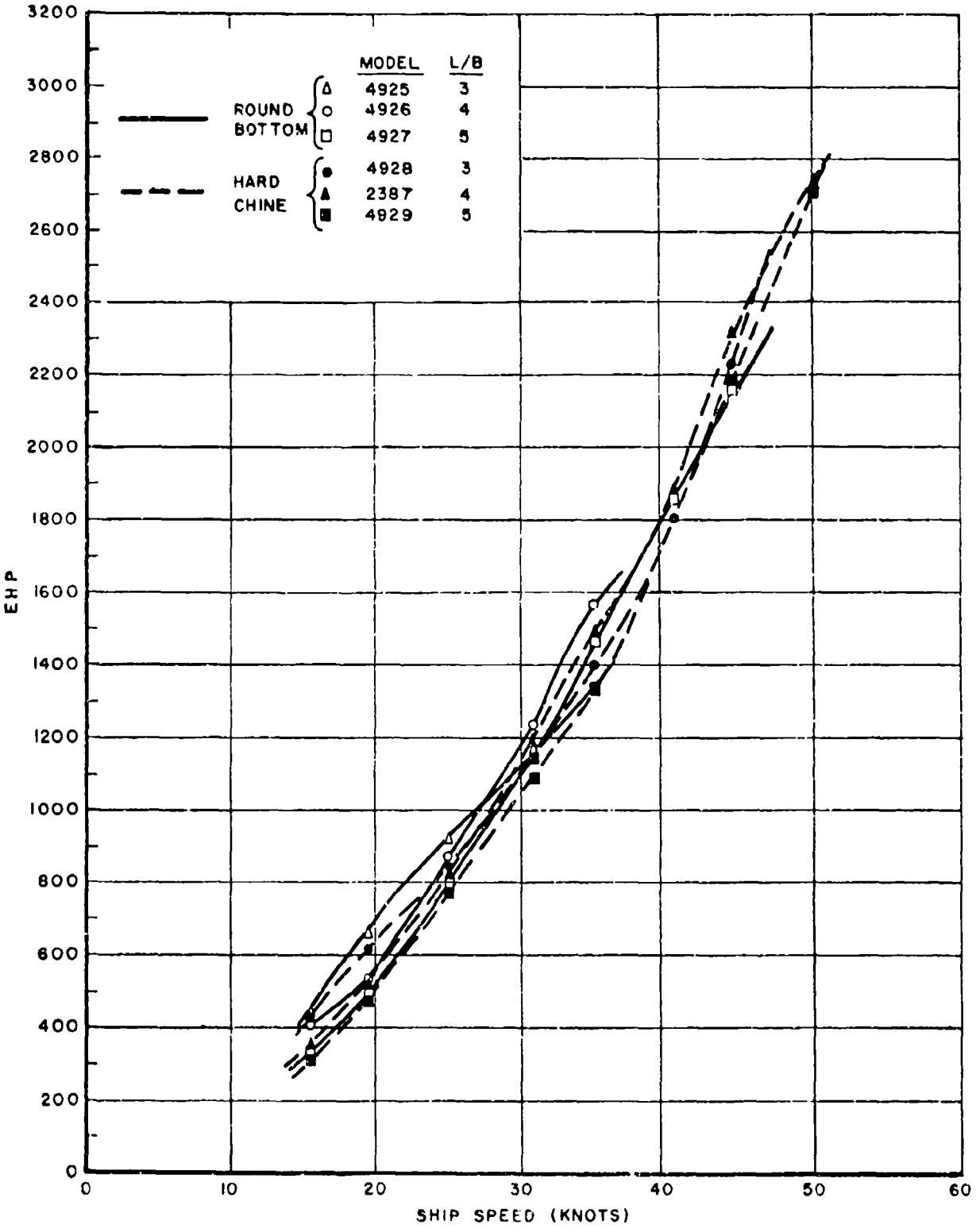

FIGURE 19. EHP IN AHEAD SEA STATE 5

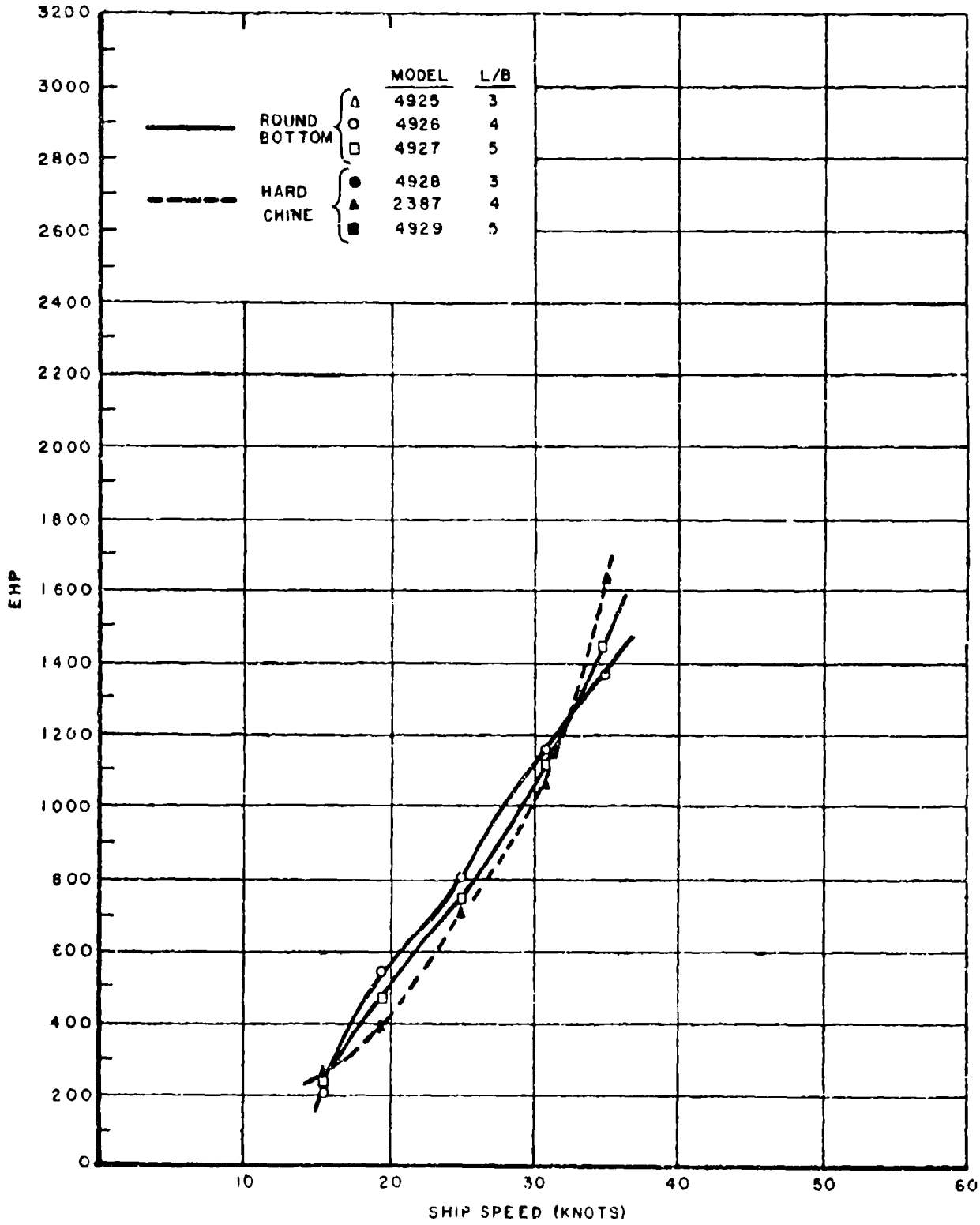

FIGURE 20. EHP IN FOLLOWING SEA OF STATE 5

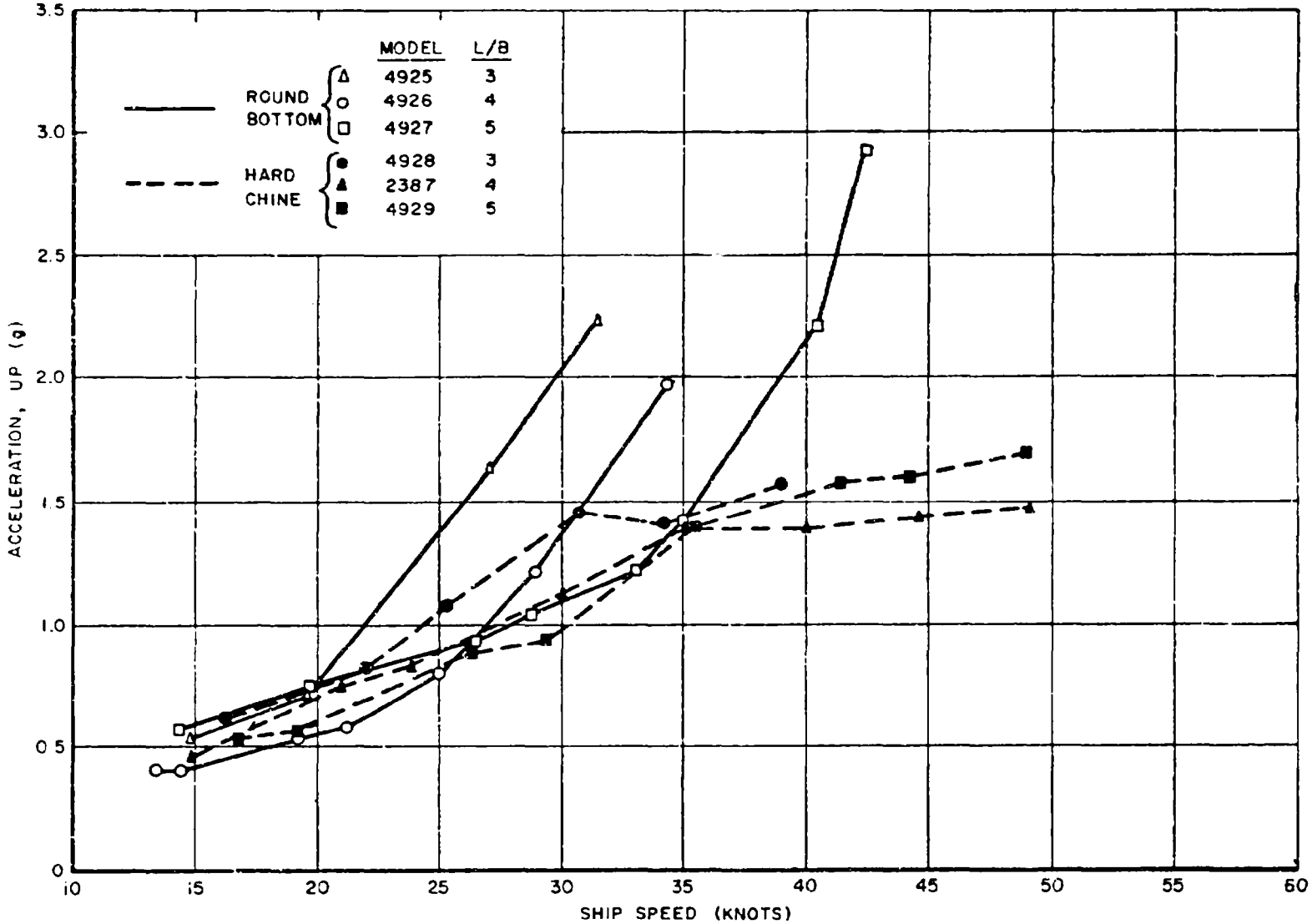

FIGURE 21. AVERAGE BOW ACCELERATION IN STATE 3-HEAD SEAS

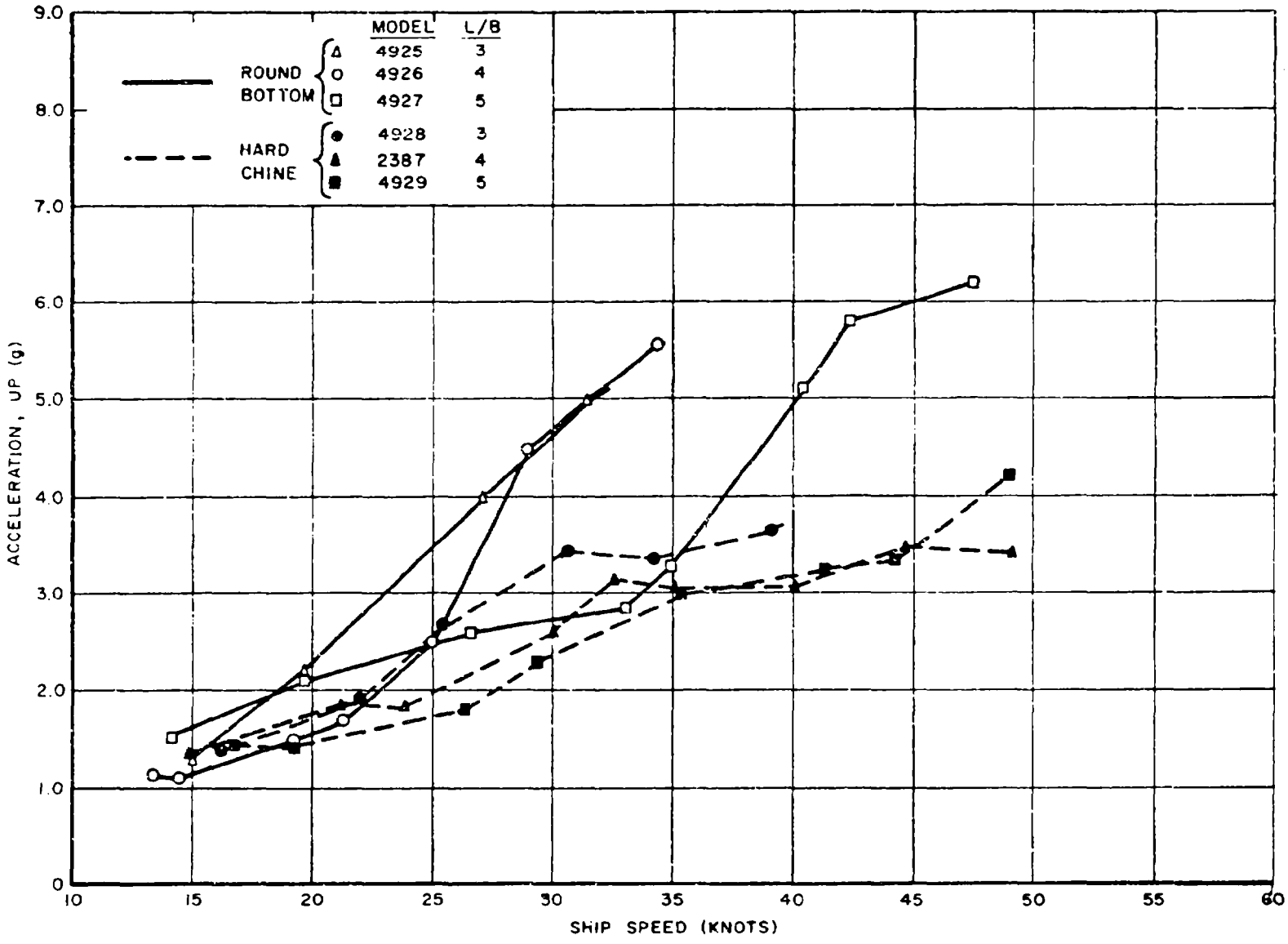

FIGURE 22. AVERAGE OF 1/10 HIGHEST BOW ACCELERATIONS IN STATE 3 – HEAD SEAS.

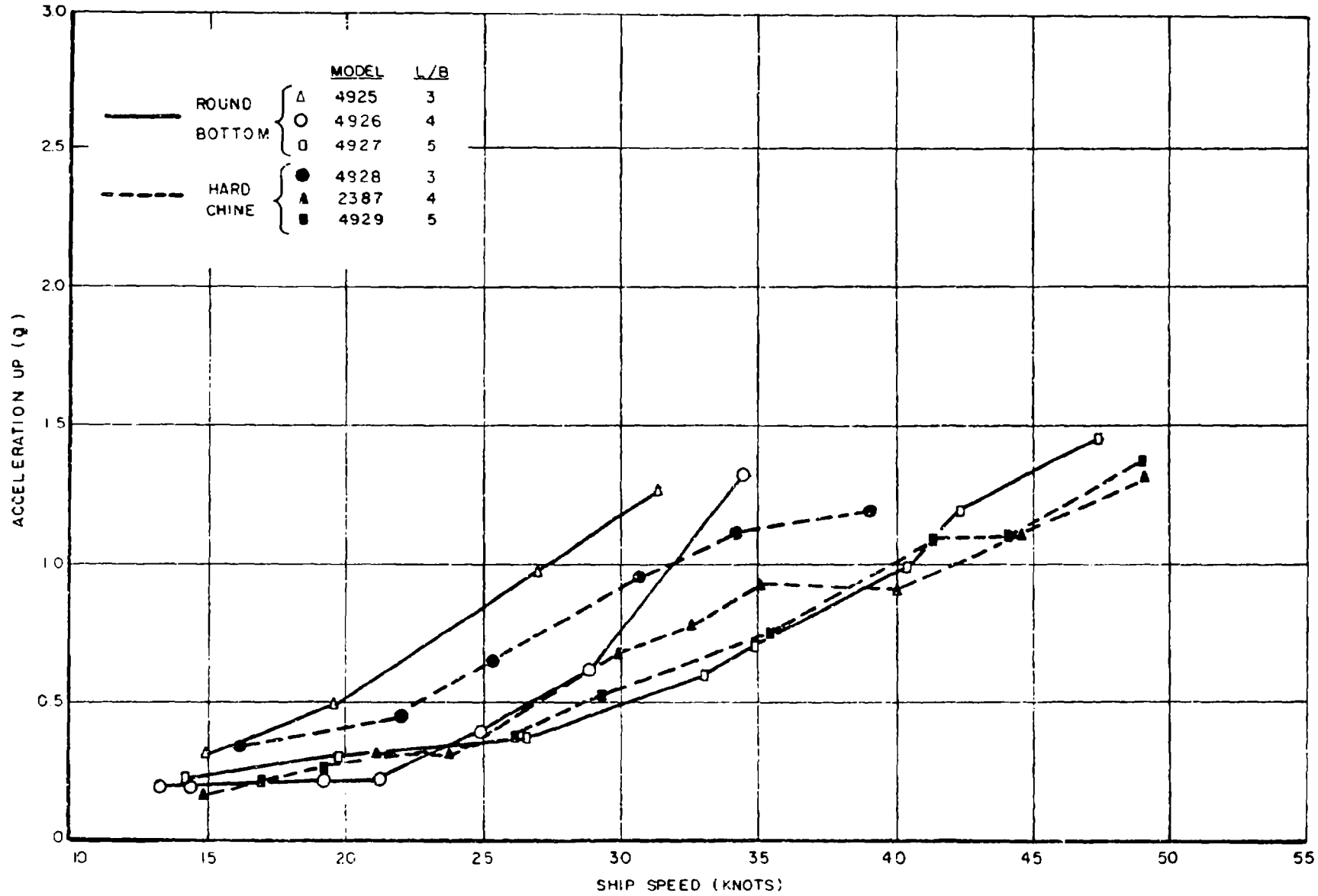

FIGURE 23. AVERAGE C.G. ACCELERATION IN STATE 3 - HEAD SEAS.

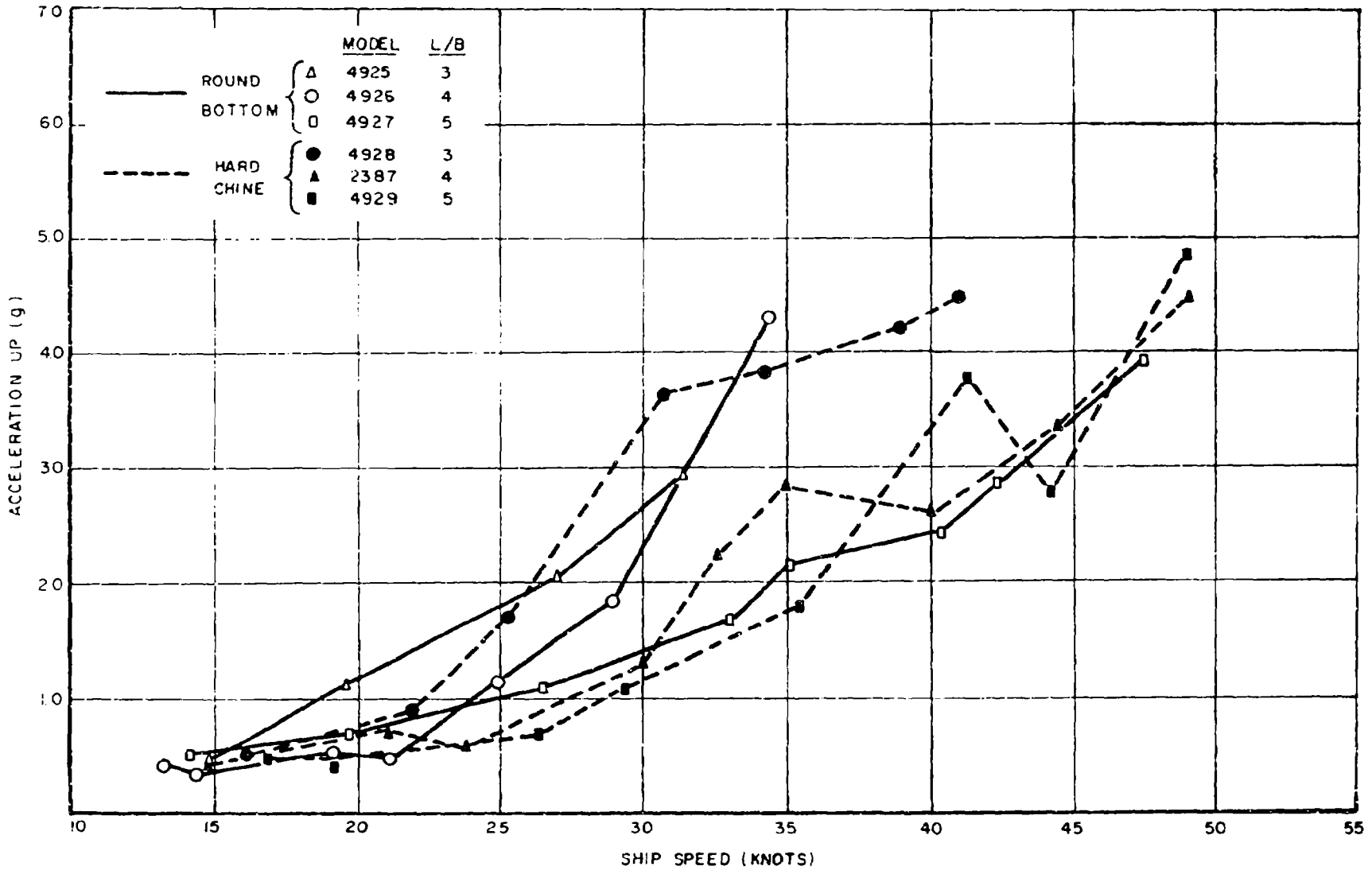

FIGURE 24. AVERAGE OF 1/10 HIGHEST C.G. ACCELERATIONS IN STATE 3 – HEAD SEAS.

R-985

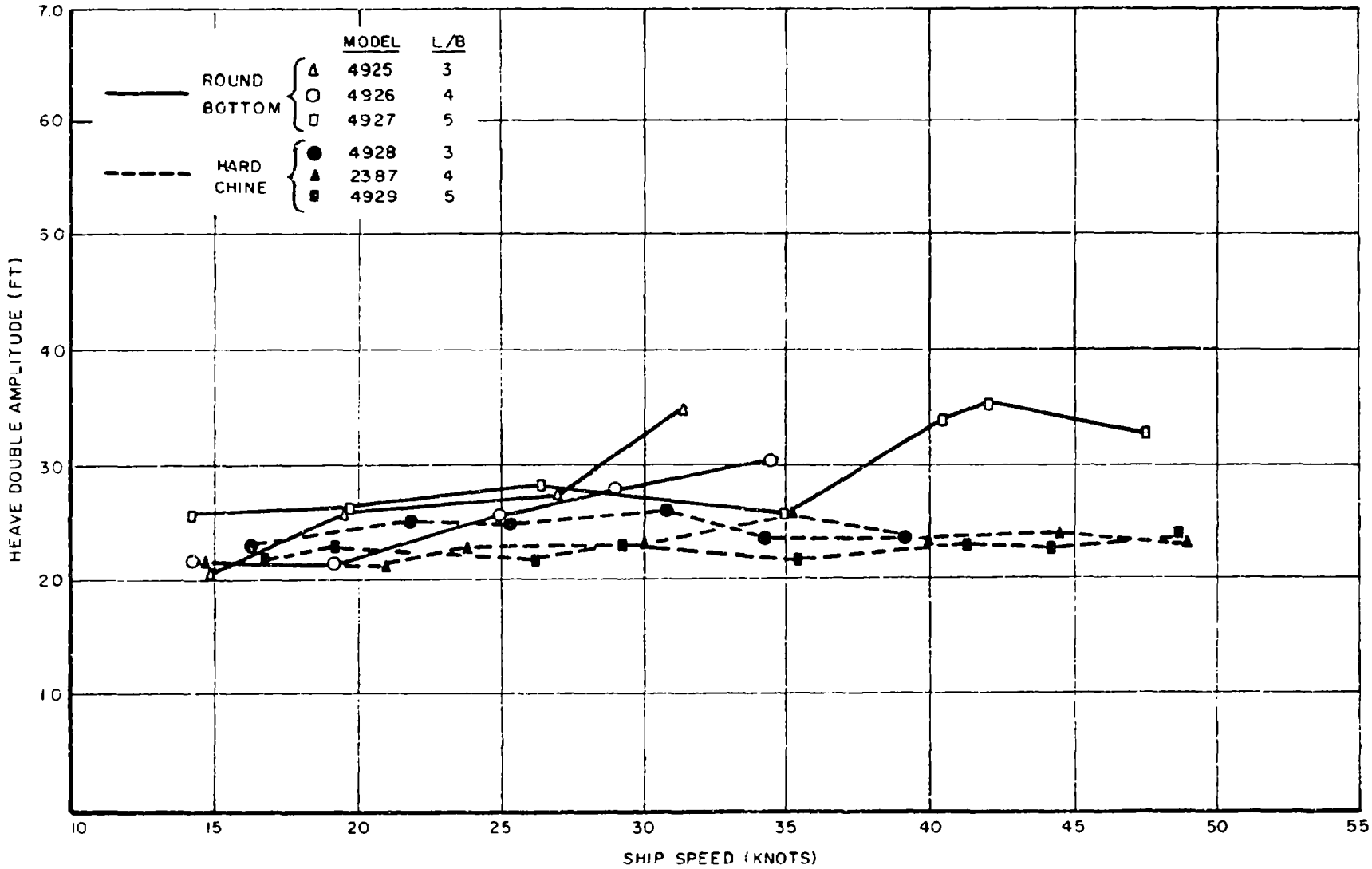

FIGURE 25. AVERAGE HEAVE DOUBLE AMPLITUDE IN STATE 3- HEAD SEAS.

R-985

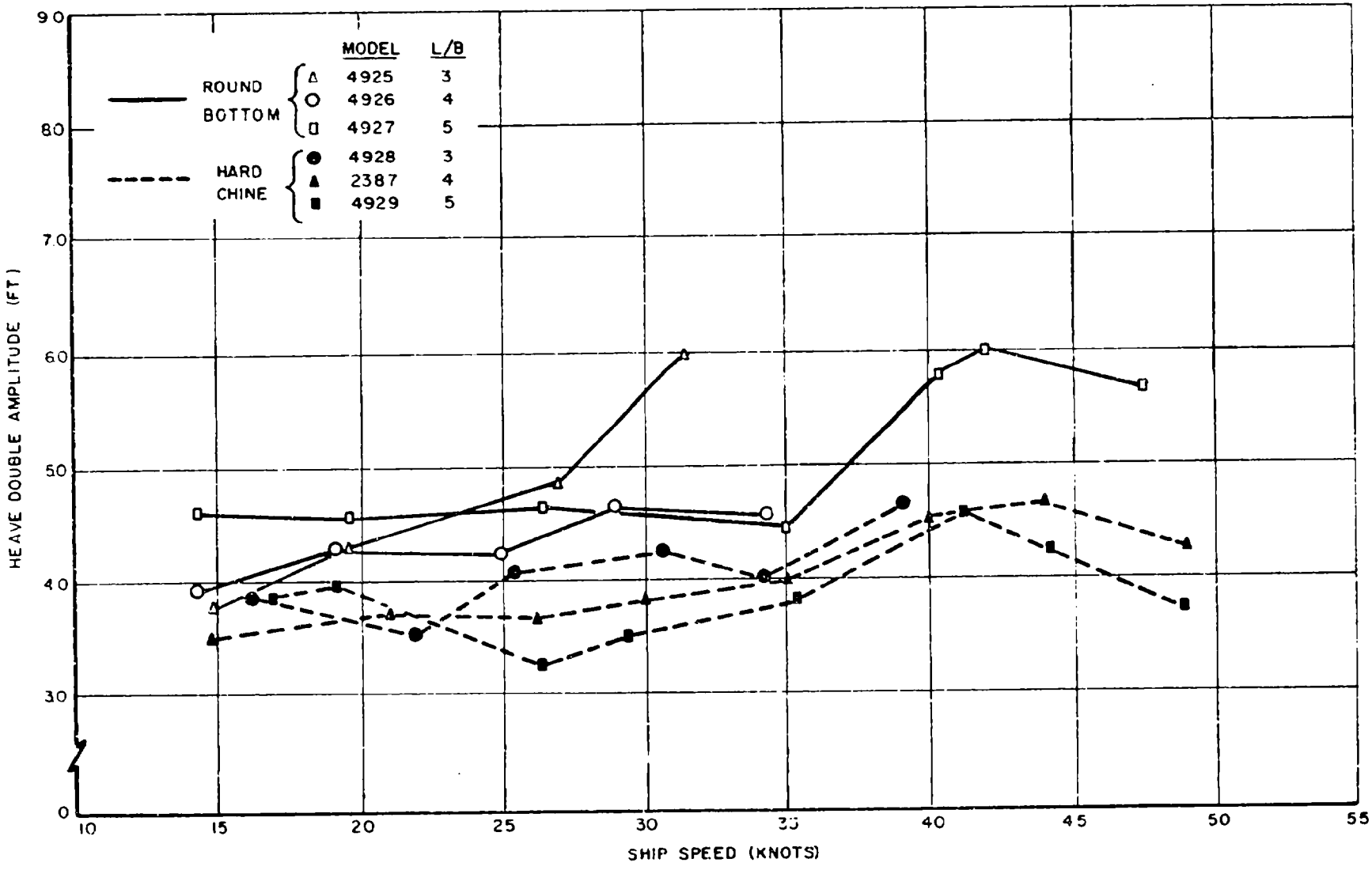

FIGURE 26. AVERAGE OF 1/10 HIGHEST HEAVE DOUBLE AMPLITUDE IN STATE 3-HEAD SEAS.

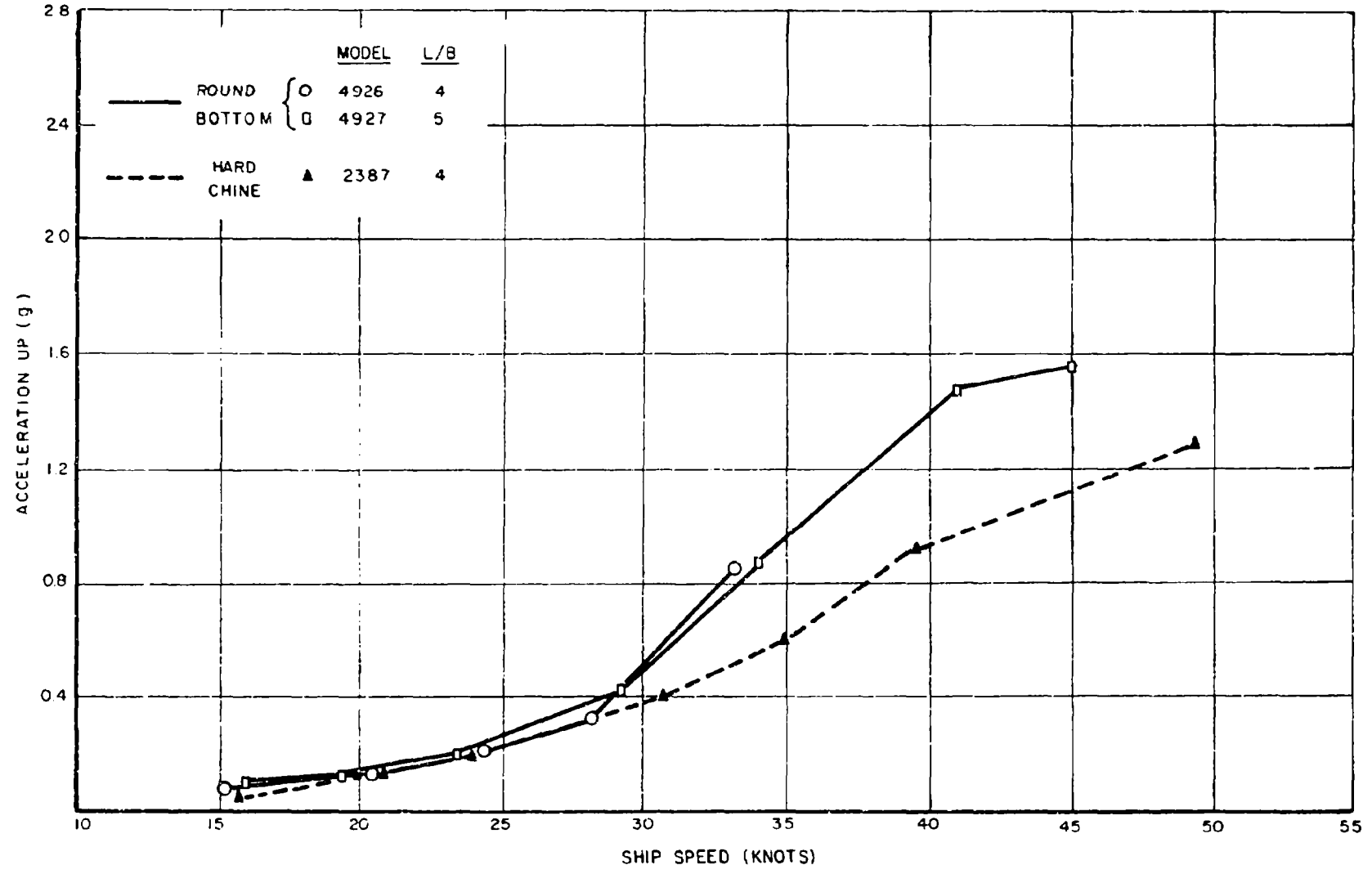

FIGURE 27. AVERAGE BOW ACCELERATION IN STATE 3 - FOLLOWING SEAS.

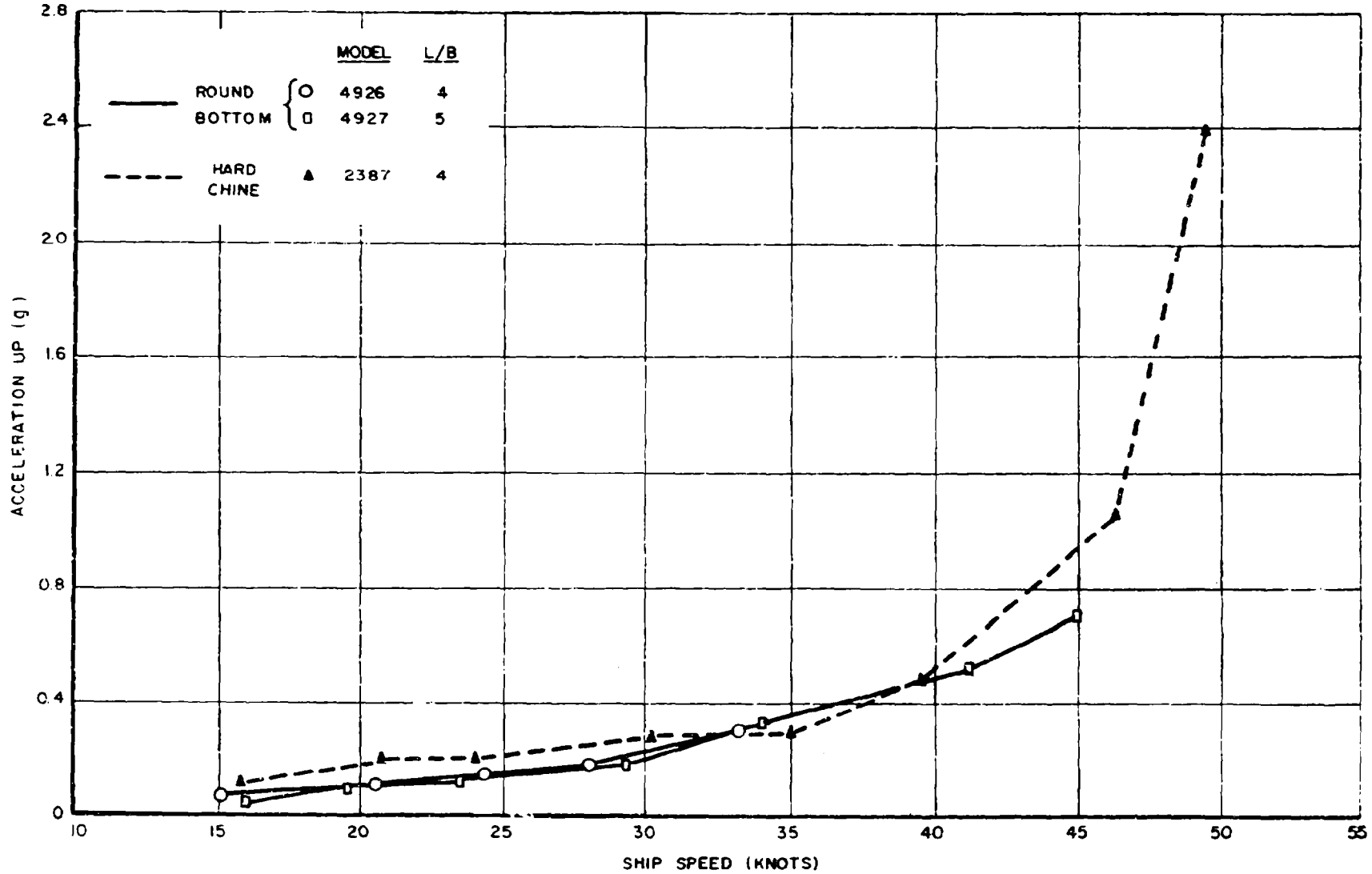

FIGURE 28. AVERAGE C.G. ACCELERATION IN STATE 3 - FOLLOWING SEAS.

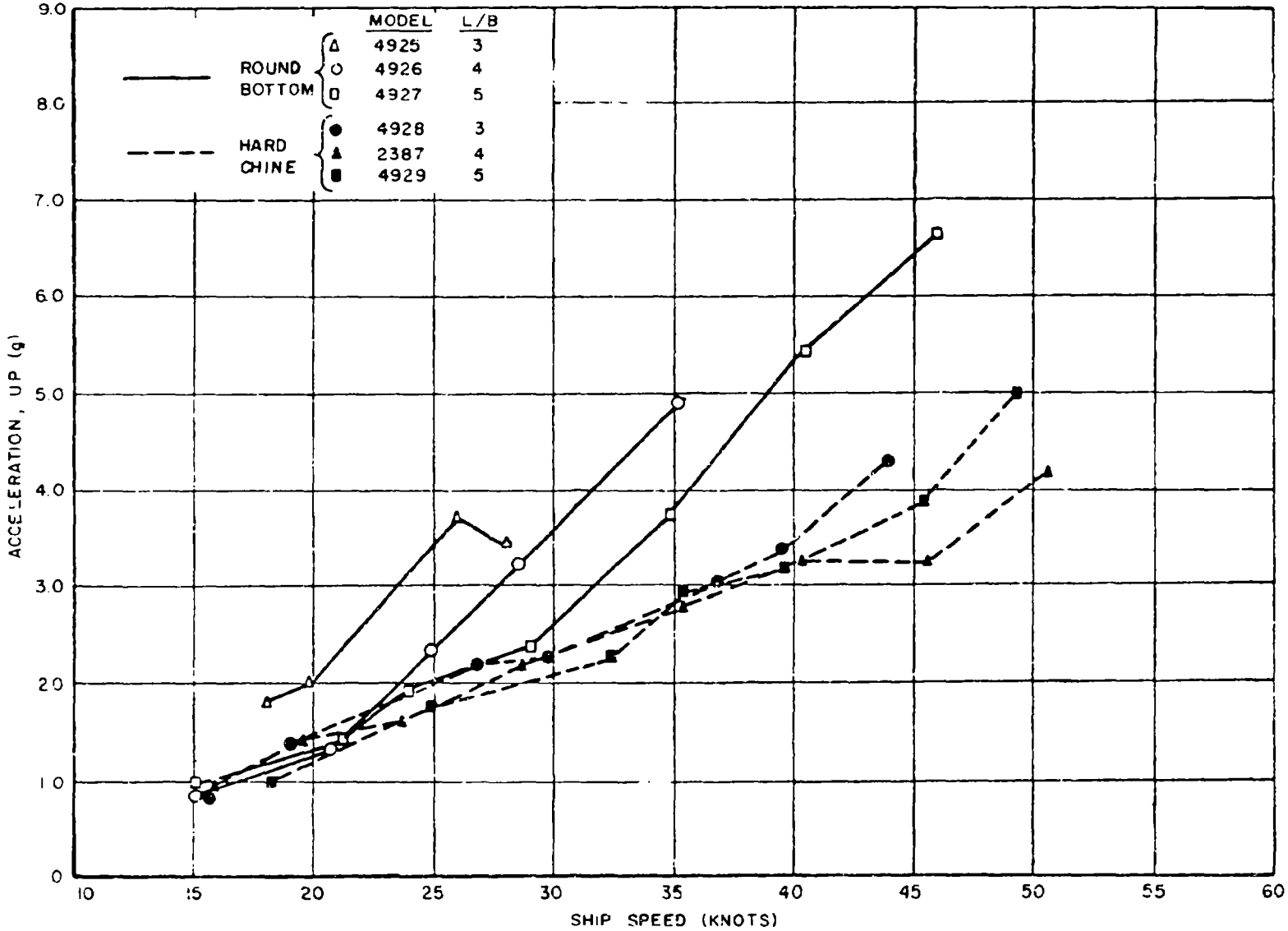

FIGURE 29. AVERAGE BOW ACCELERATION IN STATE 5 - HEAD SEAS.

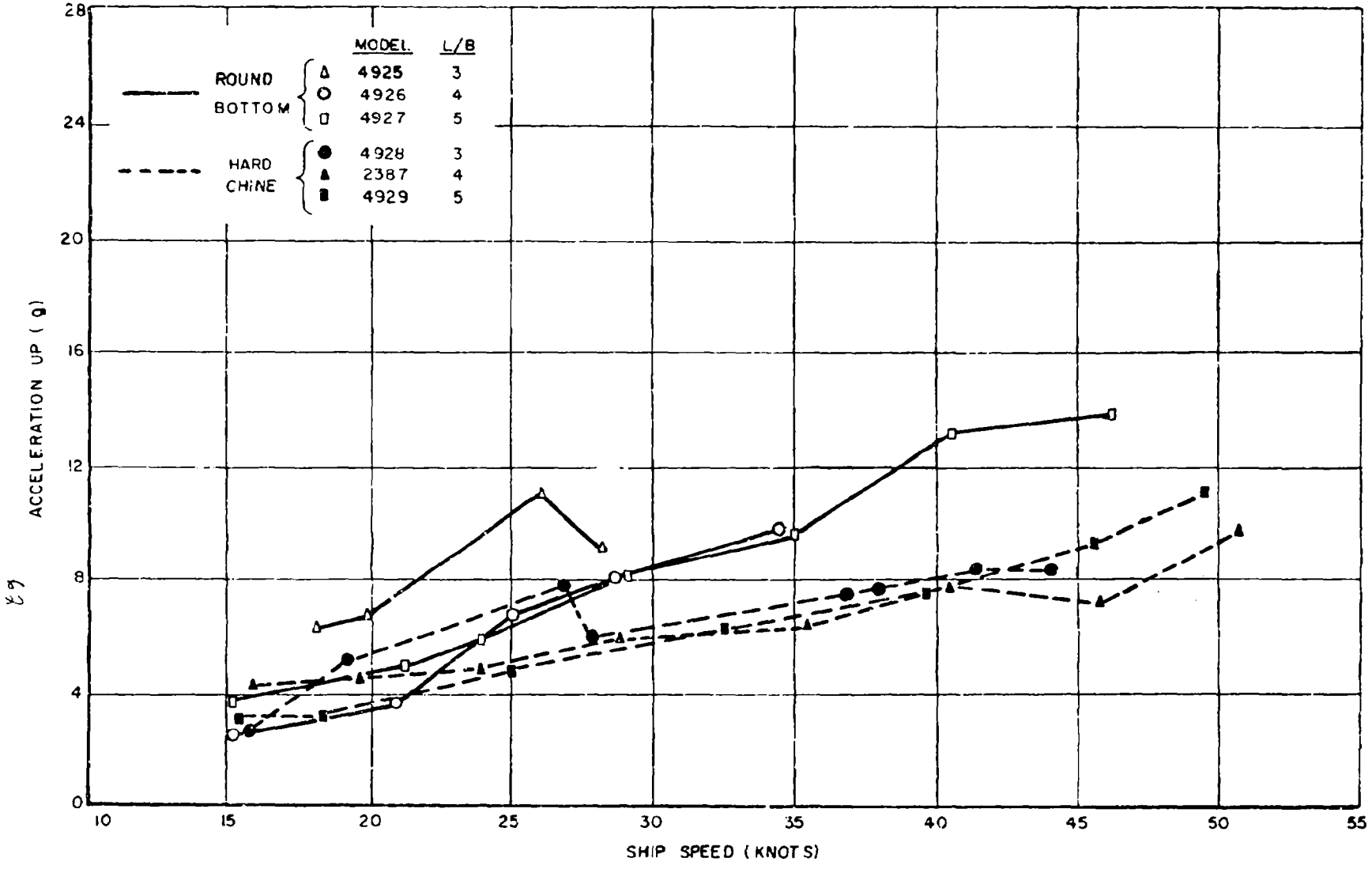

FIGURE 30. AVERAGE OF 1/10 HIGHEST BOW ACCELERATIONS IN STATE 5—HEAD SEAS.

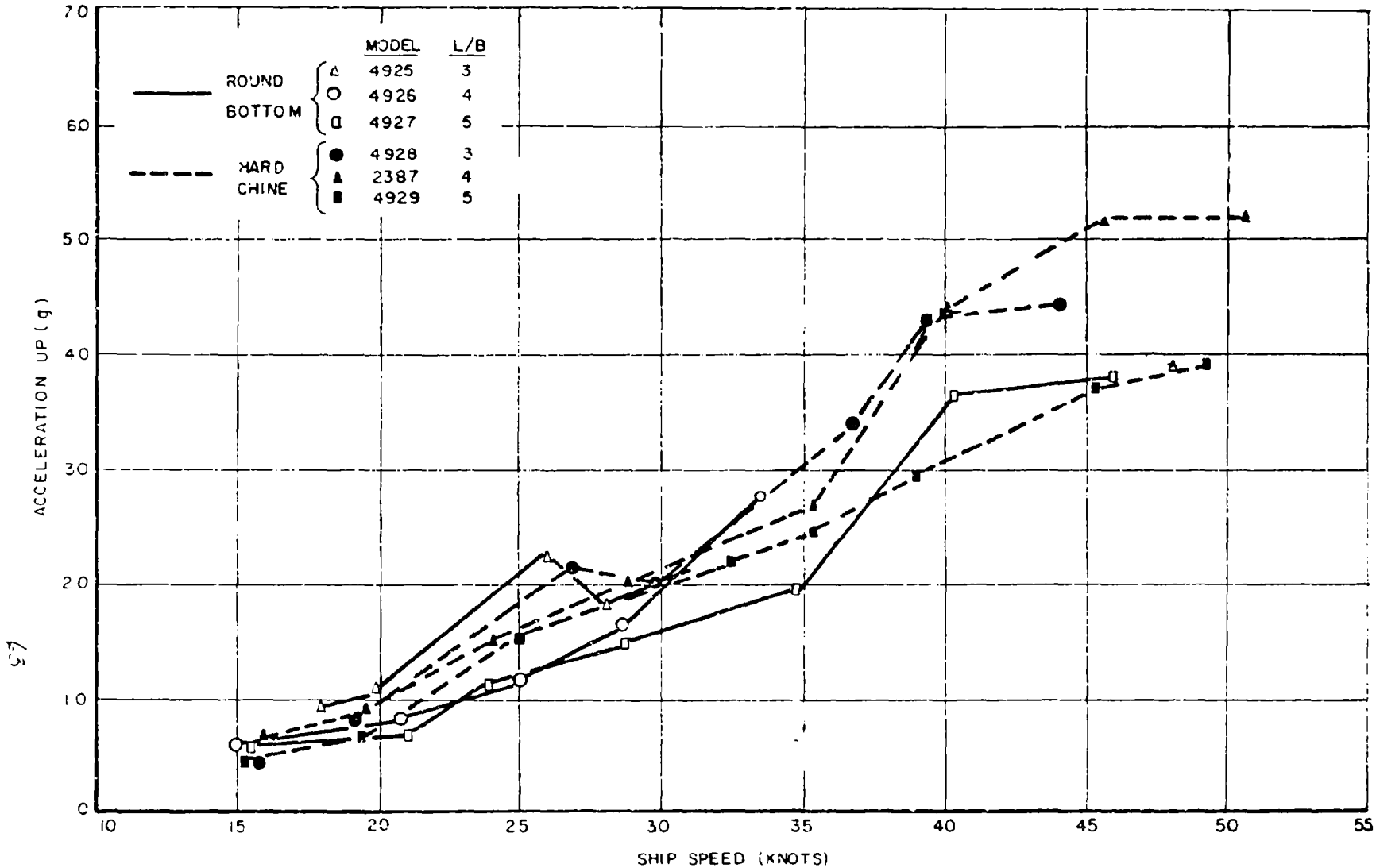

FIGURE 31. AVERAGE C.G. ACCELERATION IN STATE 5-HEAD SEAS

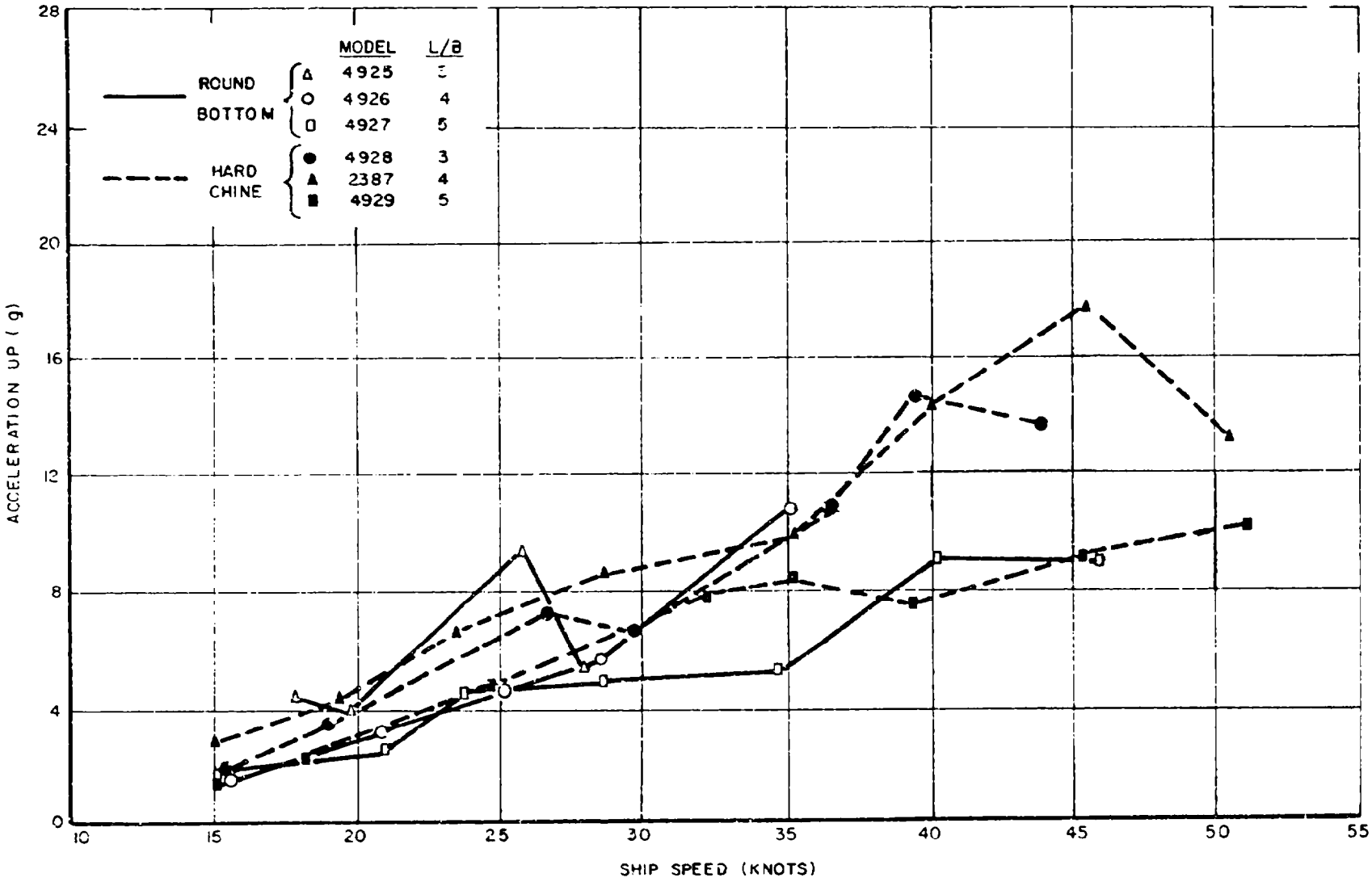

FIGURE 32 AVERAGE OF 1/10 HIGHEST C.G. ACCELERATIONS IN STATE 5 – HEAD SEAS.

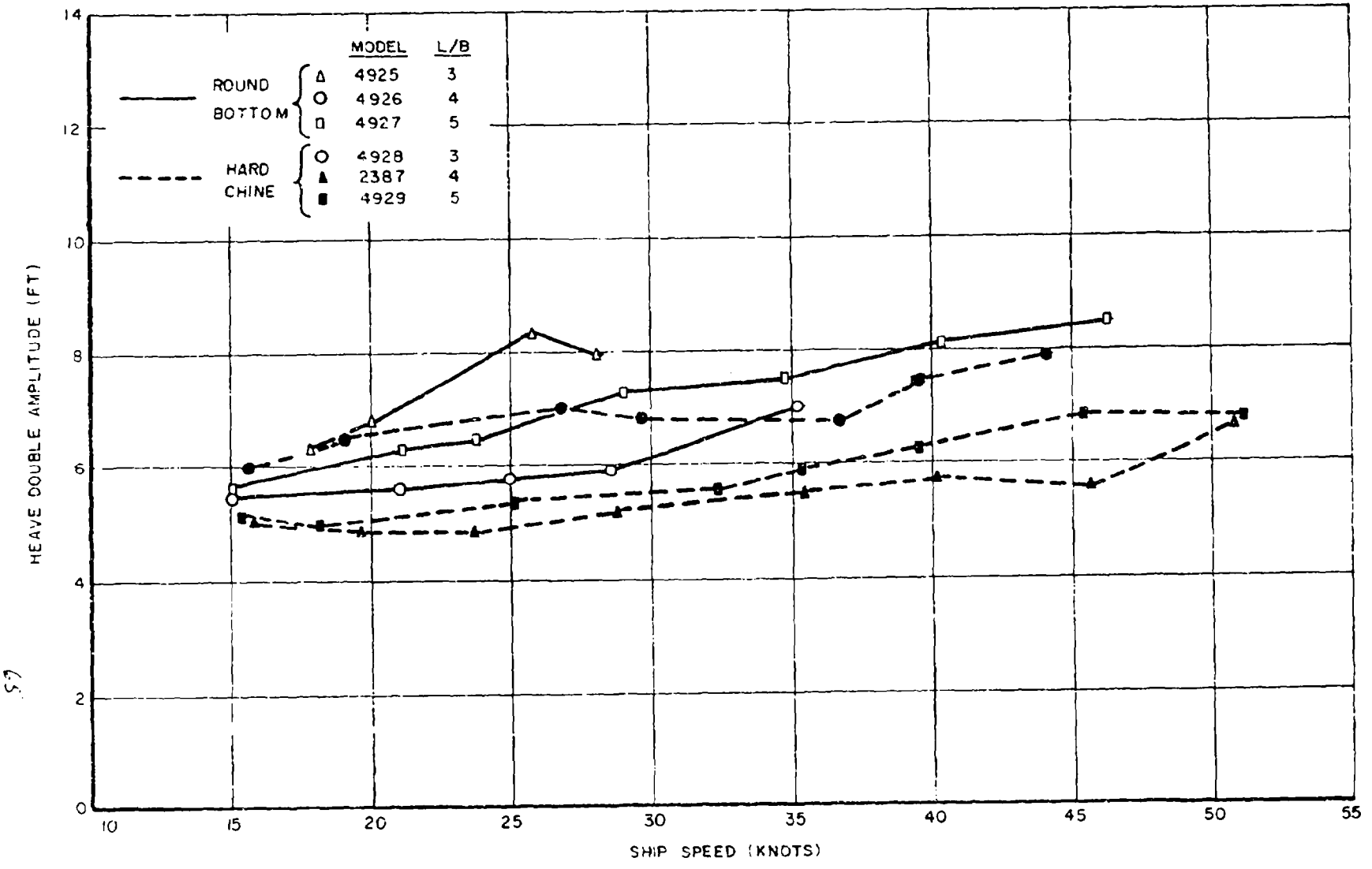

FIGURE 33. AVERAGE HEAVE DOUBLE AMPLITUDE IN STATE 5-HEAD SEAS.

R-985

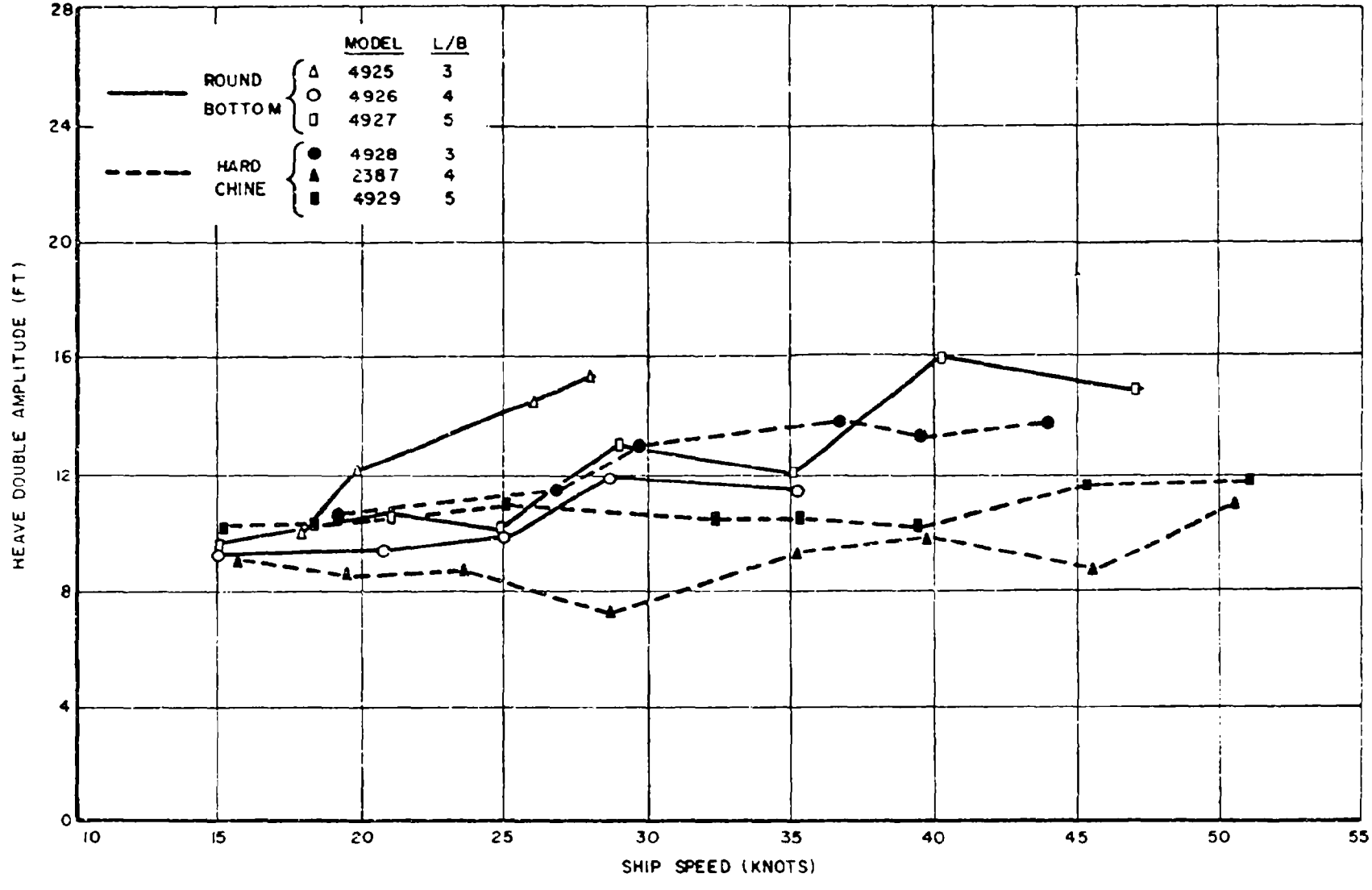

FIGURE 34. AVERAGE OF 1/10 HIGHEST HEAVE DOUBLE AMPLITUDE IN STATE 5-HEAD SEAS.

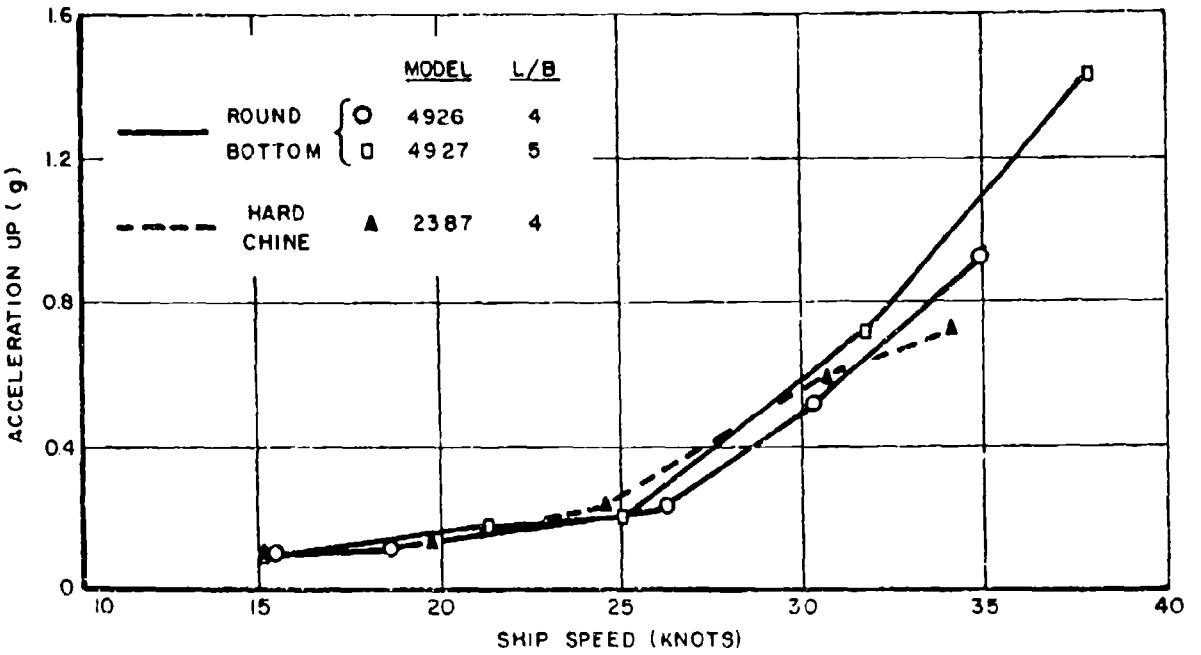

FIGURE 35. AVERAGE BOW ACCELERATION IN STATE 5 - FOLLOWING SEAS

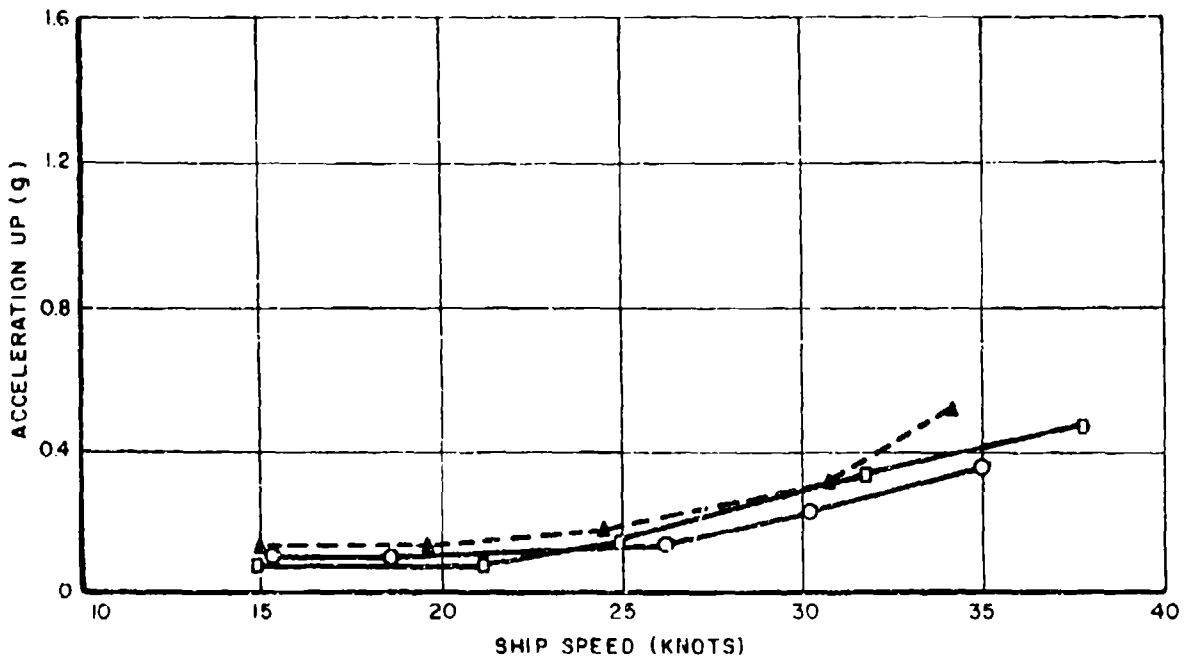

FIGURE 36. AVERAGE C.G. ACCELERATION IN STATE 5 - FOLLOWING SEAS

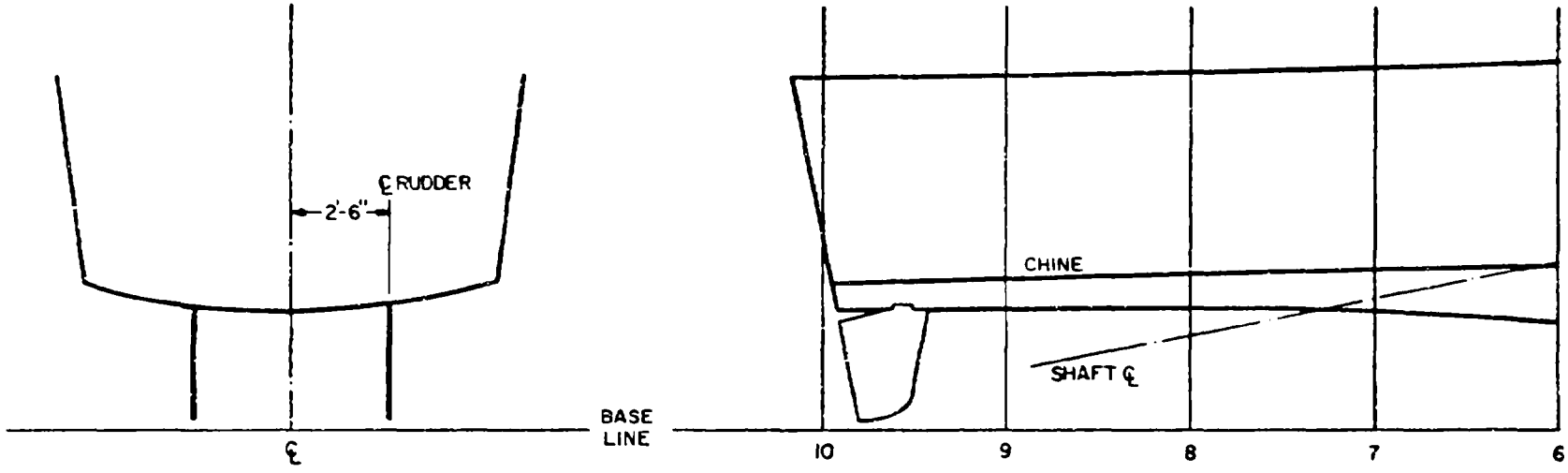

FIGURE 37 GEOMETRY AND LOCATION OF RUDDERS

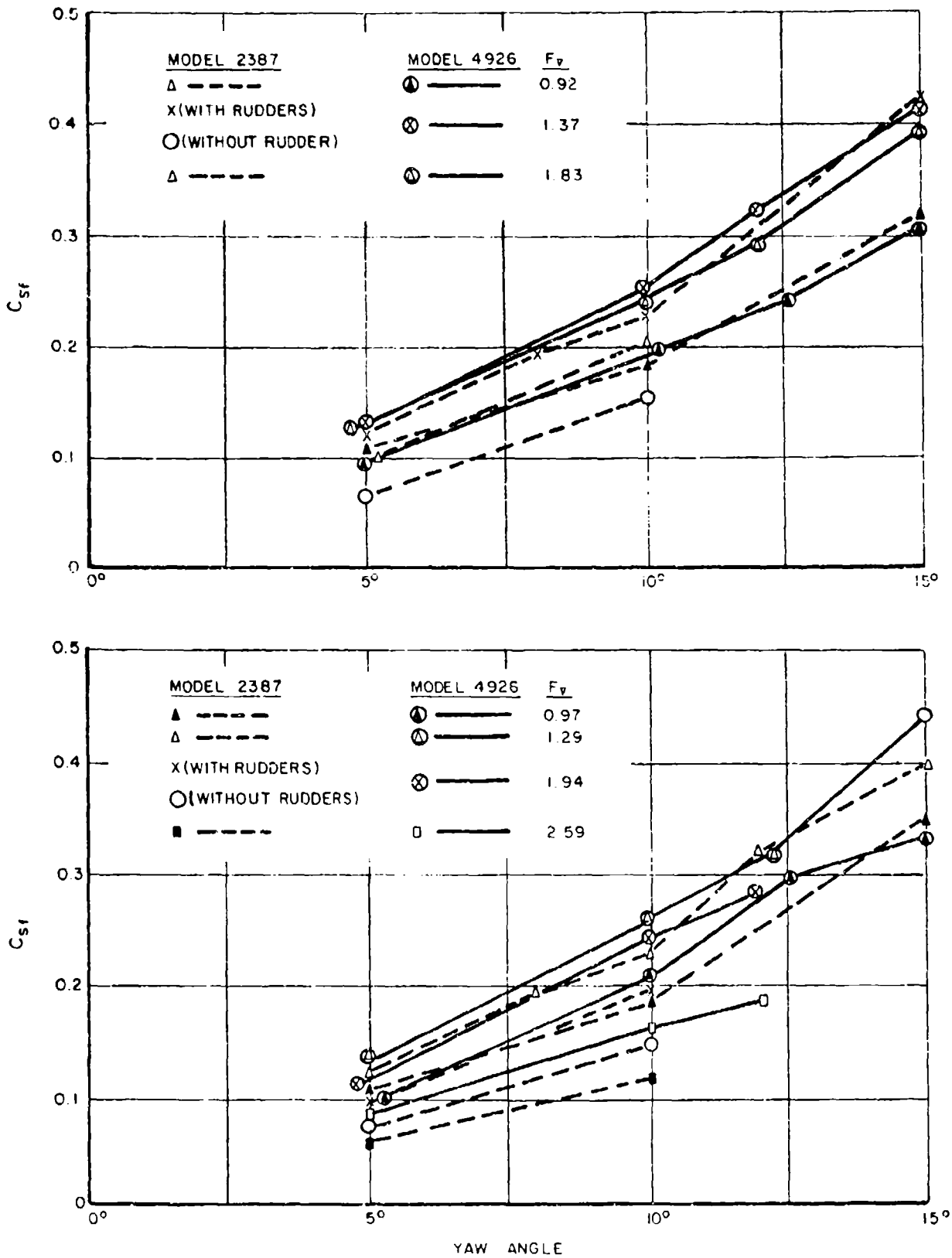

FIGURE 38. SIDE FORCE COEFFICIENTS OF MODELS IN CALM WATER.

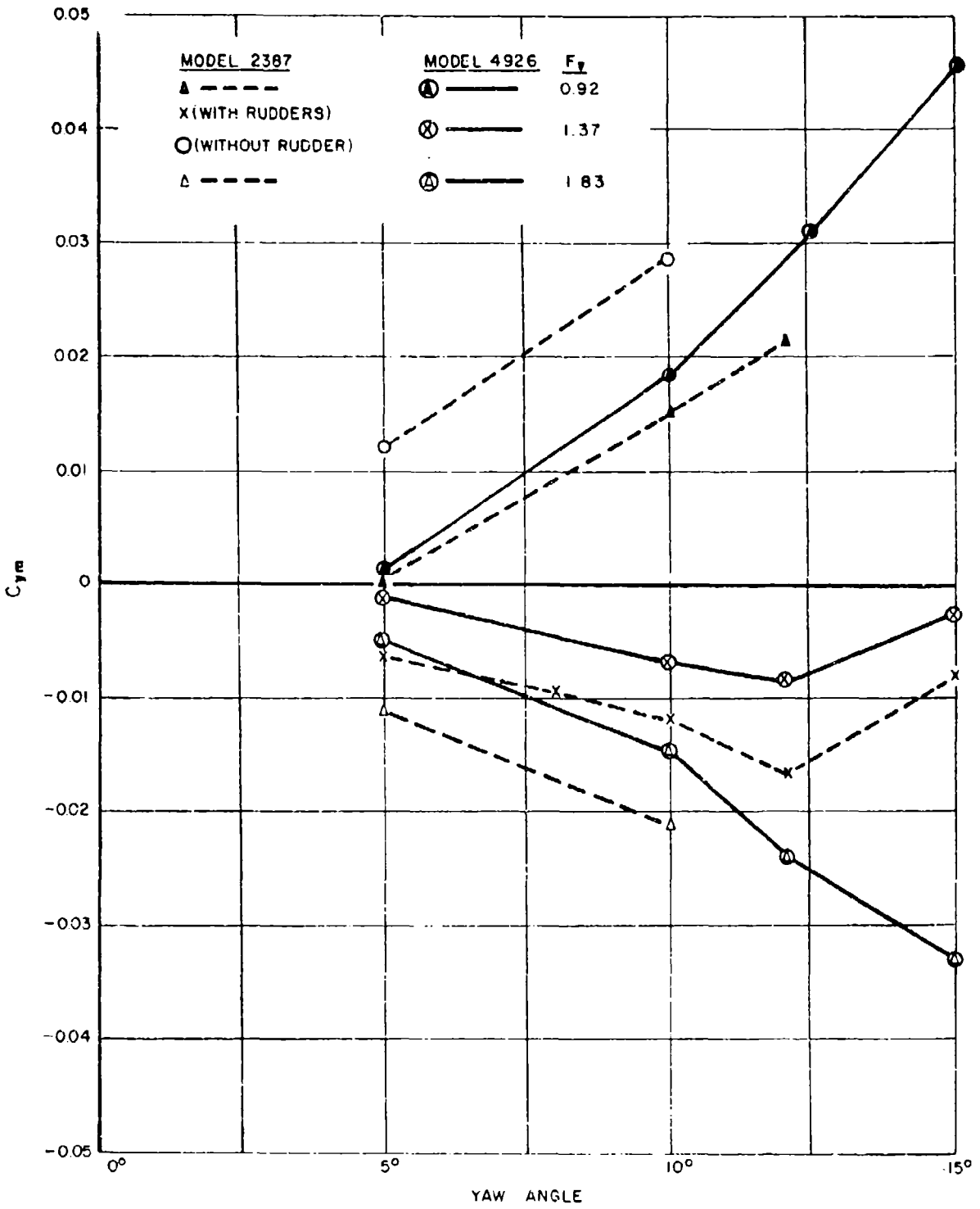

FIGURE 39. YAW MOMENT COEFFICIENTS OF MODELS IN CALM WATER.

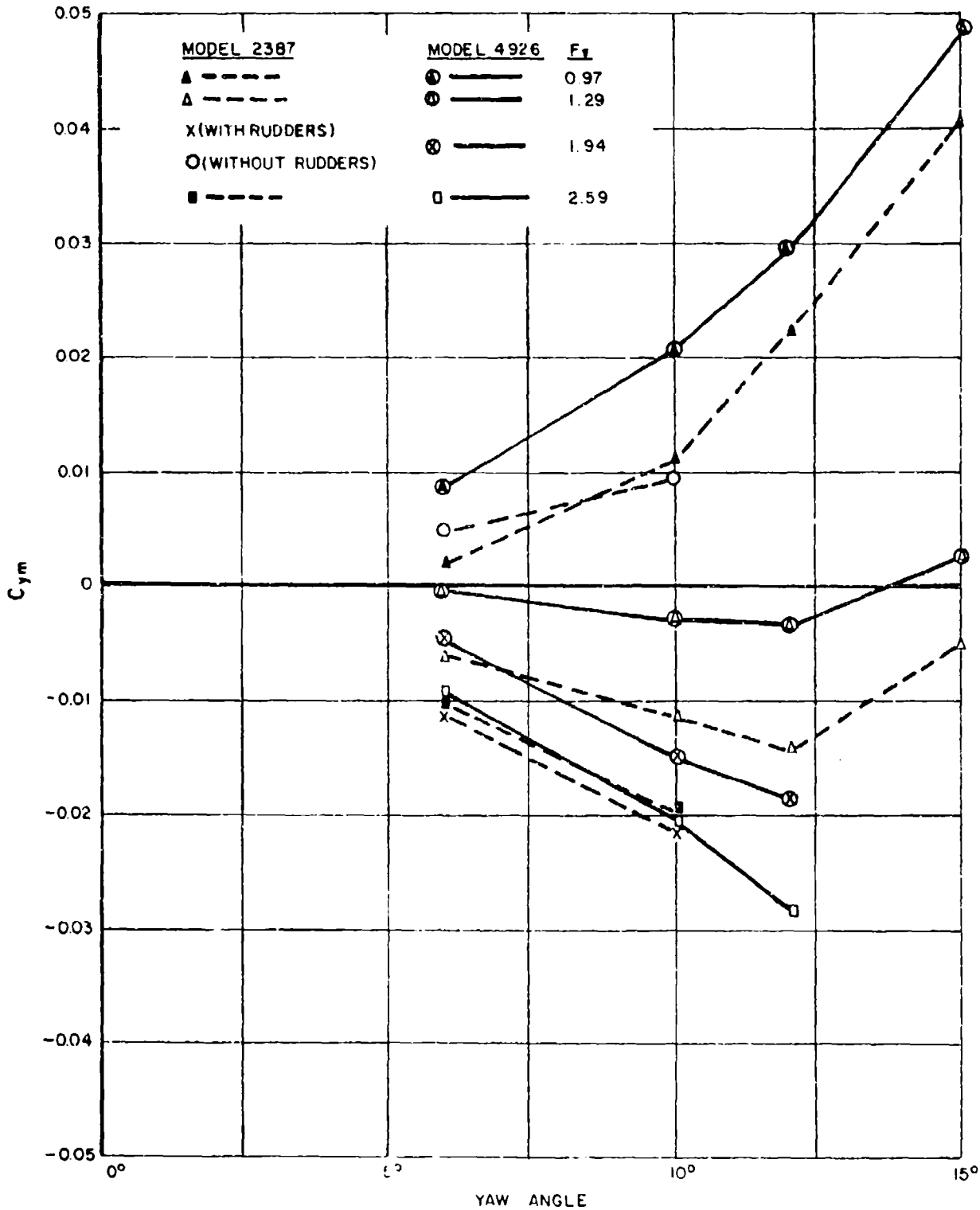

FIGURE 40. YAW MOMENT COEFFICIENTS OF MODELS IN CALM WATER.

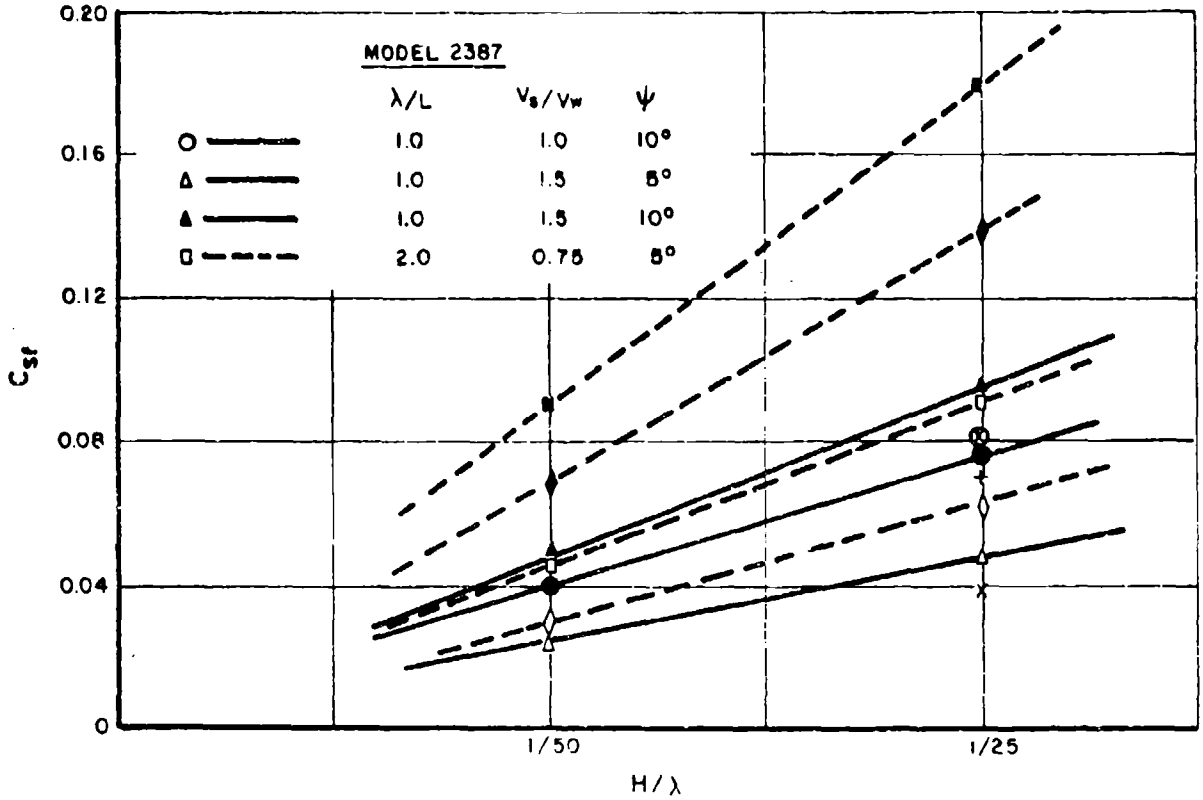

FIGURE 41. DOUBLE AMPLITUDES OF SIDE FORCE IN WAVES.

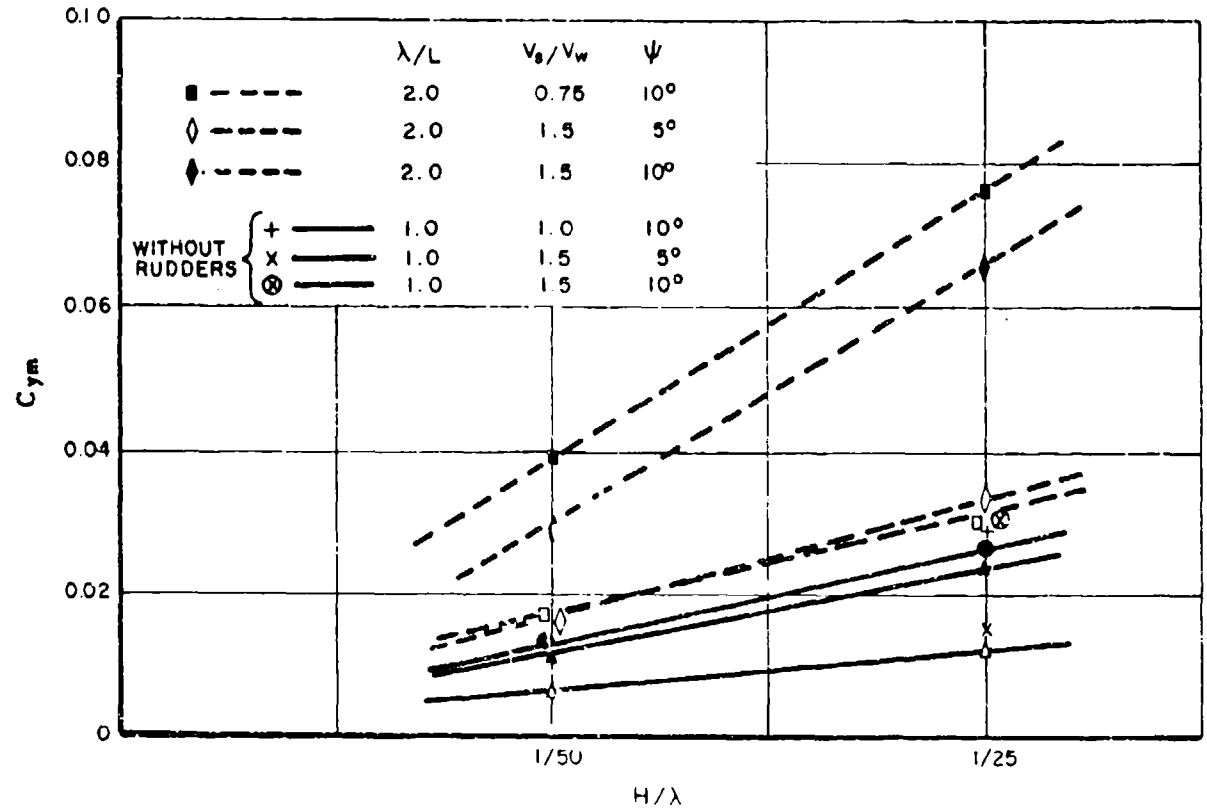

FIGURE 42. DOUBLE AMPLITUDES OF YAW MOMENT IN WAVES.

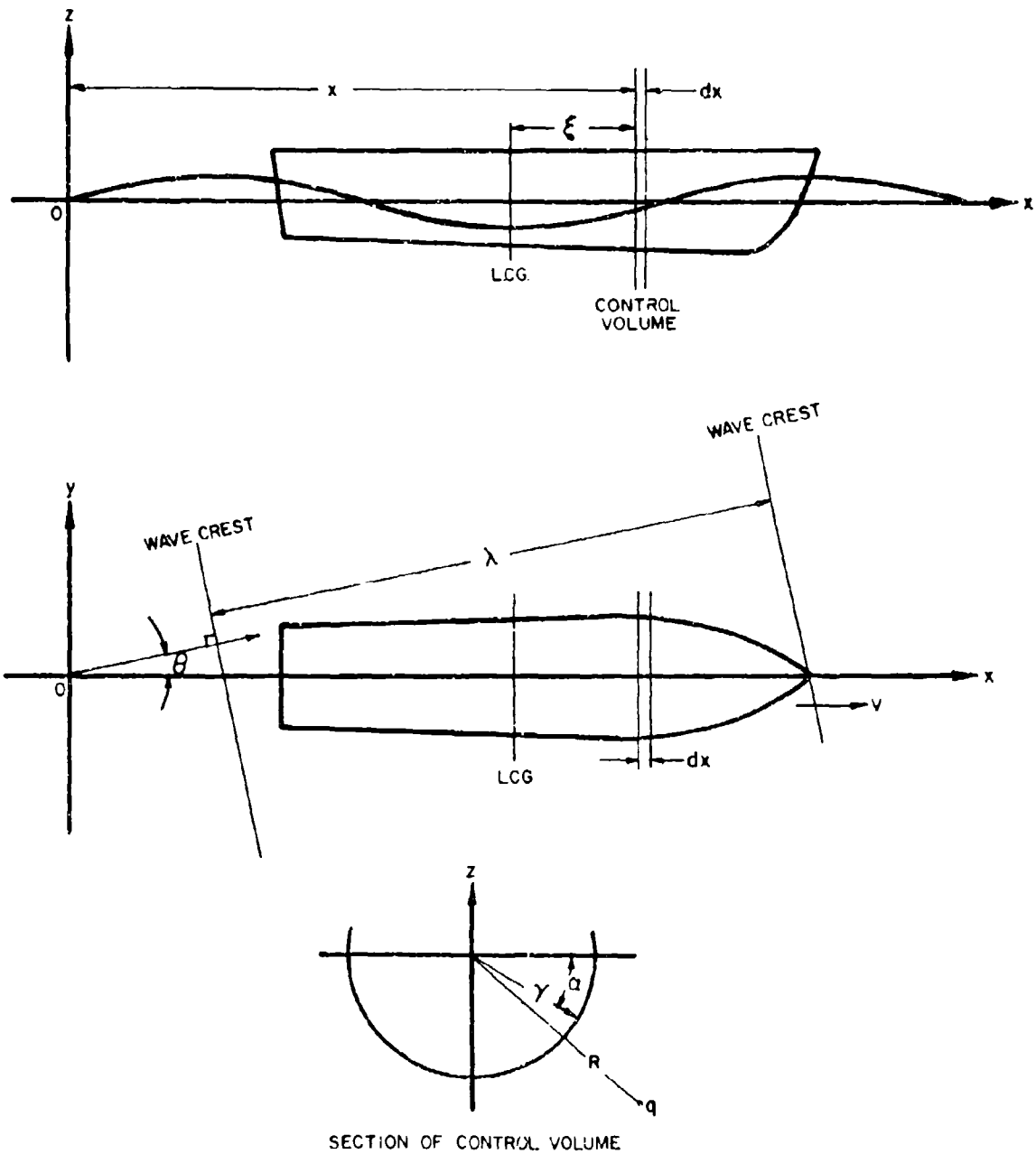

SECTION OF CONTROL VOLUME

FIGURE 43 SKETCH ILLUSTRATING NOTATION

MODEL 4927 WITH SPRAY STRIP COVERING ONLY
40 PERCENT FORWARD LENGTH

PLATE I

SPEED 25 KNOTS

SPEED 30 KNOTS

SPEED 35 KNOTS

SPEED 40 KNOTS

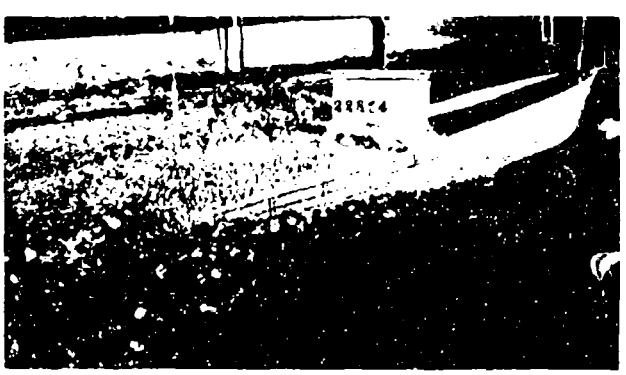

SPEED 45 KNOTS

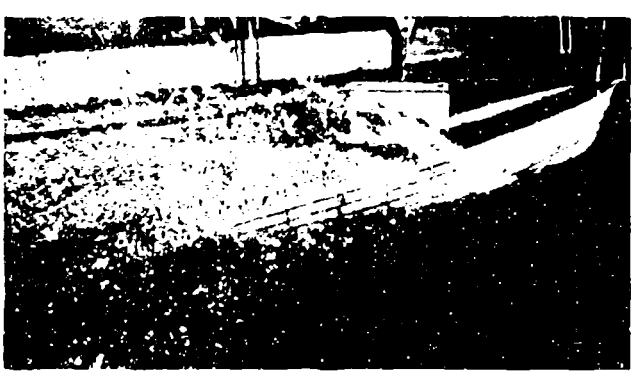

SPEED 50 KNOTS

SPEED 15 KNOTS

PLATE 2

MODEL 4925

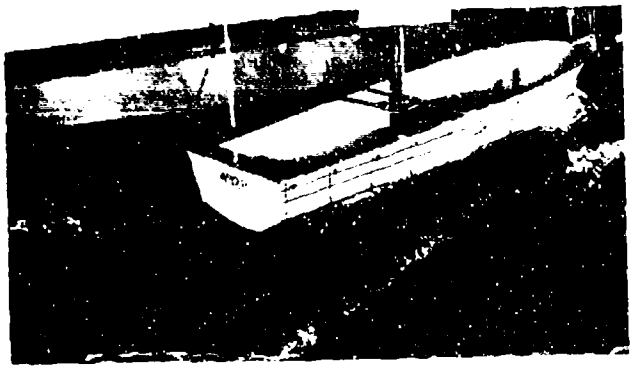

MODEL 4928

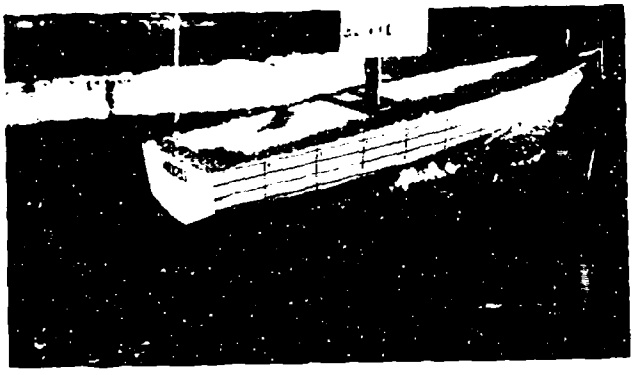

MODEL 4926

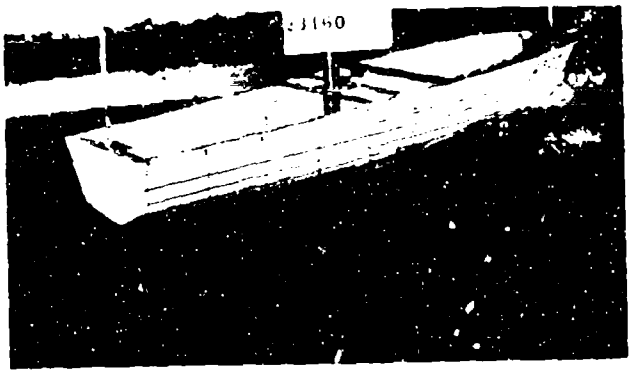

MODEL 2387

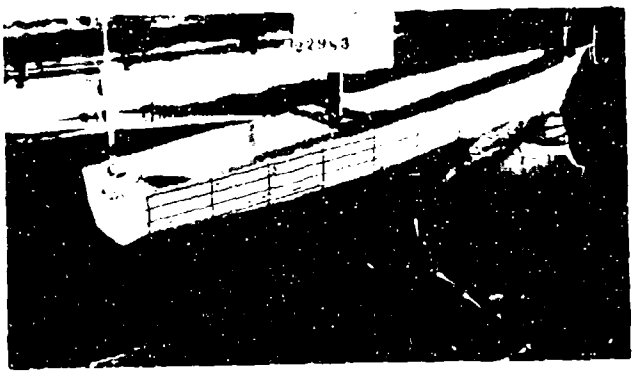

MODEL 4927

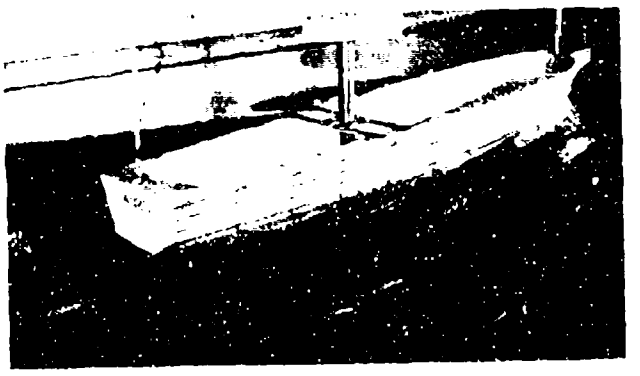

MODEL 4929

SPEED 20 KNOTS

PLATE 3

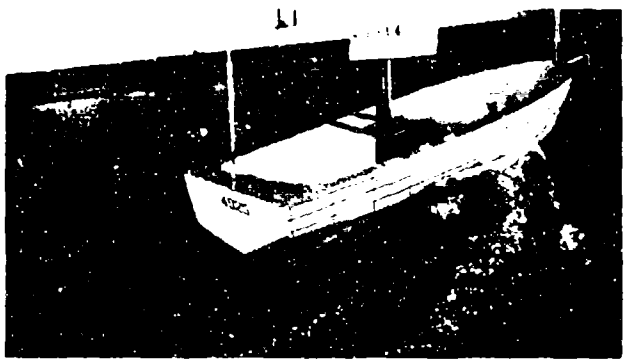

MODEL 4925

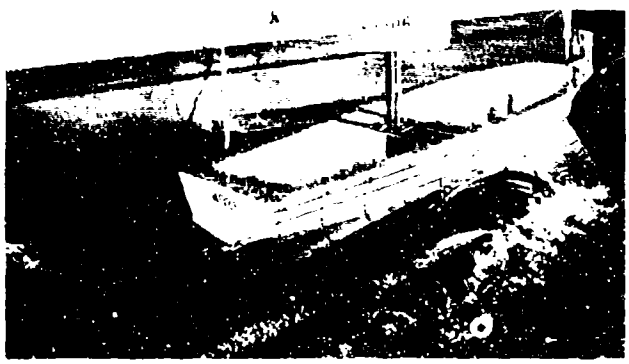

MODEL 4928

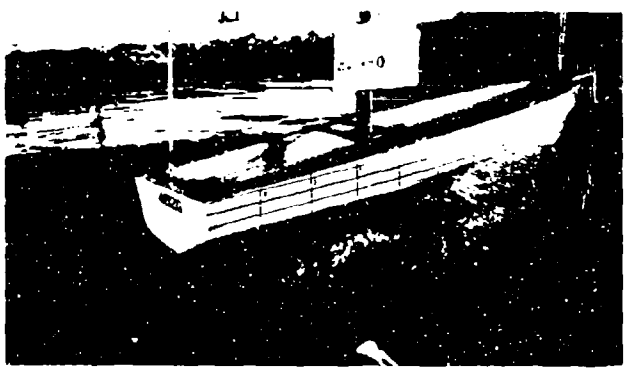

MODEL 4926

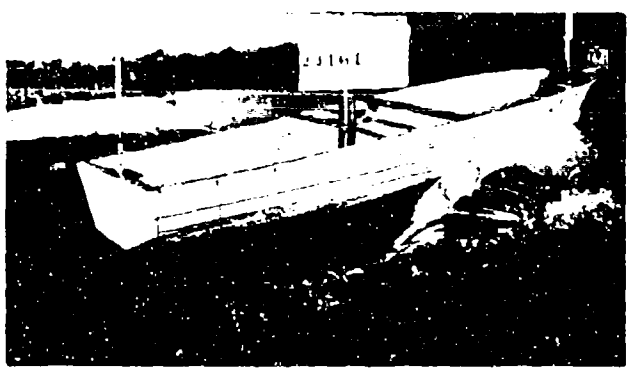

MODEL 2387

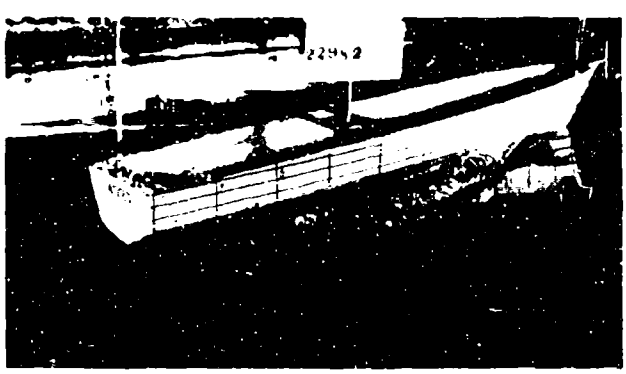

MODEL 4927

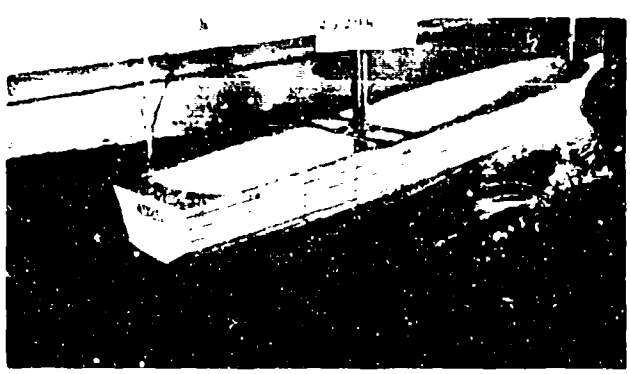

MODEL 4929

SPEED 25 KNOTS

PLATE 4

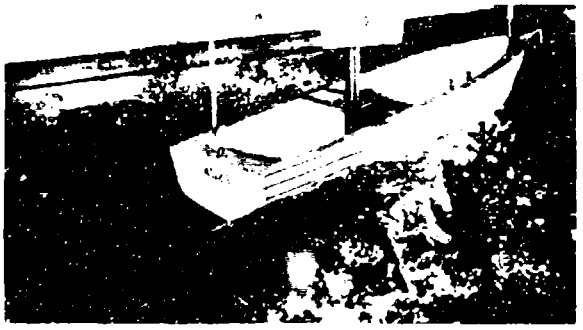

MODEL 4925

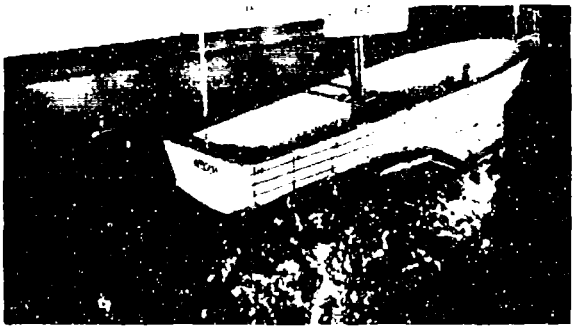

MODEL 4928

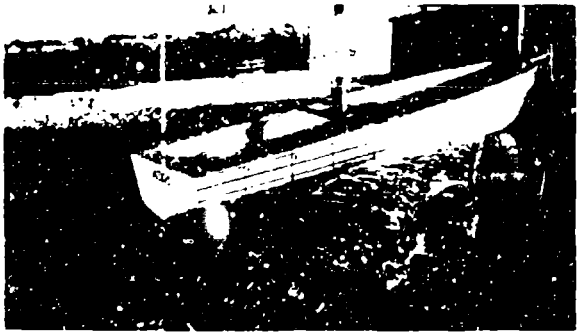

MODEL 4926

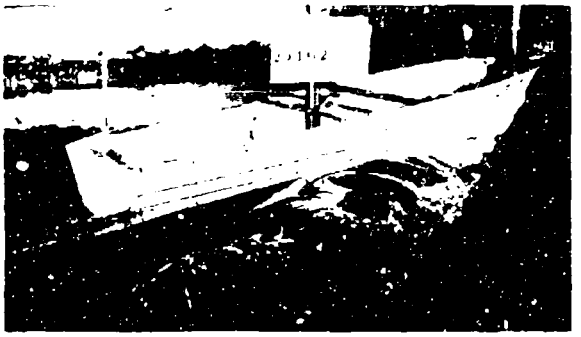

MODEL 2387

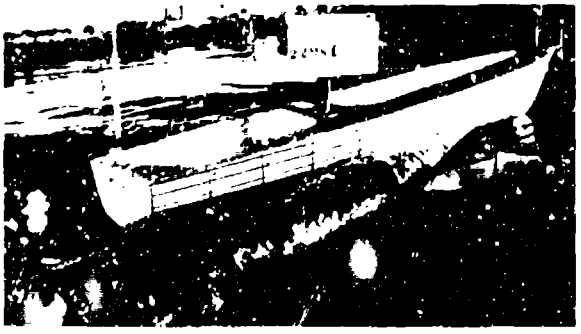

MODEL 4927

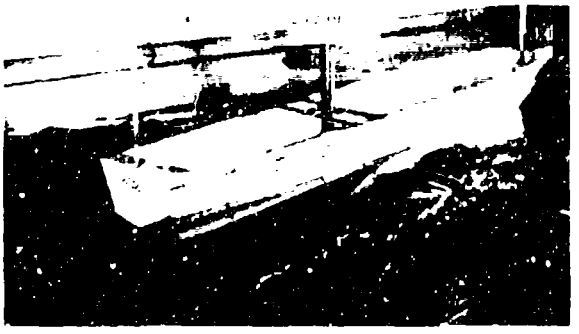

MODEL 4929

SPEED 30 KNOTS

PLATE 5

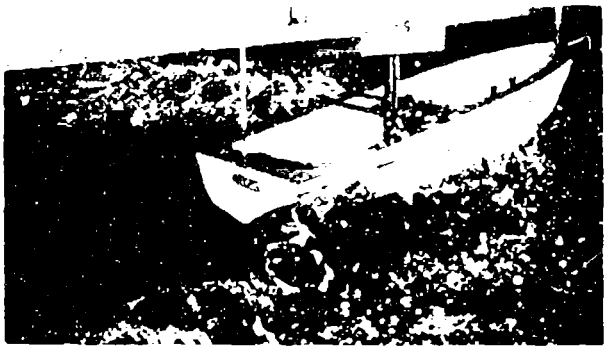

MODEL 4925

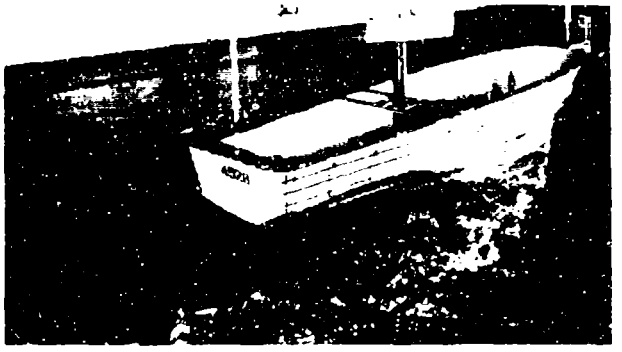

MODEL 4928

MODEL 4926

MODEL 2387

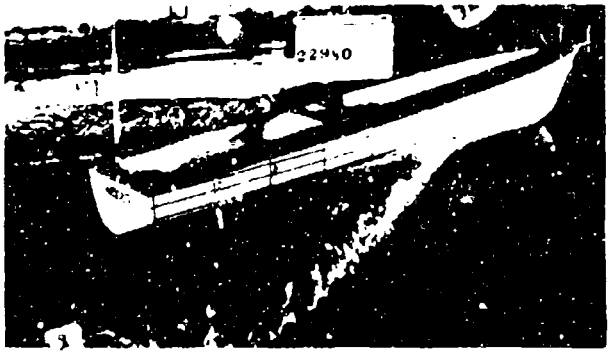

MODEL

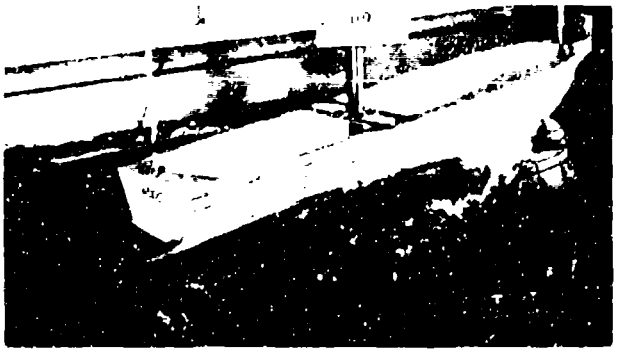

MODEL 4929

SPEED 35 KNOTS

PLATE 6

MODEL PORPOISED

MODEL 4925

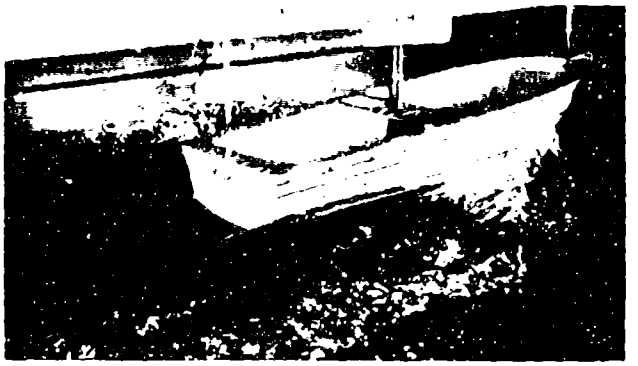

MODEL 4928

MODEL 4926

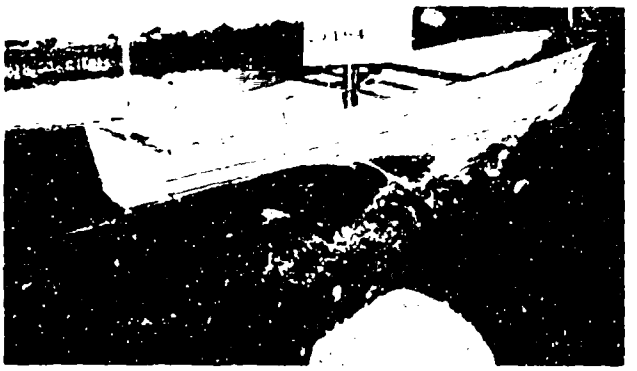

MODEL 2387

MODEL 4927

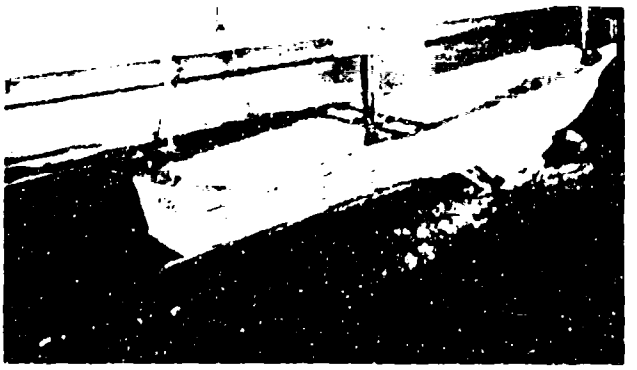

MODEL 4929

SPEED 40 KNOTS

PLATE 7

MODEL PORPOISED

MODEL 4925

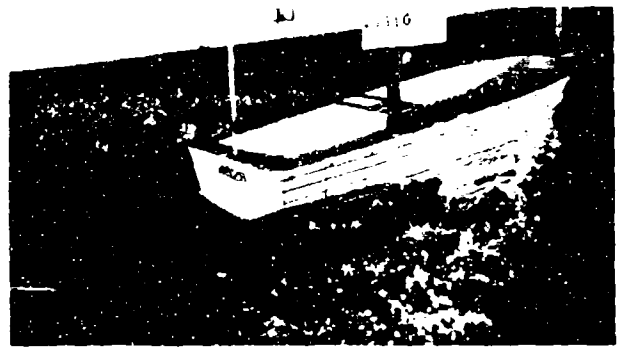

MODEL 4928

MODEL PORPOISED

MODEL 4926

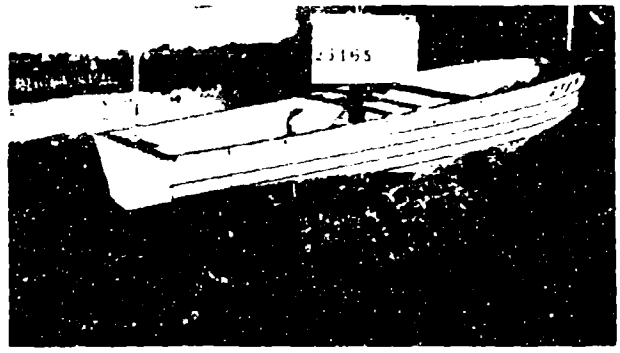

MODEL 2387

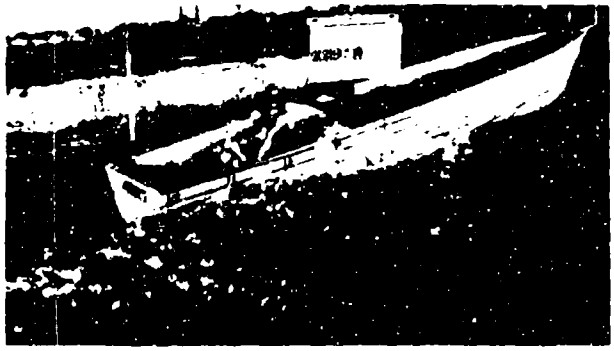

MODEL 4927

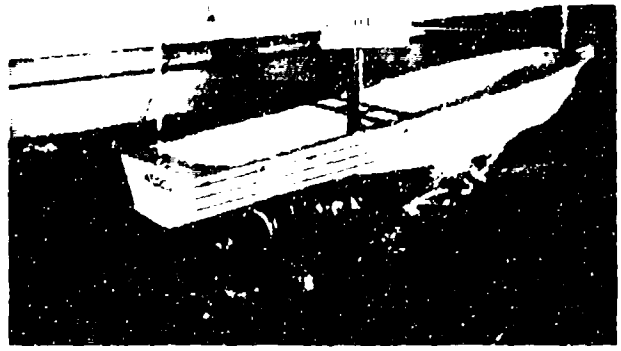

MODEL 4929

SPEED 45 KNOTS

PLATE 8

MODEL PORPOISED

MODEL 4925

MODEL PORPOISED

MODEL 4928

MODEL PORPOISED

MODEL 4926

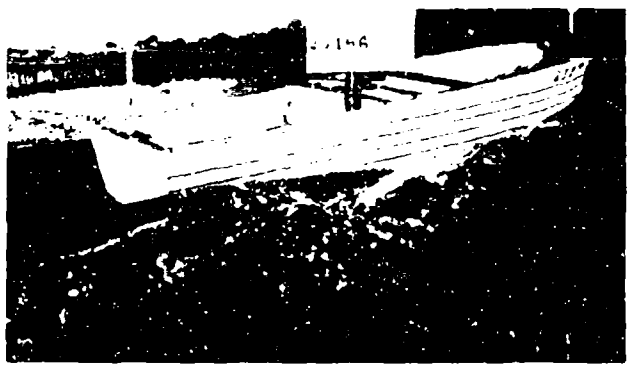

MODEL 2387

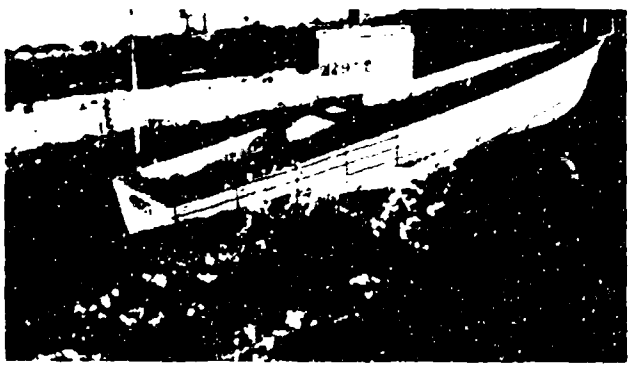

MODEL 4927

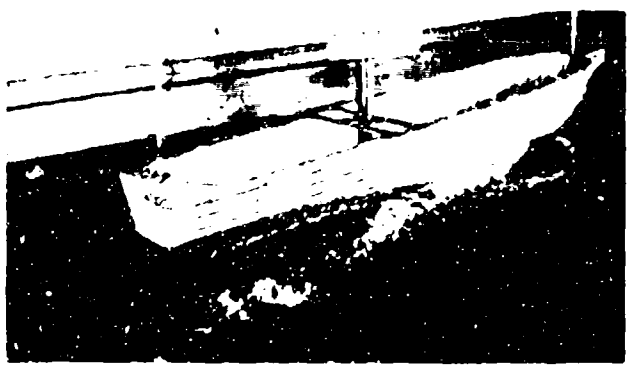

MODEL 4939

SPEED 50 KNOTS

PLATE 9

MODEL PORPOISED

MODEL 4925

MODEL PORPOISED

MODEL 4928

MODEL PORPOISED

MODEL 4926

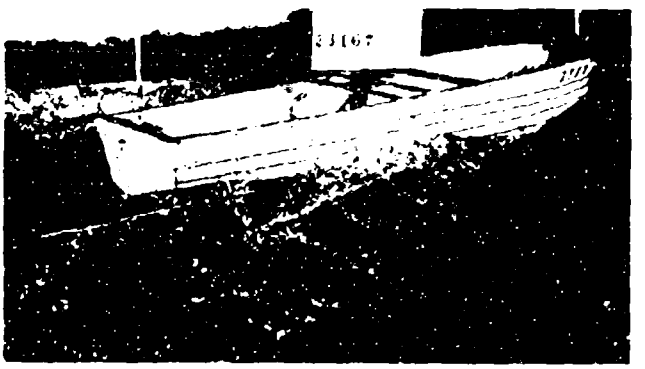

MODEL 2387

MODEL PORPOISED

MODEL 4927

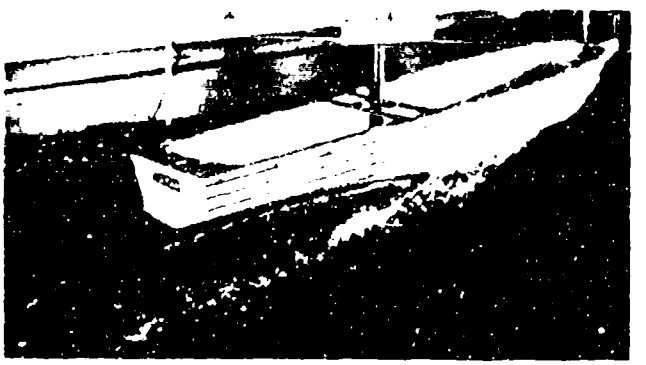

MODEL 4929

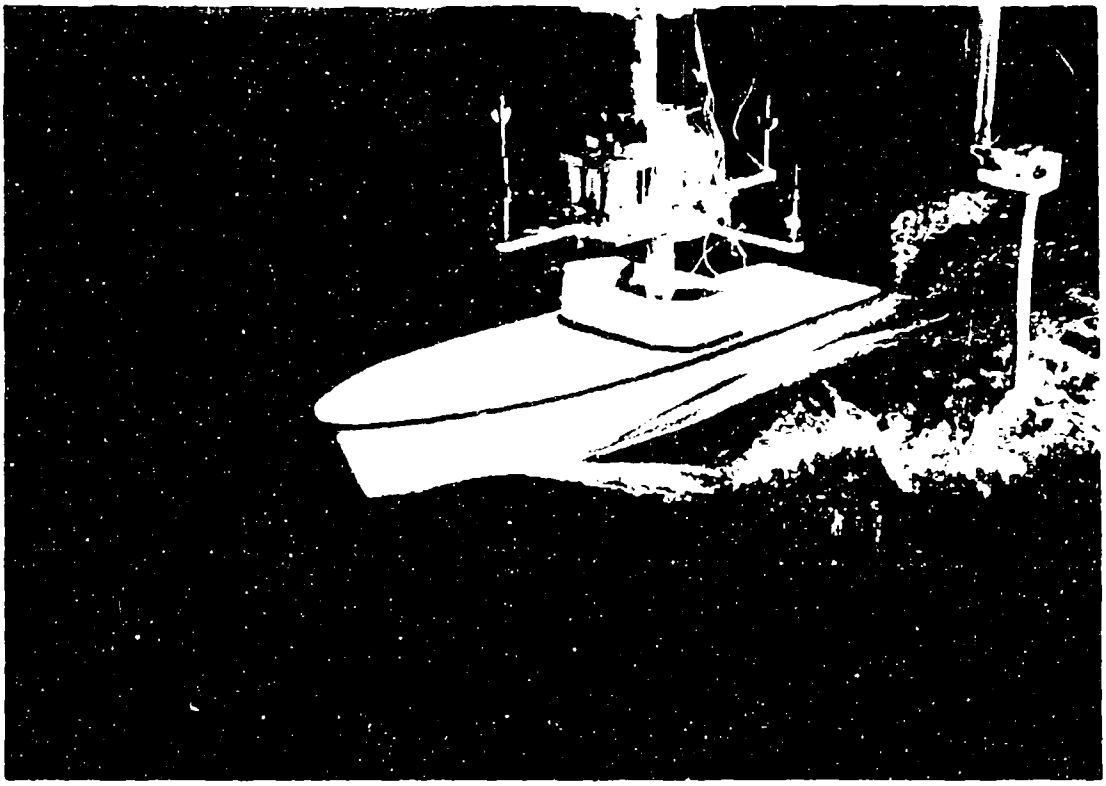

TEST FOR BROACHING TENDENCY EVALUATION

MODEL 2387 IN FOLLOWING REGULAR WAVES (100FT x 4FT)
SPEED 20 KNOTS